Theses and Dissertations

December 2013

Inverse Methods for Load Identification Augmented By Optimal Sensor Placement and Model Order Reduction

Deepak Kumar Gupta
University of Wisconsin-Milwaukee

INVERSE METHODS FOR LOAD IDENTIFICATION

AUGMENTED BY OPTIMAL SENSOR PLACEMENT

AND MODEL ORDER REDUCTION

by

Deepak Kumar Gupta

A Dissertation Submitted in

Partial Fulfillment of the

Requirements for the Degree of

Doctor of Philosophy

in Engineering

at

The University of Wisconsin – Milwaukee

December 2013

ABSTRACT

INVERSE METHODS FOR LOAD IDENTIFICATION
AUGMENTED BY OPTIMAL SENSOR PLACEMENT
AND MODEL ORDER REDUCTION

by

Deepak Kumar Gupta

The University of Wisconsin – Milwaukee, 2013
Under the Supervision of Professor Anoop K. Dhingra

Design problems require accurate characterization of loads acting on a structure. One way to estimate the loads is through experimentally measured structural response. This is known as the "inverse problem." The instrumented structure essentially acts as its own transducer. It is well known that the inverse problems tend to be highly ill-conditioned. This dissertation proposes several novel time domain and modal domain algorithms for estimating multiple dynamic loads exciting a structure from structural response measured at a finite number of optimally placed non-collocated sensors on the structure. The optimal placement of sensors is necessary to counter the inherent limitation of such inverse problems − ill-conditioning. Solution procedures based on construction of D-optimal design as well as sparse nature of mass, damping and stiffness matrices are proposed and implemented to determine the optimum locations of sensors that will provide the most precise load estimates. Both strain measurements using strain gages and acceleration measurements using accelerometers have been given due attention. Improvements in the load identification algorithms, based on model order reduction and reduced modal parameters, are further proposed to reconstruct the input forces accurately.

Load identification techniques based on dynamic programming and Markov parameters have also been studied in this work. Several limitations to these existing techniques have been identified. An attempt has been made in this dissertation to address the identified shortcomings based on D-optimal design for obtaining optimal sensor locations on the structure and model order reduction for computational cost reduction.

Both experimental measurements as well as numerical simulations have been performed in order to validate the proposed techniques. The experimental validation is done using a simple beam clamped at the base and attached to a shaker head. The focus of this example is to reconstruct the input forces exciting the structure through the shaker head. Numerical simulations are performed on the computational models developed in finite element tool ANSYS that works in close conjunction with MATLAB. Numerical sensitivity analyses are further performed to study the effect of uncertainties (noise) in experimental data as well as in the model; the techniques are validated to be robust – even with the presence of noise, the applied loads are recovered accurately.

Dedicated to my parents and my wife
for their unconditional love, support and motivation

ACKNOWLEDGEMENTS

First and foremost, I would like to express my sincere gratitude to my academic advisor - Professor Anoop Dhingra - for providing me with opportunity to pursue research under his guidance and for being an excellent academic and personal mentor throughout my graduate program. This work would not have been possible without his generous support and guidance. His advice on both research as well as my career have been invaluable.

I would also like to thank the members of my PhD Committe - Dr. Rani El-Hajjar, Dr. Ilya Avdeev, Dr. Ron Perez and Dr. Wilkistar Otieno - for taking out time to go through my work and for their insightful comments and suggestions.

I would like to acknowledge the support of my boss at work, Jay Edmundson, P.E., Vice President at Konecranes Nuclear Equipment and Services, LLC., for his motivation throughout the course of this work.

My sincere thanks goes to my colleague Dr. Pugazhendhi Kanakasabai for his invaluable inputs and suggestions. I would like to extend my appreciation to all the members of design optimization group for sharing great camaraderie in the lab. The members of the design optimization group have contributed immensely to my professional and personal time at UWM. The group has been a source of friendship as well as great advice and collaboration.

Above all, words cannot express how grateful I am to my parents who raised me with a love for science and supported me in all my pursuits, and for their unconditional love and care. Special thanks to my sister Deepika for her love and motivation. Last but not least, I would like to thank my loving wife Alka for her personal support, encouragement and great patience during the various stages of this PhD. I know I always have my family to count on when times are rough. I would not have made this far without them.

TABLE OF CONTENTS

LIST OF FIGURES

LIST OF TABLES

NOMENCLATURE

SYMBOL	DESCRIPTION
$[\ ]^{-1}$	Matrix inverse
$[\ ]^{T}$	Matrix transpose
$[\ ]^{+}$	Matrix left pseudo-inverse
$\|[\ ]\|$	Matrix determinant
$\{\dot{\ }\}$	Derivative with respect to time
$[A]$	Sensitivity matrix
$[A_c]$	System matrix for continuous case
$[A_d]$	System matrix for discrete case
$[A_d]_I$	Inverse system matrix for discrete case
a	Number of accelerometers
$[B_c]$	Input matrix for continuous case
$[B_d]$	Input matrix for discrete case
$[B_d]_{cs}$	Candidate set
$[B_d]_I$	Inverse input matrix for discrete case
b	Boundary degrees of freedom
$[C]$	Damping matrix
$[C]_{CB}$	Craig-Bampton reduced damping matrix
$[C]_{Guy}$	Guyan reduced damping matrix
$[C]_{IRS}$	Improved Reduced System (IRS) damping matrix
$[\nwarrow C \searrow]$	Diagonal modal damping matrix

$[C_c]$	Output matrix for continuous case
$[C_d]$	Output matrix for discrete case
$[C_d]_I$	Inverse output matrix for discrete case
c	Number of potential locations of sensors on the structure
$[D_c]$	Feedforward matrix for continuous case
$[D_d]$	Feedforward matrix for discrete case
$[D_d]_I$	Inverse feedforward matrix for discrete case
$\{d\}$	Measured response vector
E	Error function
e_i	Estimation error for gage i
$\{F(\omega)\}$	Force vector in frequency domain
$\{f\}, \{f(t)\}$	Force vector
f_{app}	Applied load
f_{rec}	Reconstructed load
$\{f^*\}$	Optimum reconstructed force using dynamic programming
g	Number of strain gages
$[H]$	Smoothing parameter matrix
$[H]_i$	ith forward Markov parameters matrix
$[H]_{z\_cs}$	Candidate set
$[H]_{z\_opt}$	Optimum subset of $[H]_{z\_cs}$ determined by D-optimal design
$[H(\omega)]$	Frequency Response Function (FRF) matrix
$[h]_i$	ith inverse Markov parameters matrix

$[h(t)]$	Impulse Response Function (IRF) matrix
$[I]$	Identity matrix
i	Internal degrees of freedom
j	Number of applied loads
$[K]$	Stiffness matrix
$[K]_{CB}$	Craig-Bampton reduced stiffness matrix
$[K]_{Guy}$	Guyan reduced stiffness matrix
$[K]_{IRS}$	Improved Reduced System (IRS) stiffness matrix
$[\nwarrow K \searrow]$	Diagonal modal stiffness matrix
$[M]$	Mass matrix
$[M]_{CB}$	Craig-Bampton reduced mass matrix
$[M]_{Guy}$	Guyan reduced mass matrix
$[M]_{IRS}$	Improved Reduced System (IRS) mass matrix
$[\nwarrow M \searrow]$	Diagonal modal mass matrix
m	Number of available / retained modes
n	Number of degrees of freedom
n_f	Number of forces
n_s	Number of sensors
p	Number of Craig-Bampton constrained normal modes
$[Q]$	Transformation matrix describing the locations of sensors
$[Q]_{opt}$	Transformation matrix describing the optimal locations of sensors
$\{q(t)\}$	Modal Participation Factor (MPF) vector

$\{q(t)\}_{CB}$	MPF of the Craig-Bampton reduced normal modes
$\{q(t)\}_p$	MPF of the constrained normal modes
$\{\tilde{q}(t)\}$	Modal Participation Factor (MPF) vector for retained modes
$\{\tilde{q}(t)\}_{CB}$	Approximation to $\{q(t)\}_{CB}$
$\{\tilde{\tilde{q}}(t)\}$	Approximation to $\{\tilde{q}(t)\}$
r	Primary degrees of freedom
s	Secondary degrees of freedom
$[T]$	Strain transformation matrix
$[T]_{Guy}$	Guyan reduction transformation matrix
$[T]_{IRS}$	Improved Reduced System (IRS) transformation matrix
$[T]_{DIRS}$	Dynamic IRS transformation matrix
t	Time
ti	Discretized time
t_0	Time constant
Δt	Time step
$\{u\}, \{u(t)\}$	State variables vector
$[W]$	Weighting diagonal matrix
$\{X(\omega)\}$	Displacement vector in frequency domain
$\{x(t)\}$	Displacement vector
$\{x(t)\}_{opt}$	Displacement vector at optimum accelerometer locations
$\{\tilde{x}(t)\}$	Approximate reconstructed displacement vector
$\{\tilde{\tilde{x}}(t)\}$	A random subset of $\{\tilde{x}(t)\}$

$\{x(t)\}_b$	Displacement vector corresponding to boundary degrees of freedom
$\{x(t)\}_i$	Displacement vector corresponding to internal degrees of freedom
$\{x(t)\}_r$	Displacement vector corresponding to primary degrees of freedom
$\{x(t)\}_s$	Displacement vector corresponding to secondary degrees of freedom
$\{x(t)\}_i^n$	Displacement vector due to constrained normal modes
$\{x(t)\}_i^s$	Displacement vector due to static modes
$\{y\}$	System output
δ	Unit impulse load function
$\{\varepsilon(t)\}$	Strain vector
$\{\tilde{\varepsilon}(t)\}$	Strain vector at randomly chosen locations on the structure
$\{\varepsilon(t)\}_{opt}$	Strain vector at optimum strain gage locations
ε_{ei}	Experimentally measured strain from gage i
ε_{pi}	Predicted strain for gage i
$[\varepsilon]_{xyz}$	Strain tensor in xyz coordinate system
$\varepsilon_{\%rms}$	Percent root mean square (rms) error
σ	Standard deviation
$[\phi]$	Modal matrix
$[\phi]_{CB}$	Craig-Bampton reduced modal matrix
$[\phi]_c$	Constrained modal matrix
$[\phi]_{opt}$	Optimum subset of $[\tilde{\phi}]_{cs}$ determined by D-optimal design
$[\phi]_u$	Updated modal matrix
$[\phi]_{u\_cs}$	Candidate set

$[\phi]_{u\_opt}$	Optimum subset of $[\phi]_{u\_cs}$ determined by D-optimal design
$[\tilde{\phi}]$	Truncated modal matrix retaining only m modes
$[\tilde{\phi}]_{cs}$	Candidate set
$[\tilde{\tilde{\phi}}]$	A random subset of $[\tilde{\phi}]_{cs}$
$[\psi]_{CB}$	Craig-Bampton reduction transformation matrix
$[\psi^{\varepsilon}]$	Modal strain matrix
$[\psi^{\varepsilon}]_{opt}$	Optimum subset of $[\tilde{\psi}^{\varepsilon}]_{cs}$ determined by D-optimal design
$[\tilde{\psi}^{\varepsilon}]$	Truncated modal strain matrix retaining only m modes
$[\tilde{\psi}^{\varepsilon}]_{cs}$	Candidate set
$[\tilde{\tilde{\psi}}^{\varepsilon}]$	A random subset of $[\tilde{\psi}^{\varepsilon}]_{cs}$
Ω	Frequency
ω	Circular frequency
$\omega_1, \omega_2 \cdots \omega_n$	Natural frequencies

Chapter 1 - Introduction

1.1 Problem Statement

For reliable and cost effective design and analysis of structures or engineering equipment, it is desirable to know at the design stage the locations and magnitudes of the external loads transmitted to the structure. These loads may be static or time varying dynamic loads. The stresses induced in the structure are a function of the applied loads. Knowledge of the loads early in the design process is vital for design optimization and effective analysis that ensures the structural integrity of the product. Accurate prediction of the loads leads to greater confidence in numerical simulation such as finite element analysis which, in turn, significantly reduces the reliance on expensive and time consuming experimental testing.

1.2 Limitations of Load Transducers

In many instances, it is possible to introduce load transducers (load cells) between the structure and the load transferring body that can directly measure the loads acting on a structure. This method of load measurement, however, suffers from certain limitations. For instance, an introduction of load transducers can change the system dynamic characteristics leading to inaccurate load estimation. In some applications, the input load locations may not be accessible thereby precluding insertion of a load transducer for the measurement of loads being transmitted to the structure. In several other applications, direct measurement of the excitation loads is not feasible such as aerodynamic loads,

seismic excitation, explosion forces, shock loads on ship hulls, engine torque pulses, wind loads, fluid-flow induced forces in piping systems etc.

1.3 Using Structure as a Load Transducer

In many applications, it is possible to measure the response of the structure to the unknown applied loads. The response may be quantities such as displacements, accelerations, strains etc. that depend on the loads and their measurement is more feasible than measuring the loads directly. A linear relationship (also called the system transfer function) between the loads to be estimated and the measured quantity can then be employed, along with the principle of superposition, to estimate the imposed loads. The instrumented structure, thus, behaves as its own load transducer. The simplest example utilizing this principle is a simple scale system where a weight suspended at one end of a cantilever beam is estimated by measuring the bending strains (response) at some other locations in the beam.

It is again emphasized at this point that the loads to be estimated may be static or dynamic, and different procedures may be needed depending upon whether static or dynamic loads are to be measured. It is well known that for given input time varying forces, structure response can be easily determined by using equations from dynamics and principles of elasticity. This is known as the "forward problem." In principle, it should then be possible to determine the input forces from the structure response. This is known as the "inverse problem." Solving the inverse problem may seem to be a straightforward task, but unfortunately this notion is misleading. One reason for this is that the inverse problem tends to be highly ill-conditioned, i.e., even very small variations

(noise) in the response measurement can cause large errors in the force estimation. Another challenge is that in the forward problem, the excitation forces are concentrated at a few locations on the structure and therefore, information about the forces is well known all over the structure. However, in the inverse problem, although a non-zero response is present over most of the structure, they can only be measured at a finite number of selected locations, with the response at the rest of the locations left untapped. Thus, the forward problem can be solved directly for the response, whereas the inverse problem poses significant challenges to solve for the input forces. Furthermore, a combination of different loads at different locations can result in the same level of response, while solution to the inverse problem, however, may not be unique. In fact, determining system response from input forces is working from cause to effect, whereas solving the inverse problem, i.e., determining the input forces from system response, is working from effect to cause.

Various methods have been developed and proposed to counter the challenges posed by the inverse problem which will be discussed in Chapter 2. The present work is another attempt to develop techniques to estimate the input loads applied to a structure from its measured response, i.e., to solve the inverse problem. In this dissertation, the terms loads and forces are used interchangeably. Similarly, estimation, identification and recovery mean the same in the context of this document.

1.4 Organization of Material

Chapter 1 presents a brief overview of the load estimation problem along with the identification of major challenges involved to address it.

Chapter 2 presents a broad overview of the existing literature and work done by other researchers in the areas of static as well as dynamic load recovery in frequency, modal, and time domains.

In Chapter 3, some basic concepts are laid out on which a large part of this thesis is built. Various representations into which the structural dynamics of a system can be cast are described. Furthermore, a detailed treatment of various model order reduction techniques is presented that are used extensively in later chapters.

Chapter 4 presents an in depth investigation of static load identification technique using strain data from optimally placed strain gages. With the help of static load identification, the concepts of Candidate Set and D-optimal design algorithm are introduced.

Chapter 5 develops a time domain technique for estimating dynamic loads exciting a structure from strain time response measured at a finite number of optimally placed strain gages on the structure. A novel approach is presented which utilizes the technique of model reduction that results in precise estimation of dynamic loads. This is especially useful when finite element modeling is used to study dynamics of continuous systems. Model reduction techniques presented in this chapter help recover applied loads accurately while keeping the computational costs low and without compromising on the accuracy.

Chapter 6 outlines two different algorithms for estimating time-varying loads acting on a structure by measuring acceleration time response at optimum locations on the structure. The accuracy of the load estimates is dependent on the locations of the accelerometers. A technique based on reduced modal parameters is proposed that results in higher accuracy in load estimates.

In Chapter 7, a technique based on dynamic programming is developed to identify the loads applied to a structure from experimentally measured response at optimal accelerometer locations on the structure. Since dynamic programming implementation tends to be computationally expensive, a technique based on Craig-Bampton model order reduction is proposed in the chapter that aims to reduce computation cost.

Chapter 8 deals with load identification using Markov parameters. An attempt is made to tie D-optimal design algorithm to Markov parameters technique to compute optimal accelerometer locations on the structure such that precise loads estimates are obtained. It is seen that optimum placement of accelerometer results in improvement in load estimates compared to the case when accelerometer locations are selected randomly.

Finally, Chapter 9 presents some concluding remarks on this research. In addition, potential areas of future research on this topic are also identified.

Chapter 2 - Literature Review

Over the years, several methods have been developed that can estimate the forces acting on the structure from its measured response without the use of intermediate load cells. There are several aspects of input force estimation from measured responses that have been explored to arrive at an efficient and accurate technique. Separate approaches may exist depending upon whether the forces to be estimated are static or dynamic in nature. A brief overview of many of the techniques is presented in this chapter.

2.1 Static Load Estimation Techniques

Static load estimation techniques are applicable to the case where the forces to be estimated are static in nature, i.e., they do not vary with time. These methodologies are limited to static linear elastic problems where the applied loads on the structure are estimated from the measured strains. Although, a set of static loads acting on a structure uniquely deforms it, the strains can only be measured at a finite number of locations on the deformed structure. This strain data can be used to determine the applied loads provided the principle of superposition holds. The precision with which the applied loads are estimated is dictated by the number of strain gages used along with their locations and angular orientations. While the gage locations on certain simple structures may be intuitive under certain loading conditions, the same cannot be said of a complex structure where a trial-and-error approach to gage placement can result in poor load estimates. This is because the gage may be placed at a location where it has a relatively low sensitivity to

the loads to be estimated. Further, for multi-degree of freedom force gages, the cross-sensitivity (Sommerfeld and Meyer, 1999) between the gages may not be small. As a result, the strain data obtained from many of the gages may be of little use and the load estimates may not be precisely known.

Masroor and Zachary (1991) developed a technique for determining a set of static loads acting on a structure from measured strains. They studied the effect of the number and locations of strain gages in a static load estimation problem. They formulated and defined a sensitivity parameter and argued that the variance of the force estimates is directly proportional to the sensitivity. They noted that an analysis based on all possible gage placements would be very time consuming and therefore, only a few groups of gages based on the judgment could be selected for the analysis. Since all possible gage location combinations were not taken into account, the sets selected for analysis were not guaranteed to be optimal, which in turn, might not yield the best possible load estimates.

Wickham *et al.* (1995) advanced the development by Masroor and Zachary (1991) and proposed a technique to minimize the sensitivity parameter by casting the strain gage locations problem as an optimization problem that determined the optimum locations of the gages. They utilized the k-exchange algorithm proposed by Johnson and Nachtsheim (1983) to construct the D-optimal design that provided the best estimates for the input loads. They applied this approach to recover the loads applied to a C-spring.

Dhingra and Hunter (2003) proposed a computational technique, in line with Wickham *et al.* (1995), which utilized optimum design of experiment technique to select the number, locations and angular orientations of the strain gages that will provide the

most precise load estimates. Their technique is capable of handling load recovery from 2-dimensional as well as complex 3-dimensional structures.

2.2 Dynamic Load Estimation Techniques

Dynamic load estimation techniques are applicable to the case where the forces to be estimated are dynamic in nature, i.e., they are a function of time. This area of research can be further sub-classified into three domains — (i) frequency domain, (ii) modal model domain, and (iii) time domain.

2.2.1 Frequency Domain Method

Frequency domain methods utilize a linear relationship between the applied forces and the measured response as a function of frequency. This linear relationship, also known as transfer function of the system, is called the frequency response function of the system. Consider the well known convolution integral that computes system response from the input forces:

$$\{x(t)\} = \int_0^t [h(t-\tau)]\{f(\tau)\}d\tau \tag{2.1}$$

where $\{x(t)\}$ is the $(n_s \times 1)$ response vector,

$\{f(t)\}$ is the $(n_f \times 1)$ excitation force vector,

$[h(t)]$ is the $(n_s \times n_f)$ Impulse Response Function (IRF) matrix.

Taking the Fourier transform of Eqn. (2.1), the relation can be expressed in the frequency domain as:

$$\{X(\omega)\} = [H(\omega)]\{F(\omega)\} \tag{2.2}$$

where ω is the circular frequency,

$\{X(\omega)\}$ is the $(n_s \times 1)$ response vector,

$\{F(\omega)\}$ is the $(n_f \times 1)$ excitation force vector,

$[H(\omega)]$ is the $(n_s \times n_f)$ Frequency Response Function (FRF) matrix.

The FRF can be obtained from experimentally measured data, or can be reconstructed from a modal model of the system, or can be obtained from finite element method. It completely defines the dynamic characteristics of the system. $\{X(\omega)\}$ can be measured experimentally as any of the physical quantities—displacement, velocity, acceleration, or strain. The relationship between strain frequency response function and displacement frequency response function has been explored by several authors (Li *et al.*, 1989; Tsang, 1990). Once $\{X(\omega)\}$ and $[H(\omega)]$ are known, the problem now remains that of solving for $\{F(\omega)\}$ and thereby computing the time history of the input forces $\{f(t)\}$ using the inverse Fourier transform. For square $(n_s = n_f)$ and non-singular $[H(\omega)]$, Eqn. (2.2) can be inverted to give:

$$\{F(\omega)\} = [H(\omega)]^{-1}\{X(\omega)\} \tag{2.3}$$

Unfortunately, this inverse problem is not as easy and straightforward as the mathematics suggests. Stevens (1987) presented an excellent overview of the difficulties posed by this class of inverse problems. Typically, FRF consists of a number of resonant peaks separated by anti-resonance valleys. Desanghere (1983) studied the inverse problem in frequency domain and the challenges involved in load estimation. His study suggests that at any particular frequency, especially near resonance, the response is dominated by a few modes and therefore, $[H(\omega)]$ consists of a few dominant elements

(corresponding to the resonant peaks) and many small elements (corresponding to the anti-resonance region). This leads to ill-conditioning of the matrix $[H(\omega)]$ and very small variations in the measurement of the response $[X(\omega)]$ can cause large variations in the estimated input force $\{F(\omega)\}$.

In Eqn. (2.3), there is exactly enough information so as to uniquely determine the input forces. Usually, it is possible to measure more number of response data than the number of unknown forces to be determined whereby the problem is over-determined $(n_s > n_f)$. The advantage of having more number of equations than the number of unknowns was studied by Hillary (1983) to minimize the effect of measurement errors, i.e., to improve the condition of the inverse problem. A least-squares solution to the inverse problem was, thus, suggested to take into account more data than unknowns:

$$\{F(\omega)\} = ([H(\omega)]^T [H(\omega)])^{-1} [H(\omega)]^T \{X(\omega)\} \tag{2.4}$$

where $[H(\omega)]^T$ is the Hermitian transpose of $[H(\omega)]$.

Bartlett and Flannelly (1979) were amongst the first researchers who employed the least-squares solution to estimate the forces acting on the hub of a helicopter. They estimated combinations of two orthogonal forces from fourteen response measurements at three different frequencies which were comparable to the directly measured forces.

Okubo *et al.* (1985) studied the influence of noise contaminating the measured response as well as the FRF on the accuracy of force estimation. They applied the least-squares technique to estimate force in a beam structure, cutting forces at cutting edge of a milling machine tool, forces generated on automobile engine mounts and forces transmitted to piping system and mounts of an air conditioner. They concluded that the

noise in the anti-resonance region was the greatest source of error in the input force identification than the noise in the resonance region.

Starkey and Merrill (1989) investigated the reason for the errors encountered in predicting the forces from Eqn. (2.4). They concluded that the ill-conditioned nature of the equation is due to the fact that the matrix $([H(\omega)]^T[H(\omega)])$ is frequently near-singular with the worst condition number near the natural frequencies of the system. The FRF matrix tends to be dominated by rank-one component corresponding to the dominant mode near resonance.

Hillary and Ewins (1984) used accelerometers and strain gages to measure FRF and estimated two simultaneous sinusoidal input forces on a uniform cantilever beam as test piece by employing the least-squares technique. They found that the strain related model gave more accurate results than the acceleration related model because the strain responses are more influenced by the higher modes at low frequencies; therefore, they capture the effect of higher modes better than the acceleration responses.

Boukria *et al.* (2011) applied the FRF technique to estimate the impact force magnitude and location applied to a circular plate. Tikhonov regularization was employed to stabilize the inverse problem. Determining the location of the impact force was based on the minimization of an objective function formed from the transfer function between several impact locations, forming a mesh structure with several measuring points.

Apart from the ill-conditioned nature of Eqn. (2.3) near resonance, application of the frequency domain method in force estimation has another major drawback. The FRF matrix needs to be inverted at each frequency in the range of interest, which is computationally intensive. Clearly, a better method is desired.

2.2.2 Modal Model Method

Modal model of a system is defined by its modal parameters — natural frequencies, corresponding mode shapes and modal damping factors. These parameters can be estimated experimentally from measured data, analytically for simple problems, or from finite element method. Genaro and Rade (1998) proposed the modal model method in time domain. Their approach was based upon the standard equilibrium equation in dynamics in modal coordinates:

$$[\diagdown M \diagdown]\{\ddot{q}(t)\} + [\diagdown C \diagdown]\{\dot{q}(t)\} + [\diagdown K \diagdown]\{q(t)\} = [\phi]^T\{f(t)\} \tag{2.5}$$

$$\{x(t)\} = [\phi]\{q(t)\} \tag{2.6}$$

where $[\diagdown M \diagdown]$ is the diagonal modal mass matrix,

$[\diagdown C \diagdown]$ is the diagonal modal damping matrix,

$[\diagdown K \diagdown]$ is the diagonal modal stiffness matrix,

$[\phi]$ is the modal matrix,

$\{q(t)\}$ is the vector of modal coordinates.

The input force can then be determined by inverting Eqn. (2.5):

$$\{f(t)\} = ([\phi]^T)^+([\diagdown M \diagdown]\{\ddot{q}(t)\} + [\diagdown C \diagdown]\{\dot{q}(t)\} + [\diagdown K \diagdown]\{q(t)\}) \tag{2.7}$$

where + denotes the left pseudo-inverse. They applied this method numerically to predict two simultaneously applied harmonic loads, but they failed to supplement their result with any laboratory test data.

The modal model method can as well be employed in the frequency domain as suggested by Desanghere and Snoeys (1985) where the input forces can be estimated by transforming the response from system coordinate to modal coordinate as:

$$\{F(\omega)\} = ([\phi]^T)^+(-\omega^2[\diagdown M \diagdown] + i\omega[\diagdown C \diagdown] + [\diagdown K \diagdown])[\phi]^+\{X(\omega)\} \tag{2.8}$$

The modal forces so obtained can then be transformed back to system coordinates by inverse coordinate transformation. They applied this technique to estimate forces in turbo compressor and longitudinal beam of a car frame.

Okubo *et al.* (1985) mentioned this technique in their paper, but advocated the least-squares technique as the preferred method over the modal model method. They argued that the modal model method requires extraction of modal parameters from the measured FRF and that the modal parameters are not always exact because of curve fitting problems. This introduces inaccuracy in the resulting force identification.

Busby and Trujillo (1987) cast the load estimation problem as a minimization problem of error which is defined as difference between the measured structural response and response predicted from the model. They used dynamic programming to solve this minimization problem resulting in force estimation based on a recursive reformulation of the governing equations. The utility of their approach was demonstrated numerically by applying it to a 10 degrees of freedom cantilever beam model. One of the disadvantages of the method is that the amount of computation increases dramatically as the order of the model increases. To deal with this, they proposed an eigenvalue reduction technique to reduce the order of the system. The reduction technique was based on elimination of higher modes which would lead to truncation errors.

Hollandsworth and Busby (1989) extended the previous study by Busby and Trujillo (1987) by applying it to actual experimental measurements. They estimated the impact loads on a cantilever beam by measuring acceleration response from three accelerometers placed at different locations. They found significant discrepancy between the estimated forces and actual forces. They then applied a smoothing parameter to the

measured acceleration data before subjecting it to the load identification calculations. The authors claimed that the smoothing parameter was essential in successful load estimation.

Hansen and Starkey (1990), working on a line similar to Starkey and Merrill (1989), investigated the ill-conditioned nature of the modal model method. Their study was based on the effect of locations of accelerometer placements on a steel beam on the condition number of the modal matrix. They concluded that the condition number of the modal matrix can be improved through proper selection of the accelerometer placement and modes included in the analysis.

2.2.3 Time Domain Methods

Time domain techniques are the most recent developments that aim towards estimating the input forces from measured response in time domain. The response of a structure as a function of its Impulse Response Function (IRF) and the forces acting on the structure is given by the convolution integral Eqn. (2.1) which is restated here for ease of reference:

$$\{x(t)\} = \int_0^t [h(t-\tau)]\{f(\tau)\}d\tau$$

The problem at hand is to solve this equation for unknown forces from the knowledge of the IRF and measured responses. Nashed (1976) showed that this deconvolution problem is ill-posed because the solution $f(t)$ does not continuously depend on the input data $x(t)$ and $h(t)$ and small variations in the measured data can produce large errors in the force estimation. Great deal of research has been devoted to develop techniques that aim towards deconvolving this equation to solve for the input forces.

Carne *et al.* (1992) proposed a technique referred to as the Sum of Weighted Acceleration Technique (SWAT) that estimates the input forces by summing the weight-scaled measured accelerations. The weighting factors can be determined either from inverting the modal matrix or from the free-decay response of the structure. They successfully applied this technique to estimate the impact force applied by the nose of a weapon mockup to the weapon body. This technique suffers with a drawback that only sum of the input forces can be determined without any estimation of the individual loads.

Kammer (1998) presented a method that utilizes a set of inverse system Markov parameters estimated from forward system Markov parameters using a linear predictive scheme. This computation is ill-conditioned and therefore, a regularization technique is employed to stabilize the computation. The inverse system Markov parameters can then be convolved with the measured response to estimate the input forces. This method has a limitation that the response sensors must be collocated with the input forces locations.

Steltzner and Kammer (1999) suggested a technique for input force estimation using an Inverse Structural Filter (ISF) that processes the structural response data and returns an estimate of the input forces. They successfully applied the technique to estimate the docking forces between the space shuttle and the Russian MIR space station using numerically simulated response data and also acknowledged the instances in which this technique would fail.

Liu *et al.* (2000) proposed a method to estimate the input forces with the assistance of a system identification algorithm. They applied the Kalman filter with a least-squares recursive estimator to update the estimation in real time. This method was

satisfactorily applied to predict input forces of a cantilever plate from response measured at two distinct points.

Adams and Doyle (2002) extended the work by Busby and Trujillo (1987) and applied the dynamic programming approach to load estimation for complex structures. The approach is based on the recursive reformulation of the governing equations in conjunction with finite element method and applies to multiple isolated forces as well as distributed pressures and tractions. The method was demonstrated to reconstruct impact forces on a cylindrical shell and plate with a hole.

Szwedowicz *et al*. (2002) as well as Mignolet and Choi (2003) have proposed genetic algorithm based approach for mounting strain gages on turbine blades to capture vibration modes. However, this approach is limited to the recovery of mode shapes and not the loads acting on the component.

Ma *et al.* (2003) used an on-line recursive inverse method based on the Kalman Filter and a recursive least-squares algorithm to estimate the input forces. Finite element method is used to construct the state equations of the system. The method was validated with a cantilever beam subjected to a variety of loads.

Hashemi and Kargarnovin (2007) formulated the force identification problem as an optimization problem where the objective function is calculated as the difference between analytical and measured responses and the decision variables are the location and magnitude of the applied force. Genetic Algorithm was applied to solve the optimization problem and the method effectively estimated the impact force acting on a simply supported beam.

Lu and Law (2007) suggested a method based on sensitivity of structural responses to estimate the input forces along with system parameters. The force and physical parameters are identified in a gradient-based model updating method based on dynamic response sensitivity. The method was validated with numerical simulation as well as experimental data from a simply supported steel beam.

Wu and Loh (2007) formulated a method employing the Kalman filter that establishes a regression model between the residual innovation and the input forces, based on which, a recursive least-squares estimator was proposed to estimate the input forces. They applied this method to characterize the traffic loads induced by commercial vehicles on a bridge.

Allen and Carne (2008) reviewed and compared two time domain techniques, ISF and SWAT, and revealed some of the deficiencies of the methods. They presented a number of extensions of the ISF technique which can greatly improve its performance. Inoue *et al.* (2001) presented a review of a variety of techniques that have been developed for the indirect estimation of magnitude of impact force along with its location and direction.

2.3 Summary

Though a lot of research has taken place in the field of load estimation from measured response of a structure, there are specific issues that need to be addressed with respect to computational efficiency, accuracy and practical applications. As discussed in Sec. 2.2.1, load estimation in frequency domain has some inherent drawbacks involved. The modal model method clearly has some advantages over the frequency domain

method, but it still suffers from the problem of ill-conditioning. Although a number of methods have been proposed to solve the load estimation problem in time domain, there is scope of further research to make the methods more suitable for real world applications.

It is well established that the precision of load estimates is dictated by the locations of the sensors on the structure. The condition number of the inverse problem in load estimation can be improved and precise load estimates can be obtained through proper selection of the sensor placement and modes included in the analysis; still, the work done towards addressing this is very limited and few publications exist that focus on improving the condition of the inverse problem through the optimal placement of the sensors. This thesis is an attempt to address these identified shortcomings in the existing literature.

Chapter 3 - Theoretical Framework

This chapter outlines the basic theories, equations and results that will be used frequently in the following chapters of this thesis. It is assumed throughout this work that the systems being dealt with are linear elastic in nature and the deformations are small enough so that the principle of superposition applies.

3.1 Representations of Structural Dynamics of a System

There exist a number of ways in which dynamics of a structural system can be represented. The inverse algorithms detailed in this work make use of some of these formulations. Presented next are some of the representations into which structural dynamics of a system can be cast.

3.1.1 Second-Order ODE Representation

The dynamic response of a physical structural system to applied loads can be expressed in the form of its true equations of motion as second order partial differential equations (PDE) called wave equations. Closed form solutions to wave equation exist for simple systems. When complex geometry and boundary conditions are encountered, analytical solutions to the wave equation become difficult to obtain. In such cases, the continuum of the structural system is spatially discretized into finite number of elements, following which, the continuous partial differential equations of motion for the structural

system can be written as linear second-order ordinary differential equations (ODE) in the matrix form as:

$$[M]\{\ddot{x}(t)\} + [C]\{\dot{x}(t)\} + [K]\{x(t)\} = \{f(t)\} \tag{3.1}$$

where $[M]$, $[C]$ and $[K]$ are the mass, damping and stiffness matrices respectively that are obtained herein from finite element method, $\{x(t)\}$ is the displacement vector and $\{f(t)\}$ is the load acting on the structure.

3.1.2 Generalized Coordinates Representation

The model of the system in physical coordinates given by Eqn. (3.1) can be transformed into generalized (modal) coordinates. To realize this transformation, consider the following free vibration equations of motion of an undamped system:

$$[M]\{\ddot{x}(t)\} + [K]\{x(t)\} = \{0\} \tag{3.2}$$

Assuming a harmonic solution of the form:

$$\{x(t)\} = \{\phi\}sin(\omega(t + t_0)) \tag{3.3}$$

where $\{\phi\}$ is a vector of constants, ω is the frequency (rad/s) and t_0 is a constant, the eigenvalue problem associated with Eqn. (3.2) is given by:

$$([K] - \omega^2[M])\{\phi\} = [0] \tag{3.4}$$

The eigenvectors obtained from the solution of Eqn. (3.4) form the modal matrix $[\phi]$. If the modes are normalized to the mass matrix, then:

$$[\phi]^T[M][\phi] = [I], \quad [\phi]^T[K][\phi] = [\omega^2] \tag{3.5}$$

where $[I]$ is the identity matrix and:

$$[\omega^2] = \begin{bmatrix} \omega_1^2 & 0 & \cdots & 0 \\ 0 & \omega_2^2 & \cdots & 0 \\ \vdots & \vdots & \ddots & \vdots \\ 0 & 0 & \cdots & \omega_n^2 \end{bmatrix}$$

Next, using the following transformation:

$$\{x(t)\} = [\phi]\{q(t)\} \tag{3.6}$$

where $\{q(t)\}$ is the vector of Modal Participation Factors (MPF), Eqn. (3.1) can now be transformed into modal coordinates as:

$$[M][\phi]\{\ddot{q}(t)\} + [C][\phi]\{\dot{q}(t)\} + [K][\phi]\{q(t)\} = \{f(t)\} \tag{3.7}$$

3.1.3 State-Space Representation

Another way to characterize the input-output behavior of a structural system is by writing the second-order Eqn. (3.1) as a first-order equation or in continuous time-invariant state-space form as:

$$\{\dot{u}(t)\} = [A_c]\{u(t)\} + [B_c]\{f(t)\} \tag{3.8}$$

where $\{u(t)\}$ is the vector of state variables, $[A_c]$ is the system matrix and $[B_c]$ is the input matrix for continuous case given by:

$$[A_c] = \begin{bmatrix} [0] & [I] \\ -[M]^{-1}[K] & -[M]^{-1}[C] \end{bmatrix}$$

$$[B_c] = \begin{bmatrix} [0] \\ [M]^{-1} \end{bmatrix} \tag{3.9}$$

All physical phenomena fundamentally exist in continuous time. The experimentally measured response data, however, is available only at discrete time instants. This calls for the need to transform the continuous time-invariant state-space

model into a discrete time-invariant state-space model. The transformation takes the following form:

$$\{u\}_{ti+1} = [A_d]\{u\}_{ti} + [B_d]\{f\}_{ti} \tag{3.10}$$

where *ti* is the subscript over the discretized time and $[A_d]$ and $[B_d]$ are related to their continuous case counterparts as:

$$[A_d] = e^{[A_c]\Delta t}$$

$$[B_d] = [A_c]^{-1}([A_d] - [I])[B_c] \tag{3.11}$$

where *Δt* is the time increment. Equation (3.10) is the discrete linear time-invariant state-space representation of the structural system.

3.1.4 Markov Parameter Representation

Consider the state-space model described by Eqn. (3.10); the corresponding system output is given by:

$$\{y\}_{ti} = [C_d]\{u\}_{ti} + [D_d]\{f\}_{ti} \tag{3.12}$$

where $[C_d]$ is the output matrix and $[D_d]$ is the feedforward matrix for discrete case. Given that unit impulse load is applied to the system at time $t = 0$, i.e. $\delta_0 = 1$, and assuming zero initial conditions, the impulse response at various time points is given by:

$$[H]_0 = [C_d]\{u\}_0 + [D_d]\delta_0 = [D_d]$$

$$\{u\}_1 = [A_d]\{u\}_0 + [B_d]\delta_0 = [B_d]$$

$$[H]_1 = [C_d]\{u\}_1 + [D_d]\delta_1 = [C_d][B_d]$$

$$\{u\}_2 = [A_d]\{u\}_1 + [B_d]\delta_1 = [A_d][B_d]$$

$$[H]_2 = [C_d]\{u\}_2 + [D_d]\delta_2 = [C_d][A_d][B_d] \tag{3.13}$$

$$\{u\}_3 = [A_d]\{u\}_2 + [B_d]\delta_2 = [A_d]^2[B_d]$$

$$[H]_3 = [C_d]\{u\}_3 + [D_d]\delta_3 = [C_d][A_d]^2[B_d]$$

$$\vdots$$

$$[H]_i = [C_d][A_d]^{i-1}[B_d]$$

Given the impulse response, the response at any time is given by the convolution of the input force with the impulse response as:

$$\{y\}_{ti} = \sum_{i=0}^{ti}[H]_i\{f\}_{ti-i} \tag{3.14}$$

where the matrices $[H]_i$ are called forward Markov parameters and summarized as:

$$[H]_0 = [D_d]$$

$$[H]_i = [C_d][A_d]^{i-1}[B_d] \qquad i = 1, 2, 3 \dots \tag{3.15}$$

The forward Markov parameters represent the response of the discrete system to applied unit impulse and thus contain the dynamic properties of the system. They can either be obtained analytically from the discretized model of the structural system or experimentally by measuring the output of the system due to a known input, computing the corresponding frequency response function and then taking its inverse discrete Fourier transform. Equation (3.14) is the Markov parameter representation of the structural system.

3.2 Model Order Reduction

Model order reduction methods (Paz, 1985), also referred to as condensation methods, aim at reducing the number of degrees of freedom in a model without changing its dynamic characteristics significantly. The technique of model order reduction will be used extensively in this thesis; therefore, it is imperative to discuss some of the existing model reduction methods before their application to dynamic load recovery is presented.

3.2.1 Static Condensation

This method, also known as Guyan reduction, was first proposed by Guyan (1965). The method ignores the dynamic components (both inertia and damping) of the model, hence the name static condensation method. In order to accomplish the reduction of the stiffness matrix $[K]$, the primary (master) degrees of freedom are arranged as the first r coordinates and the remaining eliminated or secondary (slave) degrees of freedom form the last s coordinates. Following this arrangement and ignoring damping, Eqn. (3.1) can be written using partitioning matrices as:

$$\begin{bmatrix} [M]_{rr} & \vdots & [M]_{rs} \\ \cdots & \vdots & \cdots \\ [M]_{sr} & \vdots & [M]_{ss} \end{bmatrix} \begin{Bmatrix} \{\ddot{x}(t)\}_r \\ \cdots \\ \{\ddot{x}(t)\}_s \end{Bmatrix} + \begin{bmatrix} [K]_{rr} & \vdots & [K]_{rs} \\ \cdots & \vdots & \cdots \\ [K]_{sr} & \vdots & [K]_{ss} \end{bmatrix} \begin{Bmatrix} \{x(t)\}_r \\ \cdots \\ \{x(t)\}_s \end{Bmatrix} = \begin{Bmatrix} \{f(t)\}_r \\ \cdots \\ \{0\} \end{Bmatrix} \qquad (3.16)$$

where $\{x(t)\}_r$ is the displacement vector corresponding to the primary degrees of freedom and $\{x(t)\}_s$ is the displacement vector corresponding to the secondary degrees of freedom. To simplify the explanation, it is assumed without loss of generality that the external forces are zero at the secondary degrees of freedom. Using the second set of equations from Eqn. (3.16) and ignoring the inertia components, the eliminated or the

secondary degrees of freedom can be expressed in terms of the primary degrees of freedom as:

$$\{x(t)\}_s = [\bar{T}]\{x(t)\}_r \tag{3.17}$$

where $[\bar{T}]$ is given by:

$$[\bar{T}] = -[K]_{ss}^{-1}[K]_{sr}\{x(t)\}_r \tag{3.18}$$

Ignoring the inertia components in Eqn. (3.16) and substituting $\{x(t)\}_s$ from Eqn. (3.17) into Eqn. (3.16):

$$\begin{bmatrix} [K]_{rr} & \vdots & [K]_{rs} \\ \cdots & \vdots & \cdots \\ [K]_{sr} & \vdots & [K]_{ss} \end{bmatrix} \begin{bmatrix} [I] \\ \cdots \\ [\bar{T}] \end{bmatrix} \{x(t)\}_r = \begin{Bmatrix} \{f(t)\}_r \\ \cdots \\ \{0\} \end{Bmatrix} \tag{3.19}$$

where $[I]$ is the identity matrix. Writing transformation matrix $[T]_{Guy} = \begin{bmatrix} [I] \\ \cdots \\ [\bar{T}] \end{bmatrix}$ and pre-multiplying Eqn. (3.19) by $[T]_{Guy}^T$ results in:

$$[K]_{Guy}\{x(t)\}_r = \{f(t)\}_r \tag{3.20}$$

where the reduced stiffness matrix $[K]_{Guy}$ is expressed as a transformation of full model stiffness matrix $[K]$ as:

$$[K]_{Guy} = [T]_{Guy}^T[K][T]_{Guy} \tag{3.21}$$

In order to reduce the mass and damping matrices, it is assumed that the same static relationship between the primary and secondary degrees of freedom remains valid in the dynamic problem. The transformation given by Eqn. (3.21) can also be applied to reduce the mass matrix $[M]$ and the damping matrix $[C]$ as:

$$[M]_{Guy} = [T]_{Guy}^T[M][T]_{Guy}$$

$$[C]_{Guy} = [T]_{Guy}^T[C][T]_{Guy} \tag{3.22}$$

Though the static condensation method is very simple to apply, in general, it is not very accurate and introduces errors in the results when applied to dynamic problems. The magnitude of the errors depends on the relative number of degrees of freedom eliminated as well as on the specific choice of these degrees of freedom.

3.2.2 Improved Reduced System (IRS)

O'Callahan (1989) proposed a method for dynamic model reduction known as the Improved Reduced System (IRS) method. In this modified approach, an extra term is added to the static condensation transformation $[T]_{Guy}$ to account for the inertia forces. The modified transformation matrix $[T]_{IRS}$ is given by:

$$[T]_{IRS} = [T]_{Guy} + [S][M][T]_{Guy}[M]_{Guy}^{-1}[K]_{Guy} \tag{3.23}$$

where $[S] = \begin{bmatrix} [0] & [0] \\ [0] & [K]_{ss}^{-1} \end{bmatrix}$.

The reduced stiffness matrix $[K]_{IRS}$, reduced mass matrix $[M]_{IRS}$ and reduced damping matrix $[C]_{IRS}$ are obtained by:

$$[K]_{IRS} = [T]_{IRS}^{T}[K][T]_{IRS}$$

$$[M]_{IRS} = [T]_{IRS}^{T}[M][T]_{IRS} \tag{3.24}$$

$$[C]_{IRS} = [T]_{IRS}^{T}[C][T]_{IRS}$$

Friswell *et al.* (1995) extended the IRS method by using the transformation from dynamic reduction instead of static reduction as the basic transformation. The dynamic IRS transformation matrix $[T]_{DIRS}$ at a given frequency Ω is given by:

$$[T]_{DIRS} = [T]_d + [S]_d[M][T]_d[M]_{Guy}^{-1}([K]_{Guy} - \Omega^2[M]_{Guy}) \tag{3.25}$$

where $[S]_d = \begin{bmatrix} [0] & [0] \\ [0] & ([K]_{ss} - \Omega^2[M]_{ss})^{-1} \end{bmatrix}$ and

$$[T]_d = \begin{bmatrix} [I] \\ -([K]_{ss} - \Omega^2[M]_{ss})^{-1}([K]_{sr} - \Omega^2[M]_{sr}) \end{bmatrix}.$$

The reduced stiffness, mass and damping matrices are then given by expressions similar to Eqn. (3.24).

The transformation mentioned in Eqn. (3.23) relies on the reduced mass and stiffness matrices obtained from the static reduction. Once the transformation is computed, improved estimates of the reduced matrices are available from Eqn. (3.24). These improved estimates can be substituted back in Eqn. (3.23) to give a more accurate transformation matrix. For subsequent iterations, the transformation matrix can be obtained by:

$$[T]_{IRS,i+1} = [T]_{Guy} + [S][M][T]_{IRS,i}[M]_{IRS,i}^{-1}[K]_{IRS,i} \tag{3.26}$$

where i denotes the ith iteration. The transformation $[T]_{IRS,i}$ is the current IRS transformation and $[M]_{IRS,i}$ and $[K]_{IRS,i}$ are the associated reduced mass and stiffness matrices given by Eqn. (3.24). A new transformation is then obtained from Eqn. (3.26) which then becomes the current transformation for the next iteration. The procedure converges to produce the reduced stiffness, mass and damping matrices. This method is known as the iterated IRS technique.

3.2.3 Component Mode Synthesis (CMS)

This dynamic condensation method was first proposed by Craig and Bampton (1968); therefore, it is also known as Craig-Bampton model order reduction method. This method is especially useful when substructuring is used, where the degrees of freedom of each substructure can be divided into two sets — boundary degrees of freedom b and internal degrees of freedom i. Boundary degrees of freedom of a substructure are those

which are common with other substructures, while internal degrees of freedom are those belonging only to the relevant substructure. In order to accomplish model reduction, boundary degrees of freedom together with some of the modal coordinates of the substructure constrained at its boundary are considered as primary or retained degrees of freedom.

Ignoring damping, Eqn. (3.1) can be written using partitioning matrices as:

$$\begin{bmatrix} [M]_{bb} & \vdots & [M]_{bi} \\ \cdots & \vdots & \cdots \\ [M]_{ib} & \vdots & [M]_{ii} \end{bmatrix} \begin{Bmatrix} \{\ddot{x}(t)\}_b \\ \cdots \\ \{\ddot{x}(t)\}_i \end{Bmatrix} + \begin{bmatrix} [K]_{bb} & \vdots & [K]_{bi} \\ \cdots & \vdots & \cdots \\ [K]_{ib} & \vdots & [K]_{ii} \end{bmatrix} \begin{Bmatrix} \{x(t)\}_b \\ \cdots \\ \{x(t)\}_i \end{Bmatrix} = \begin{Bmatrix} \{f(t)\}_b \\ \cdots \\ \{f(t)\}_i \end{Bmatrix} \qquad (3.27)$$

where $\{x(t)\}_i$ is the displacement vector corresponding to the internal degrees of freedom and $\{x(t)\}_b$ is the displacement vector corresponding to the boundary degrees of freedom. It is proposed that $\{x(t)\}_i$ can be assumed to be equal to the sum of static modes $\{x(t)\}_i^s$, i.e., the deformation due to $\{x(t)\}_b$ when no force acts on the substructure, and the constrained normal modes $\{x(t)\}_i^n$, i.e., the natural modes of free vibration of the substructure when the boundary displacement vector $\{x(t)\}_b$ is set to zero. The static modes $\{x(t)\}_i^s$ can be obtained, assuming zero inertia effects and $\{f(t)\}_i = \{0\}$, from the second set of equations in Eqn. (3.27) as:

$$\{x(t)\}_i^s = -[K]_{ii}^{-1}[K]_{ib}\{x(t)\}_b \qquad (3.28)$$

The constrained normal modes $\{x(t)\}_i^n$ can be computed by solving the eigenvalue problem $-\omega^2[M]_{ii} + [K]_{ii} = \{0\}$. Solution of the eigenvalue problem provides the constrained modal matrix $[\phi]_c$, whereby, the constrained normal modes $\{x(t)\}_i^n$ are given by:

$$\{x(t)\}_i^n = [\phi]_c\{q(t)\}_p \qquad (3.29)$$

where p is the number of Craig-Bampton constrained normal modes. The displacement vector $\{x(t)\}$ can then be expressed as:

$$\{x(t)\} = \begin{Bmatrix} \{x(t)\}_b \\ \{x(t)\}_i \end{Bmatrix} = \begin{Bmatrix} \{x(t)\}_b \\ -[K]_{ii}^{-1}[K]_{ib}\{x(t)\}_b + [\phi]_c\{q(t)\}_p \end{Bmatrix} = [\psi]_{CB} \begin{Bmatrix} \{x(t)\}_b \\ \{q(t)\}_p \end{Bmatrix} \tag{3.30}$$

where $[\psi]_{CB}$ is the transformation matrix that transforms the reduced coordinates to the full model coordinates given as:

$$[\psi]_{CB} = \begin{bmatrix} [I] & [0] \\ -[K]_{ii}^{-1}[K]_{ib} & [\phi]_c \end{bmatrix} \tag{3.31}$$

Thus the reduced stiffness matrix $[K]_{CB}$, reduced mass matrix $[M]_{CB}$ and reduced damping matrix $[C]_{CB}$ can be expressed as a transformation of the respective full model matrices as:

$$[K]_{CB} = [\psi]_{CB}^T[K][\psi]_{CB}$$

$$[M]_{CB} = [\psi]_{CB}^T[M][\psi]_{CB} \tag{3.32}$$

$$[C]_{CB} = [\psi]_{CB}^T[C][\psi]_{CB}$$

As stated previously, static condensation produces reasonable results only at lower frequencies and tends to be inaccurate when applied to higher frequency range dynamic problems, thus, leading to errors in the analysis. Among the more accurate condensation techniques are dynamic reduction, component mode synthesis (CMS), improved reduced system (IRS) etc. that have been proposed to improve upon the Guyan condensation. Each of them has certain advantages and disadvantages over the others. Dynamic reduction (Qu, 2004) requires a guess on initial frequency which may not be trivial. It has been observed by Koutsovasilis and Beitelschmidt (2008) that CMS produces better results than dynamic reduction at higher frequencies. IRS is computationally intense due to the inherent iterations involved. CMS is used in this work

as it provides a good balance between accuracy and computational expense. The choice between fixed interface CMS and free interface CMS is subtle. Fixed interface CMS, also known as Craig-Bampton model reduction, is selected to be used in the remainder of this work as it has better convergence properties.

3.3 Error Quantification

A possible means to quantify the error in the recovered loads with respect to the applied loads is presented in this section. The percent root mean square (rms) error $\varepsilon_{\%rms}$ in the recovered loads with respect to the actual applied loads can be calculated as:

$$\varepsilon_{\%rms} = \left(\frac{\sqrt{\Sigma\left(f_{app} - f_{rec}\right)^2}}{\sqrt{\Sigma f_{app}^2}} \times 100 \right) \%$$

(3.33)

where f_{app} is the applied load and f_{rec} is the reconstructed load. The above equation can be used to quantify errors in the load estimates.

Chapter 4 -   Static and Quasi-Static Load Identification from Strain Measurements

Measurement of strains at certain locations on a structure by strain gages and using these measurements to recover the loads acting on the structure by inverse analysis has been used extensively over the years. Strain gages provide one of the most inexpensive, robust and reliable methods of measuring the system responses to the applied loads. It is well established (Hillary and Ewins, 1984) that the strain related models give more accurate results than the acceleration related models because the strain responses are more influenced by the higher modes at low frequencies and therefore, they capture the effect of higher modes better than the acceleration responses. An in depth investigation of the existing static load identification technique using strain measurements is the subject of this chapter. Sec. 4.1 introduces the technique to estimate the static loads applied to a structure. Sec. 4.2 builds upon the concepts presented in Sec. 4.1 to identify a set of quasi-static loads acting on a structure. By means of static load estimation, this chapter also marks the introduction of Candidate set and D-optimal design algorithm. These developments will be used extensively in future chapters of this thesis when the subject of identification of dynamic loads acting on a structure will be taken up.

4.1 Static Load Estimation

The static load estimation problem can be written as a system of linear equations as:

$$\{\varepsilon\} = [A]\{f\} \tag{4.1}$$

where $\{\varepsilon\}$ is a $(g \times 1)$ vector of strains measured at g distinct locations on the structure,

$[A]$ is a $(g \times n_f)$ sensitivity matrix, a_{ij} represents the strain at location i due to a unit load applied at location j,

$\{f\}$ is an $(n_f \times 1)$ vector of n_f applied forces on the structure.

Equation (4.1) simply states that the strain at any location on the structure can be written as a linear combination of strains produced at that location by each load applied individually. It applies to linear elastic problems and assumes that the deformations are small enough such that the principle of superposition holds. Assuming that $[A]$ is known and $\{\varepsilon\}$ is measured, the least-squares estimate of the unknown forces $\{f\}$ is given by:

$$\{f\} = ([A]^T[A])^{-1}[A]^T\{\varepsilon\} \tag{4.2}$$

In practice, the strain vector is prone to measurement errors. If the errors in strain measurements are independently and identically distributed and the standard deviation of each of them is σ, then the variance-covariance matrix for the load estimates (Masroor and Zachary, 1991) can be obtained by:

$$var(\{f\}) = \sigma^2([A]^T[A])^{-1} \tag{4.3}$$

The matrix $([A]^T[A])^{-1}$ is known as the sensitivity of $[A]$. For a given variance in strain measurements σ^2, minimization of the sensitivity of $[A]$ leads to an increased precision in the load estimates. The sensitivity of $[A]$ is a function of the number, locations and angular orientations of the strain gages mounted on the structure. Therefore, optimal selection of the locations, angular orientations and the number of strain gages, so as to minimize the sensitivity of $[A]$, can lead to the minimization of the variation in the load estimates. A solution procedure exists that can be used to provide the most precise

estimates of the applied loads by the optimal selection of the locations, angular orientations and the number of strain gages on the structure. This procedure can be divided into three steps — (i) generation of the candidate set, (ii) determination of the number of strain gages to be used, and (iii) determination of the D-optimal design. These steps are discussed in detail in the following subsections.

4.1.1 Generation of the Candidate Set

Typically, there is a large number of locations on the surface of a structure on which strain gages can be mounted. These locations exclude the inaccessible areas such as the regions of load application. Each combination of strain gage location and angular orientation is termed a candidate point. Each candidate point provides a potential row for inclusion in the matrix $[A]$. All possible combinations of the strain gage locations and the orientation angles constitute a set, called the candidate set. The matrix $[A]$ is such a subset of the candidate set that provides the most precise estimates of the applied loads. The number of rows g of the matrix $[A]$ represents the number of strain gages mounted on the structure and the number of columns n_f represents the number of applied loads. The elements in each row of the matrix $[A]$ represent the response of a strain gage at a particular location and angular orientation to each individual unit load.

The candidate set can be generated analytically for a structure of any complexity by utilizing the finite element model of the structure. There are some practical considerations that must be followed before generating the candidate set. Since the strain gages are to be mounted on the surface of the structure, the finite element model should be prepared such that surface strain information is available in all the regions being

considered as possible locations for the strain gages. The surface strain information can easily be obtained if shell elements are used to model the structure. If shell elements are not used, but say 3-D solid elements are used to model the structure, then the solid elements can be coated with shell elements to obtain the surface strain information. The meshing is done such that the element size is compatible with the physical dimensions of the strain gages to be used.

From a numerical standpoint, the elemental strain information is preferred over the nodal strain information; the reasons for this can be understood as follows. Since a node on the surface of the model can be a common node for up to four adjacent elements, the nodal strain is an average of the four elemental strains. By using the elemental strains, the errors due to the strain averaging are avoided. Moreover, the optimum gage orientation angle is measured with respect to the element coordinate system located at the centroid of the element. This implies that the gage orientation angle is determined uniquely if the elemental strain information is used; whereas for the nodal strain case, since the four adjacent elements can have their local coordinate system in four different orientations, the determination of the gage orientation angle becomes much more complicated. For these two reasons, it is recommended that elemental strain information be used for all the calculations. Further, the centroids of the shell elements are considered as the locations for mounting the strain gages.

Next, unit loads are applied to the finite element model, one at a time, at the locations corresponding to the unknown loads to be recovered. For each applied unit load, strain tensors are obtained at all the elements suitable for mounting strain gages. Since the strain gage sensitivity varies as the gage orientation angle changes, the

computed strain tensors need to be transformed to determine strain values for a number of different gage orientations. The strain tensors can be transformed from the xyz coordinate system to any $x'y'z'$ coordinate system as (Budynas, 1999):

$$[\varepsilon]_{x'y'z'} = [T][\varepsilon]_{xyz}[T]^T \tag{4.4}$$

where $[T]$ denotes the transformation matrix that contains the direction cosines for the $x'y'z'$ system with respect to the xyz system. For the shell elements used herein, the element coordinate system is oriented such that the element z-axis is always normal to the plane of the element. Therefore, the strain transformations involve rotation about the z-axis with the transformation matrix given as:

$$[T] = \begin{bmatrix} \cos\theta & \sin\theta & 0 \\ -\sin\theta & \cos\theta & 0 \\ 0 & 0 & 1 \end{bmatrix} \tag{4.5}$$

By allowing θ to vary from 0 to 170 degree in a pre-selected increment, say 10 degree, the strain tensors for all the relevant elements at the intermediate gage locations are obtained for each applied unit load. It is to be noted that since a strain gage is mostly sensitive in its axial direction, the candidate set consists of all the x'-direction strain components, i.e., the first element of all the transformed strain tensors.

4.1.2 Determination of Number of Strain Gages

As more strain gages are used, the additional information on the strains helps to obtain a more precise estimate of the applied loads, but practical and financial constraints place limitations on the number of strain gages to be used. If the number of forces to be estimated is n_f, then the number of strain gages g must satisfy the criterion $g \geq n_f$. If ε_{ei} denotes the experimentally measured strain from gage i and ε_{pi} denotes the predicted

strain for gage i (using Eqn. (4.1)), then the estimation error for gage i is given by $e_i = \varepsilon_{ei} - \varepsilon_{pi}$ and for an overconstrained system of linear equations with $g - n_f$ degrees of freedom, the variance in strain measurement errors is given by (Chatterjee and Hadi, 1988):

$$\sigma^2 = \frac{\sum_{i=1}^{g} e_i^2}{g - n_f} \tag{4.6}$$

Given the maximum allowable variance in strain measurement errors that is acceptable, the number of required strain gages can be calculated using Eqn. (4.6).

4.1.3 Determination of the D-optimal Design

For a given number of strain gages g, the candidate set is searched to determine g gage locations and angular orientations that provide the least variance in the load estimates. If the candidate points to be included in matrix $[A]$ such that the sensitivity of $[A]$ is minimized are determined by trial and error, the set so obtained may not be the optimum set and would lead to a higher variability in the estimated loads. Also, it would be too time consuming to take into account all the possible combinations of gage placements to arrive at the set that would produce the best estimates of the forces.

A variety of criteria have been studied in the statistical literature (Kammer, 1991; Atkinson and Donev, 1992) to minimize the sensitivity of $[A]$. The criterion of most relevance to the current application involves the maximization of $|[A]^T[A]|$, the determinant of $[A]^T[A]$. Design that maximizes $|[A]^T[A]|$ is called D-optimal design (Mitchell, 1974), where D denotes determinant. The D-optimality criterion is used to

select the best candidate points from the candidate set which will provide the most precise load estimates.

In order to construct a *g*-point D-optimal design, the *g* strain gage locations and angular orientations that maximize $|[A]^T[A]|$ must be selected from the candidate set. To select the *g*-point D-optimal design, algorithms based on the principles of optimal augmentation and reduction of an existing design can be implemented. With optimal augmentation, the candidate point with maximum prediction variance is added as a row to the matrix. Similarly, optimal reduction of the augmented design is achieved by eliminating the candidate point or row of the matrix having minimum prediction variance. This process of augmenting and deleting candidate points in an optimal fashion continues until no further improvement in the objective function can be made. Such procedures are called exchange algorithms; two such types of procedures are the sequential exchange algorithm (Galil and Keifer, 1980) and the k-exchange algorithm (Johnson and Nachtsheim, 1983).

The basic idea behind the sequential exchange algorithm is as follows. Given the candidate set, the number of strain gages *g* and the number of applied loads n_f, the first step is to randomly select *g* distinct candidate points from the candidate set to initialize the $(g \times n_f)$ matrix $[A]$. Out of the remaining candidate set, a candidate point is then selected and the corresponding row is augmented to the matrix $[A]$ to form matrix $[A]_+$ such that $|[A]_+^T[A]_+|$ is maximum. Next, out of the *g+1* rows in matrix $[A]_+$, a row is deleted to arrive at matrix $[A]_-$ such that $|[A]_-^T[A]_-|$ is maximum. This process of augmenting and deleting rows continues until there is no further improvement in the value of $|[A]^T[A]|$. The final $[A]$ so obtained is the D-optimal design and provides the

information on the optimum strain gage locations and angular orientations. A flowchart depicting this algorithm is shown in Fig. 4.1.

As the candidate set gets bigger and bigger, increasingly large number of determinants and matrix inverses need to be calculated. A very naïve way to compute the determinant is to obtain $M = [A]^T[A]$ and then calculate the determinant $|M|$. This approach of determinant calculation is computationally very expensive. An alternate formula for computing the determinant $|M_+| = |[A]^T_+[A]_+|$ from that of $|M|$ when a row y^T is augmented to the matrix $[A]$ is:

$$|M_+| = |M|(1[+]y^T M^{-1}y) \tag{4.7}$$

where $[+]$ denotes addition and is replaced by subtraction in the case of deleting a row y^T from $[A]_+$. In order to be able to use Eqn. (4.7), M^{-1} can be maintained and updated as the row y^T is augmented to the matrix $[A]$ by:

$$|M_+|^{-1} = |M|^{-1}[-]\frac{(M^{-1}y)(M^{-1}y)^T}{(1[+]y^T M^{-1}y)} \tag{4.8}$$

where $[-]$ denotes subtraction and is replaced by addition in the case of deleting a row y^T from $[A]_+$.

Once the optimum strain gage locations and angular orientations are determined, strain gages are mounted at those locations and angular orientations on the structure before the application of the unknown loads. The strains $\{\varepsilon\}$ thus measured, together with the optimum $[A]$ computed, are then used to estimate the unknown forces $\{f\}$ in accordance with Eqn. (4.2).

4.1.4 Example: Plate with a Hole

A numerical example, the classical problem of a plate with a hole, is chosen to illustrate how the static load estimation method is applied in practice. The problem is to estimate two uniform pressure loads acting simultaneously on two orthogonal faces of a rectangular flat plate with a hole at its center. The plate model along with the locations and directions of the applied loads is shown in Fig. 4.2. The plate is of uniform thickness and composed of isotropic material.

Taking advantage of the problem symmetry, a finite element model of a quarter of the plate was developed in ANSYS and meshed with SOLID45 element type which has 3 degrees of freedom per node. Considering the top face of the plate as the region of potential strain gage placements, it was meshed with SHELL41 element type to facilitate evaluation of the surface strains. SHELL41 was selected as it offers 3 degrees of freedom per node and therefore has better compatibility with SOLID45 as compared to any other shell element type. The shell elements were given near zero values for the modulus of elasticity and the thickness so that they do not change the elastic characteristics of the problem. The left face of the plate was constrained in the x-direction and the lower face of the plate was constrained in the y-direction. Next, loads of unit magnitudes were applied to the right face in the x-direction and the upper face in the y-direction, one at a time. The mesh, boundary conditions and the two load cases are shown in Fig. 4.3. Strain tensors were obtained at the centroid of each shell element in the element coordinate system for each load case.

All further processing of the strain data and calculations were performed in MATLAB. To generate the candidate set, the strain tensors were transformed using Eqn.

(4.4) at each shell element centroid for angular orientations ranging from 0 to 170 degree in 10 degree increments. Since the number of loads to be estimated was 2, the number of strain gages to be used must be ≥ 2; for illustration purposes, a total of 4 gages were used. The D-optimality criterion, as discussed in Sec. 4.1.3, was used to find the optimum gage locations and angular orientations for the given number of strain gages. The optimum gage locations and angular orientations are listed in Table 4.1. The shell element numbers in the region of the optimum gage locations are shown in Fig. 4.4 and the elements corresponding to the optimum gage locations are depicted in Fig. 4.5. It is to be noted that the optimum angular orientations of the strain gages are with respect to the x-axes of the element coordinate systems. The element coordinate systems for the shell elements in the region of interest are depicted in Fig. 4.6.

Next, loads with arbitrary values of 257 and 364 were simultaneously applied to the finite element model and strains were calculated corresponding to the optimum strain gage locations and angular orientations listed in Table 4.1. Input loads were then estimated using Eqn. 4.2; the recovered loads were found equal to the applied loads.

4.2 Quasi-Static Load Estimation

The recovery of static loads leads to a way where quasi-static loads acting on a structure can be estimated. Quasi-static loading refers to time varying loading which is slow enough such that the inertial effects are negligible, i.e., response to the loads applied at a certain instant of time is independent of the loading history at all the earlier instants of time. Although time is associated with quasi-static analysis, it is a process of conducting an independent static analysis at each instant of time. The steps involved in

estimating the quasi-static loads are parallel to that of the estimation of static loads and are explained with the help of a numerical example of a bent cantilever beam.

4.2.1 Example: Bent Cantilevered Beam

The problem at hand is to recover three mutually perpendicular quasi-static loads acting at a point on a bent cantilevered beam. The beam model along with the applied load directions is shown in Fig. 4.7. A finite element model of the beam was developed in ANSYS using SOLID45 element type to mesh it. Considering the top and the bottom face of the beam as the regions of potential strain gage location sites, they were meshed with SHELL41 element type (for reasons mentioned in Sec. 4.1.4) so that the surface strain information can be obtained. The shell elements were given near zero values for the modulus of elasticity and the thickness so that they do not change the elastic characteristics of the model. The left end of the beam was fixed in all degrees of freedom. Next, three unit loads, each of magnitude 1, were applied to a corner node in the x, y and z-directions, one at a time. Figure 4.8 shows the mesh, boundary conditions and the three load cases. Strain tensors were obtained at the centroid of each shell element in the element coordinate system for each load case.

The candidate set was generated as discussed in Sec. 4.1.1 using the obtained strain tensors, in line with the procedure followed in Sec. 4.1.4. Since the number of loads to be estimated was 3, the number of strain gages to be used was chosen to be 4. The candidate set was subjected to the optimization algorithm presented in Sec. 4.1.3 to arrive at the D-optimal design that provides the information on the optimum strain gage locations and angular orientations on the structure. The optimum gage locations and

angular orientations with respect to the x-axes of the shell element coordinate systems are listed in Table 4.2. The shell elements corresponding to the optimum gage locations and their coordinate systems are depicted in Fig. 4.9.

Next, three time varying loads were simultaneously applied to the beam model. The time history of the loads is shown in Fig. 4.10 and their description is as follows:

- Sine wave of amplitude 5 and frequency 0.04 Hz in the x-direction.

- Random wave in the range [-10, 10] in the y-direction.

- Square wave of amplitude 5 and frequency 0.04 Hz in the z-direction.

At different instants of time, strains were calculated corresponding to the optimum strain gage locations and angular orientations listed in Table 4.2. Each time instant constitutes an independent static analysis. Applied loads were then recovered as a function of time by processing the strain tensors generated at different instants of time using Eqn. (4.2). The applied and recovered loads are plotted in Figs. 4.11 to 4.13 and the 95% confidence bounds on the load estimates (Neter *et al*., 1990) are plotted in Figs. 4.14 to 4.16. It can be concluded from the plots that there was accurate recovery of the applied quasi-static loads.

Table 4.1 Optimum Gage Locations and Angular Orientations

Element Number	Angular Orientation (degree)
688	90
689	90
937	0
947	0

Table 4.2 Optimum Gage Locations and Angular Orientations

Element Number	Angular Orientation (Degree)
335	0
451	0
837	80
901	20
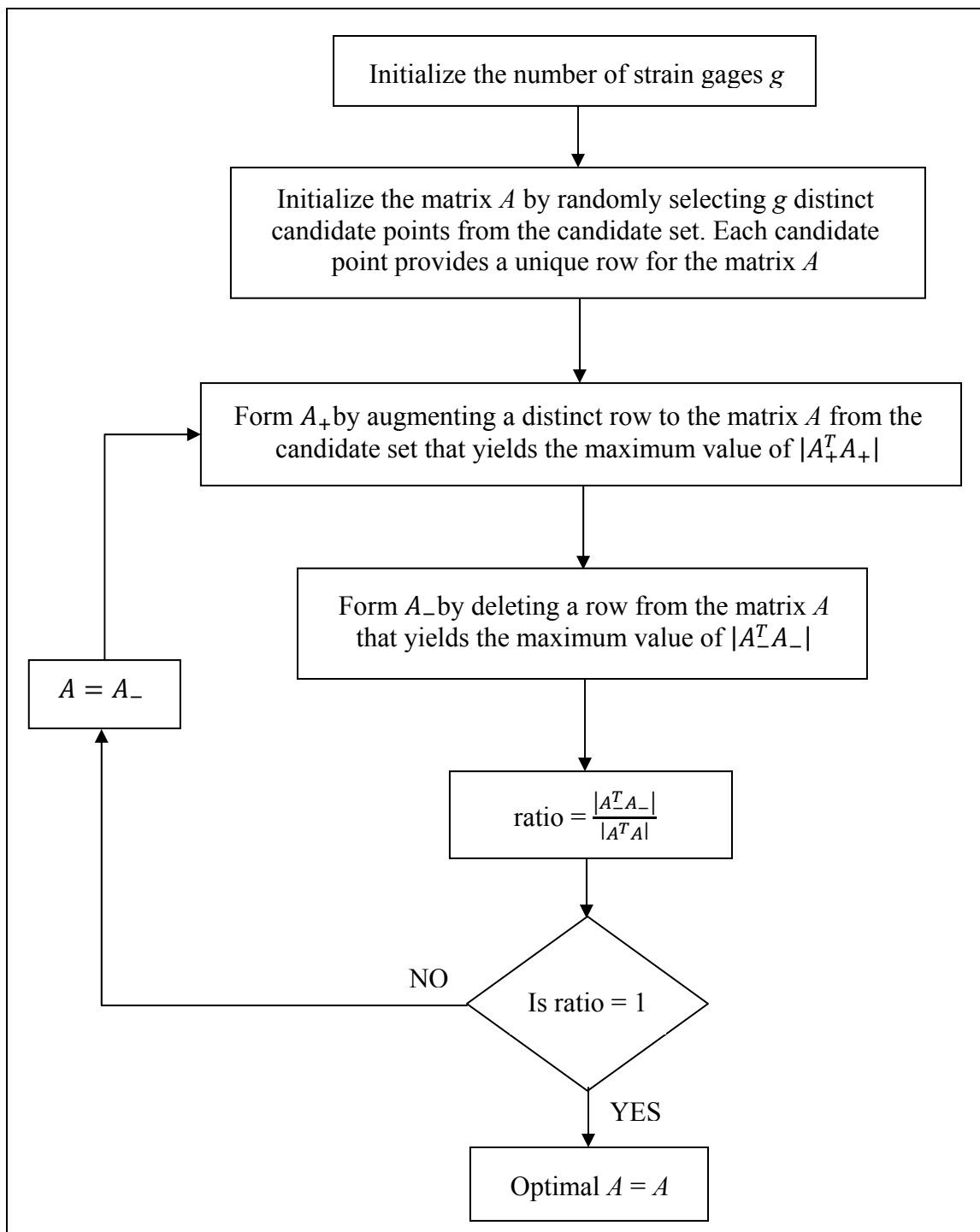
Figure 4.1 Flowchart of the Sequential Exchange Algorithm
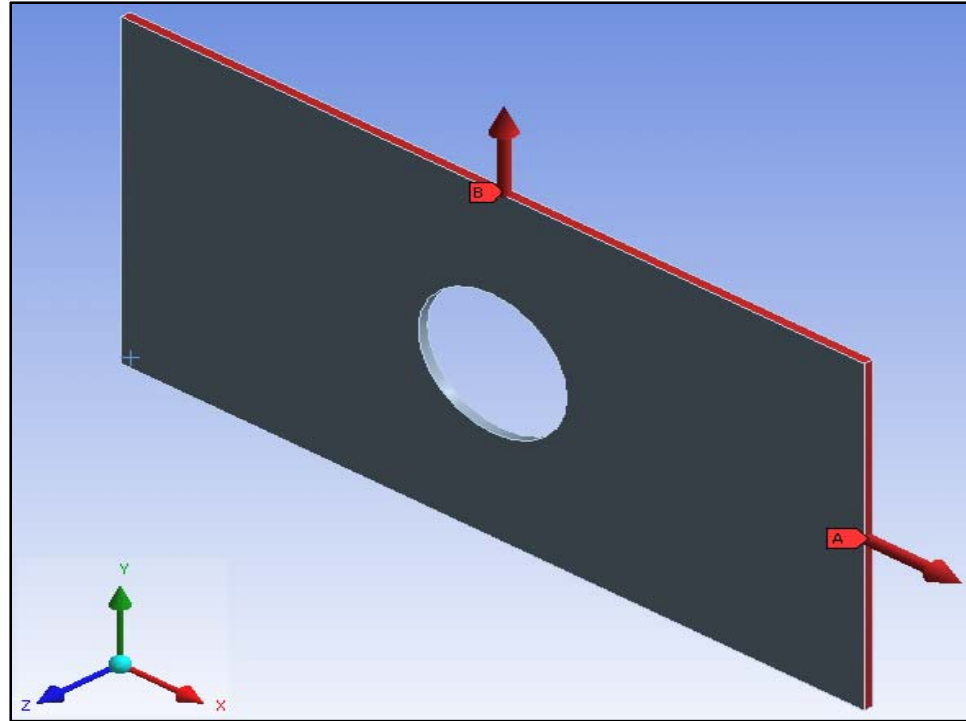
Figure 4.2 Plate Model with Applied Loads
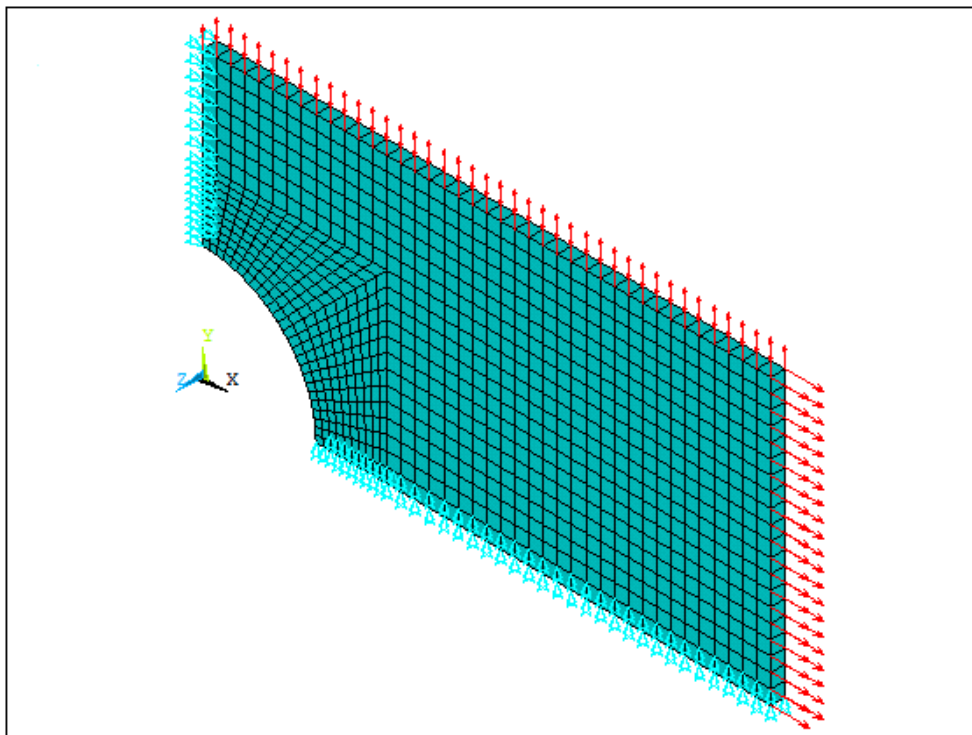
Figure 4.3 Finite Element Model of Plate
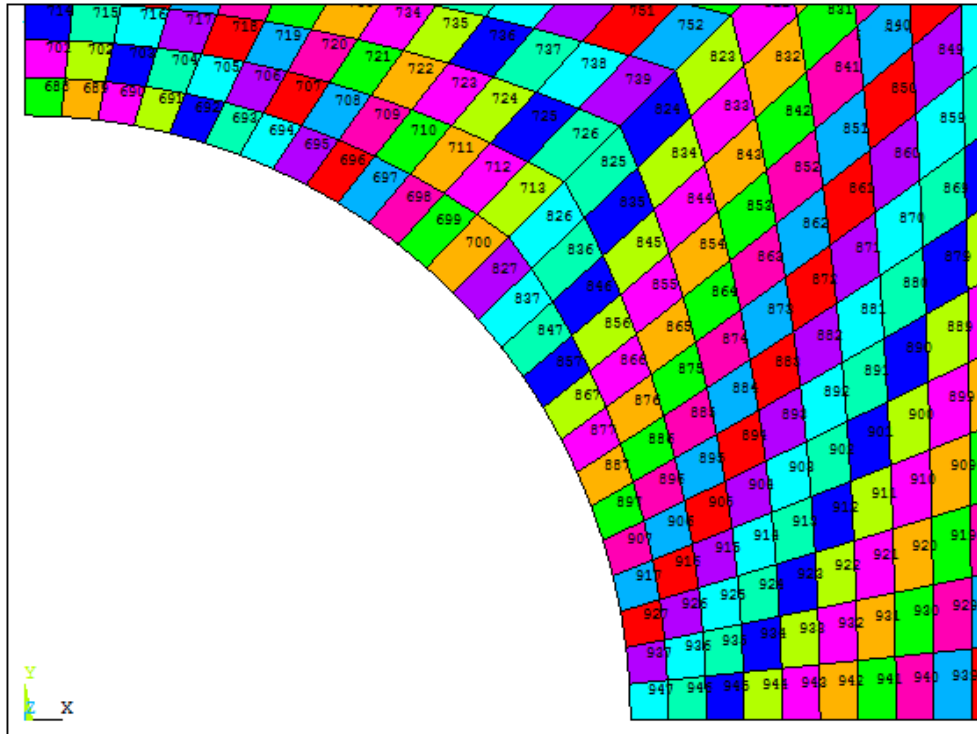
Figure 4.4 Numbered Shell Elements
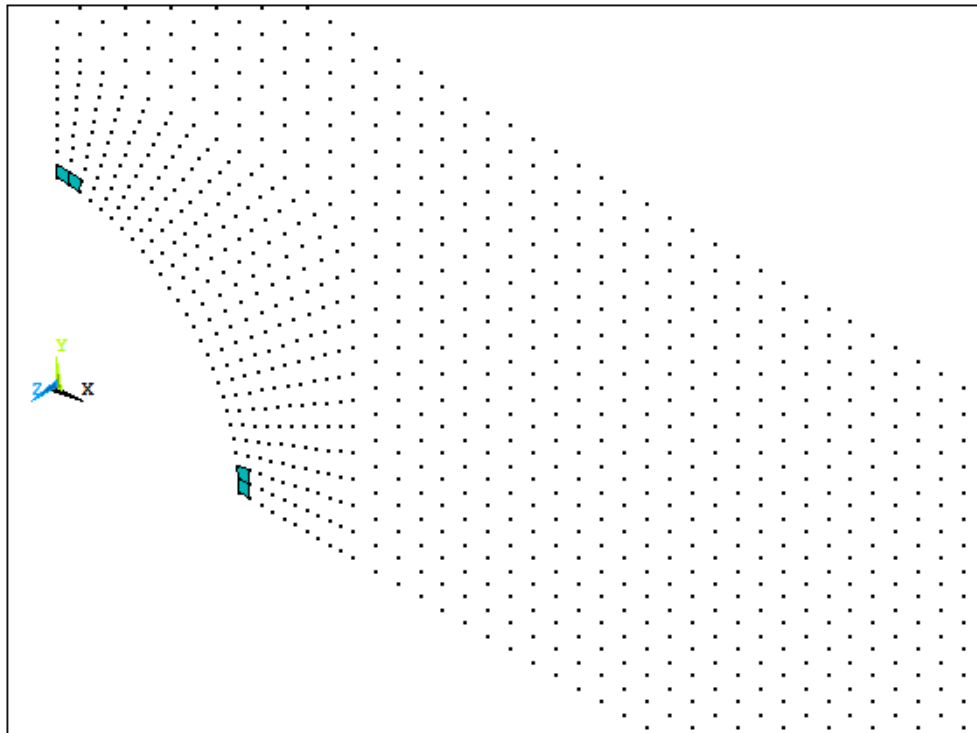
Figure 4.5 Shell Elements Corresponding to Optimum Gage Locations
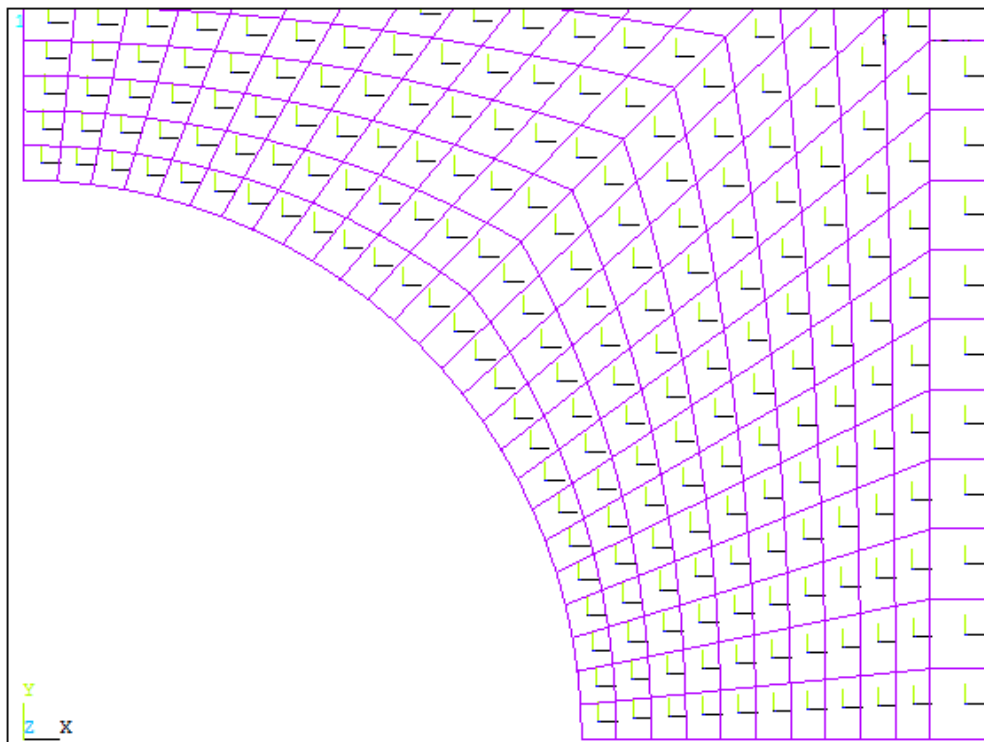
Figure 4.6 Shell Element Coordinate Systems
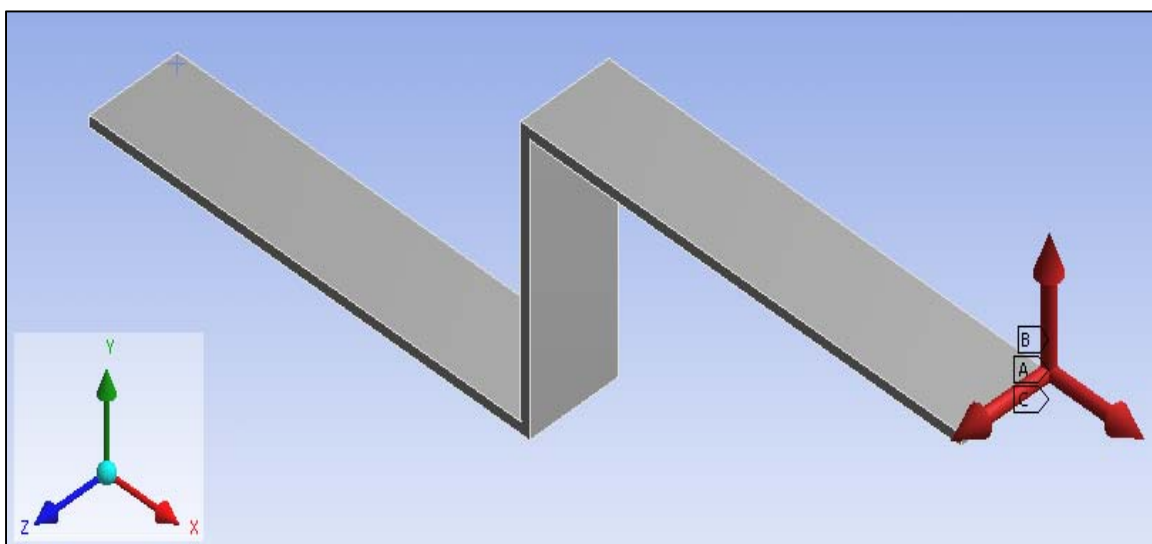
Figure 4.7 Bent Cantilever Beam with Applied Loads
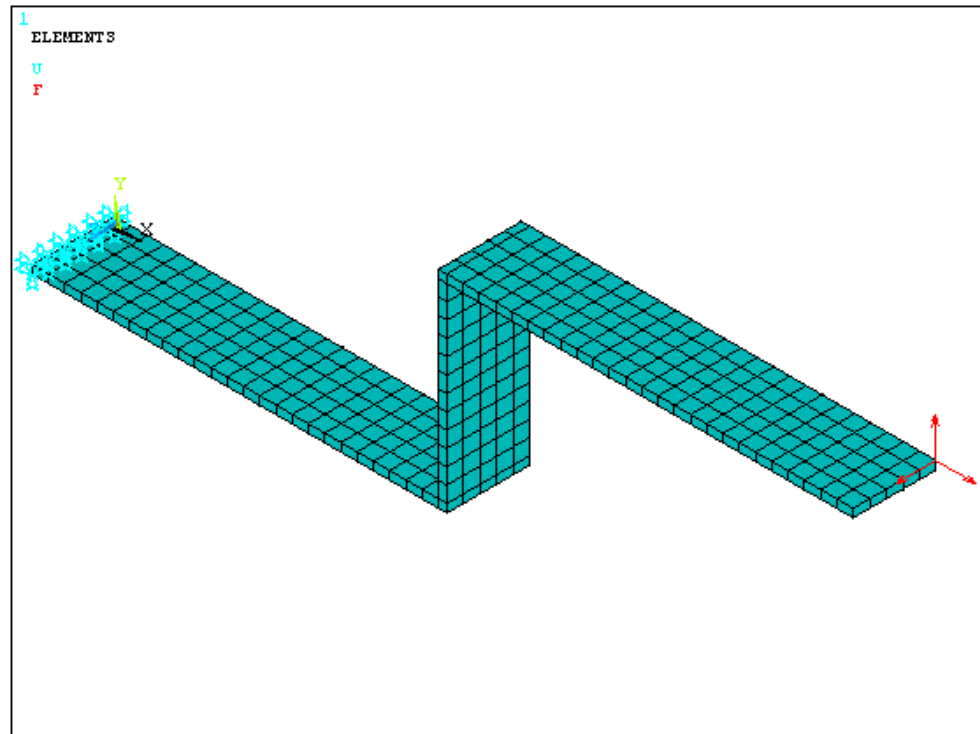
Figure 4.8 Finite Element Model of Bent Beam
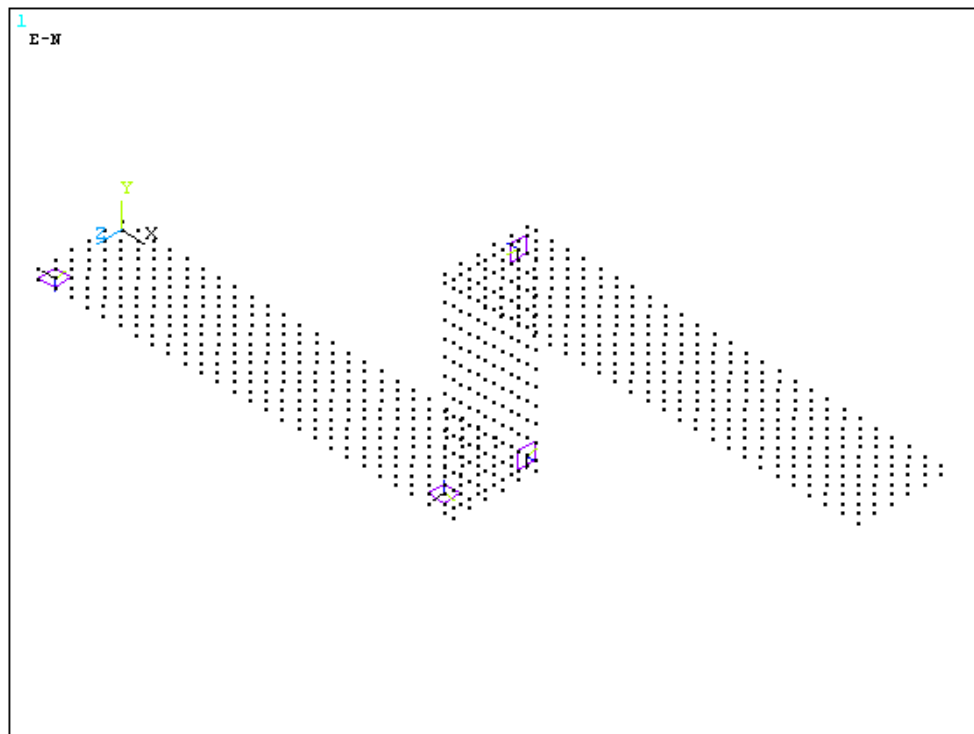
Figure 4.9 Shell Elements Corresponding to Optimum Gage Locations
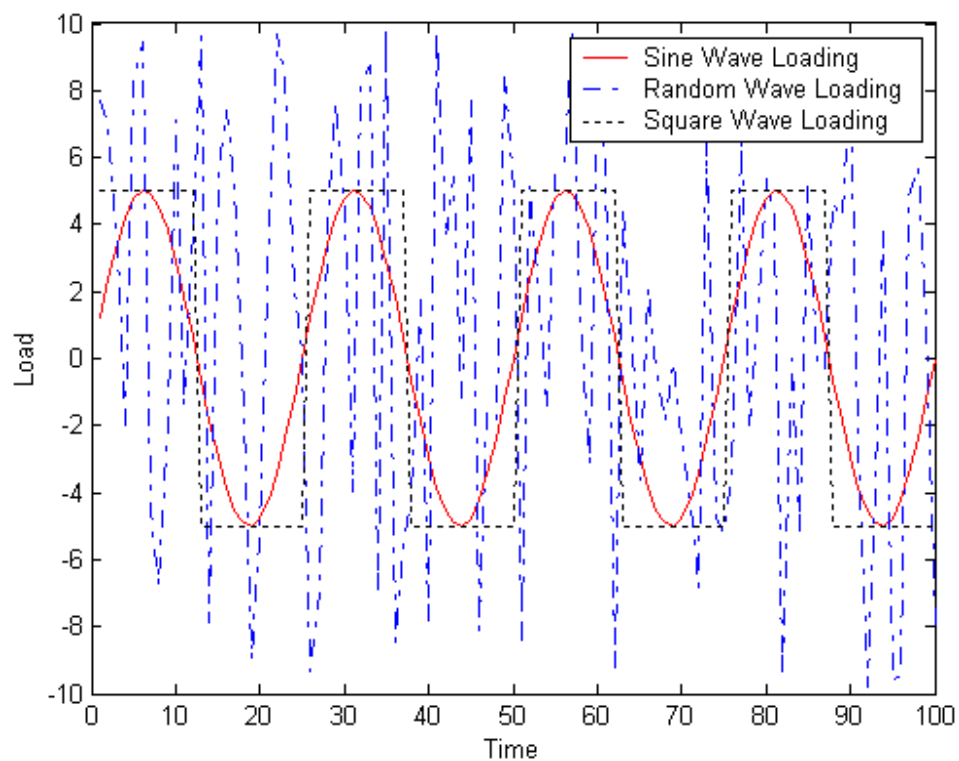
Figure 4.10 Time History of Applied Loads
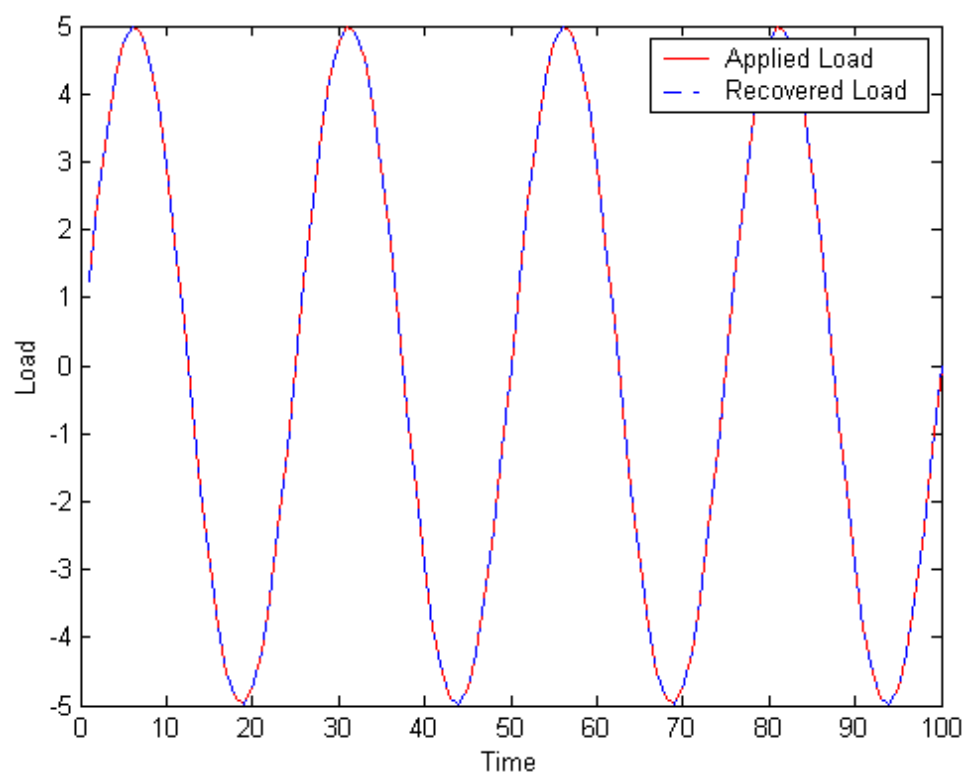
Figure 4.11 Recovery of Sine Wave Loading
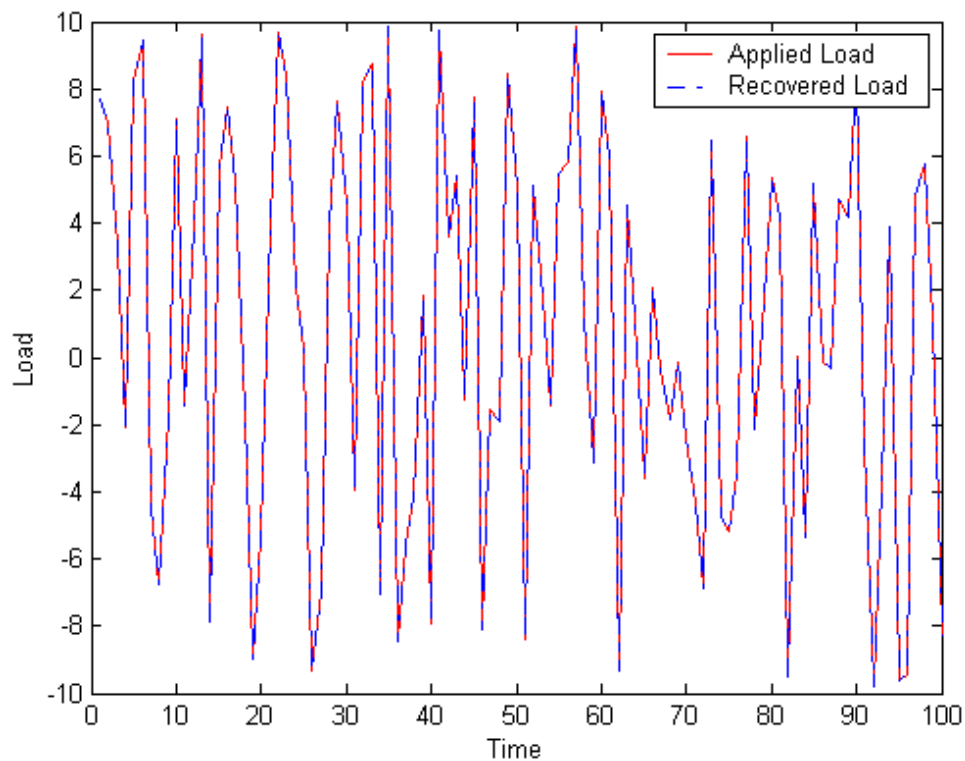
Figure 4.12 Recovery of Random Wave Loading
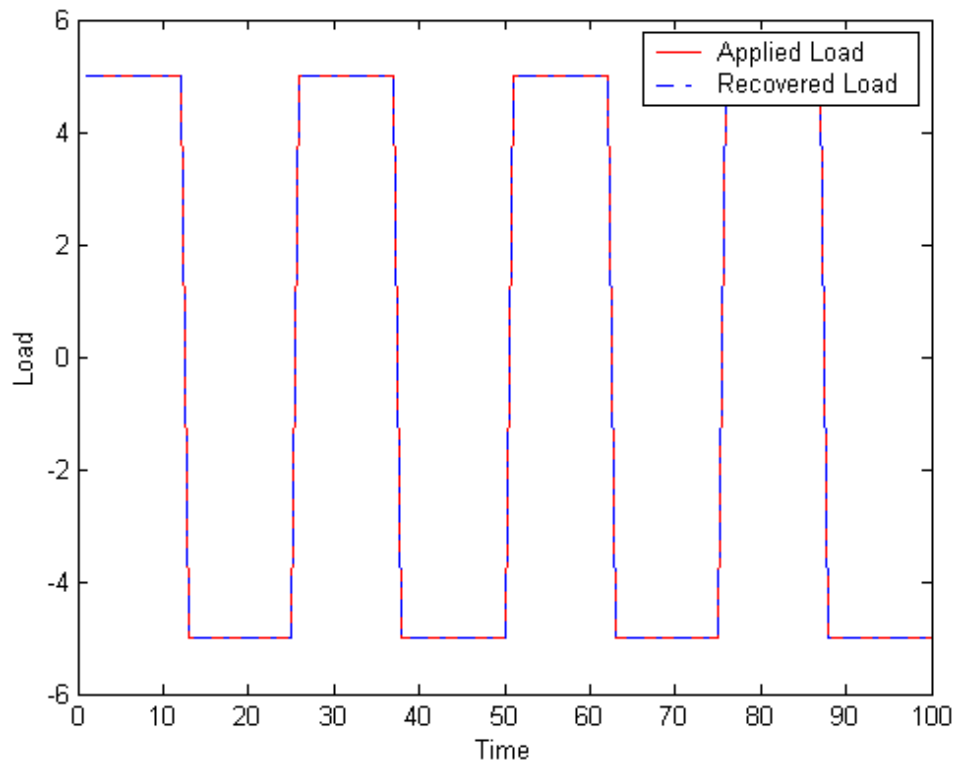
Figure 4.13 Recovery of Square Wave Loading
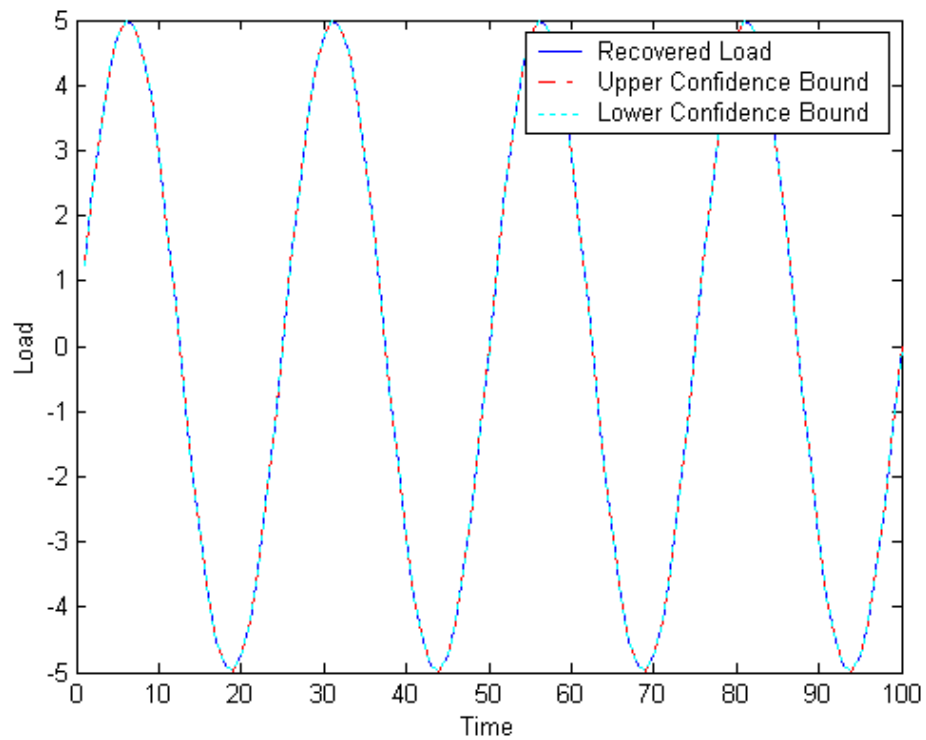
Figure 4.14 95% Confidence Bounds on Recovered Sine Wave Load
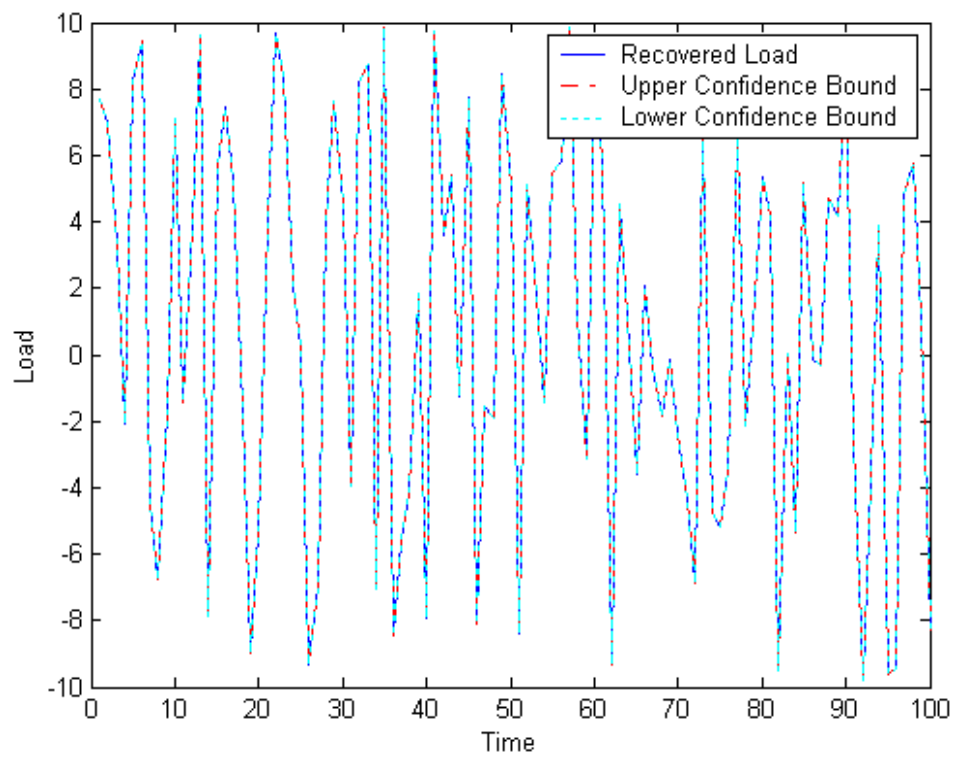
Figure 4.15 95% Confidence Bounds on Recovered Random Wave Load
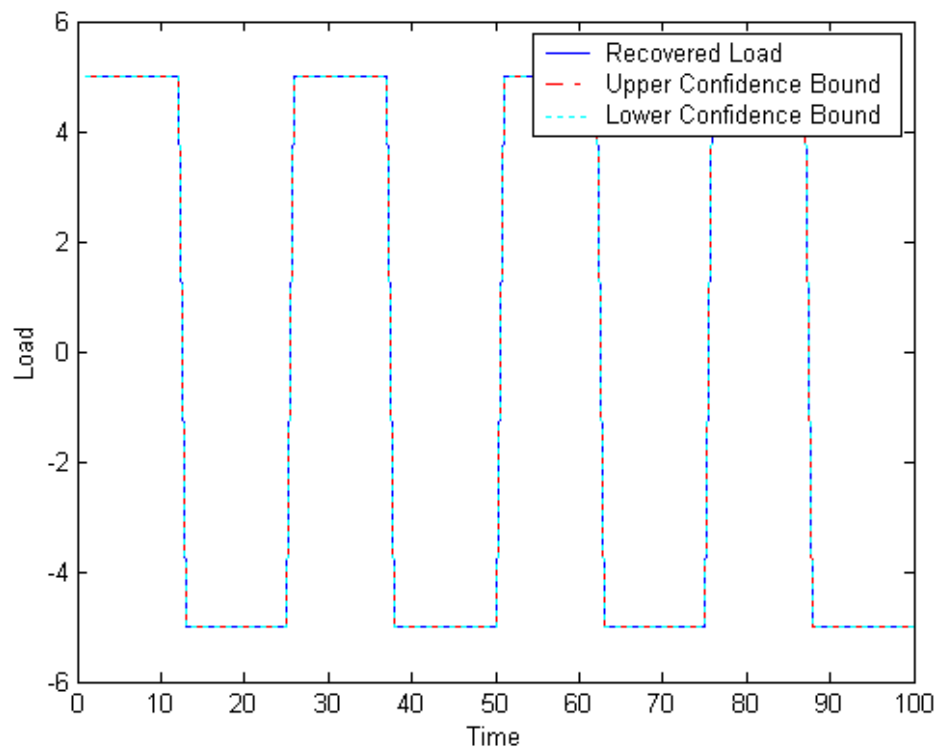
Figure 4.16 95% Confidence Bounds on Recovered Square Wave Load

Chapter 5 - Dynamic Load Identification from Strain Measurements

This chapter presents a time domain technique for estimating dynamic loads acting on a structure from strain time response measured at a finite number of optimally placed strain gages on the structure. The technique utilizes model reduction to obtain precise load estimates. The structure essentially acts as its own load transducer. The approach is based on the fact that the strain response of an elastic vibrating system can be expressed as a linear superposition of its strain modes. Since the strain modes as well as the normal displacement modes are intrinsic dynamic characteristics of a system, the dynamic loads exciting a structure are estimated by measuring induced strain fields.

As already discussed in the previous chapter, the accuracy of estimated loads is dependent on the number and placement of gages on the instrumented structure. It will be further shown in this chapter that the accuracy of the estimated loads also depends on the number of retained strain modes obtained from strain modal analysis. A solution procedure based on the construction of a D-optimal design is implemented to determine the optimum locations and orientations of strain gages that will provide the most precise load estimates. The concepts of D-optimal design algorithm and candidate set have already been presented in the previous chapter with the help of static load estimation. A novel approach is proposed in this chapter which makes use of model reduction technique, resulting in significant improvement in accuracy in the dynamic load estimation. Validation of the proposed approach through experimental as well as

numerical example problems is also presented which reveals the effectiveness and robustness of the technique, even in the presence of errors (noise) in strain measurements.

5.1 Modal Analysis and Strain Modes

Consider the spatially discretized linear second-order ordinary differential equation (ODE) of an n degrees of freedom (DOFs) structural system in the matrix form given by Eqn. (3.1). For simple systems, $[M]$, $[C]$ and $[K]$ may be obtained by writing the system equations of motion; for complex systems, they can be generated from the finite element model of the structure. With the availability of system response $\{x(t)\}$ to dynamic loads $\{f(t)\}$, which as shown later will be constructed using modal analysis and strain measurements, $\{\dot{x}(t)\}$ and $\{\ddot{x}(t)\}$ can be obtained upon successive numerical differentiation of $\{x(t)\}$. Given all the terms on the left-hand-side in Eqn. (3.1), the dynamic loads $\{f(t)\}$ acting on the structure can be estimated.

For structural continuum, the displacements $\{x(t)\}$ at any point in a deformed structure are related to the strains $\{\varepsilon(t)\}$ by a linear differential operator D (Bernasconi and Ewins, 1989) as:

$$\{\varepsilon(t)\} = D\{x(t)\} \tag{5.1}$$

which leads to:

$$\{\varepsilon(t)\} = [\psi^{\varepsilon}]\{q(t)\} \tag{5.2}$$

where $[\psi^{\varepsilon}]$ denotes the modal strain matrix containing the strain modes. Equation (5.2) simply states that at any particular time, the strain response at any point on the structure can be expressed as a linear combination of the modal strains. It applies to linear elastic problems and assumes that the deformations are small enough such that the principle of

superposition holds. The modal strains are an intrinsic property of a structure's dynamic behavior, as are the displacement mode shapes. While both strain and displacement modes are intrinsic dynamic characteristics of a structure and correspond to each other, it has been noted by Yam *et al.* (1996) that for sensitivity reasons, strain modal analysis is more useful in dynamic design of structures with features such as holes, grooves and cracks.

Since, in real world applications, seldom is the case when all the modes in $[\psi^\varepsilon]$ are available, one generally has a reduced number of modes m available either from experimental modal strain analysis or finite element modal strain analysis, leading to truncated $[\tilde{\psi}^\varepsilon]$ retaining only m modes. Equation (5.2) then gets approximated as:

$$\{\varepsilon(t)\} = [\tilde{\psi}^\varepsilon]\{\tilde{q}(t)\} \tag{5.3}$$

where $\{\tilde{q}(t)\}$ is the mode participation factor for the retained modes. As will be made clear in due course of this chapter, it is desired to determine $\{\tilde{q}(t)\}$ at this point. Assuming that $[\tilde{\psi}^\varepsilon]$ is known and $\{\varepsilon(t)\}$ is measured, the least-squares estimate of $\{\tilde{q}(t)\}$ is given by:

$$\{\tilde{q}(t)\} = \left([\tilde{\psi}^\varepsilon]^T[\tilde{\psi}^\varepsilon]\right)^{-1}[\tilde{\psi}^\varepsilon]^T\{\varepsilon(t)\} \tag{5.4}$$

While the above development is presented for a discretized system, it is equally applicable to continuous systems spatially discretized using a finite element based approach. There are a number of problems associated with estimating $\{\tilde{q}(t)\}$, to name a few:

- Each element in the vector $\{\varepsilon(t)\}$ corresponds to strain measured at a unique location out of the infinitely many possible locations on the structure. It is not

feasible to place strain gages at all the possible locations on the structure to obtain

$\{\varepsilon(t)\}$ in full.

- Some means needs to be devised that allows for estimating $\{\tilde{q}(t)\}$ by taking strain

  measurements at few finite number of locations on the structure.

- Since the input force locations may not be available to mount the strain gages, the

  measurements cannot be taken at or around these locations.

- Since there can be a large number of locations on the structure where the gages

  can potentially be mounted, a natural question arises: if a finite number of gages

  is to be used, where all should they be located on the structure such that precise

  load estimates are obtained.

The following sections outline procedures that deal with the above mentioned problems.

5.2 Candidate Set

First of all, the number of strain gages g to be used is identified based upon the

methodology discussed in Sec. 4.1.2., i.e. $g \geq m$. Next, as described in Sec. 4.1.1, the

candidate set is generated analytically by utilizing the finite element model of the

structure. In this respect, a finite element model of the structure is developed following

the recommendations reported in Sec. 4.1.1 and a modal analysis of the model is

performed. The maximum number of modes obtainable from a finite element model is

equal to the total number of degrees of freedom of the model, which can be a large

number. Decision needs to be made on the number of modes to be retained to

approximate the response of the structure; these are the modes whose MPF will be

estimated at a later stage from the structure response to applied loads. The fraction of

effective modal mass captured by the retained modes can be used to decide upon the number of modes to be retained in the analysis. It has been observed through experience that sufficient number of modes must be retained in the analysis such that the Mass Participation Factor captured by the retained modes is at least 90%. The modal matrix $[\phi]$ for the retained modes and $[M]$, $[C]$, $[K]$ matrices are obtained from the finite element model.

Each retained normal mode is then applied to the finite element model as a displacement load case, one at a time. Each normal mode yields the corresponding strain mode of the structure in accordance with Eqn. (5.3). Let the number of shell elements suitable for mounting strain gages be c; strain tensors are obtained at all the elements suitable for mounting strain gages for each load case. Since the strain gage sensitivity varies as the gage orientation angle changes, the computed strain tensors are transformed to determine strain values for a number of different gage orientations per Eqns. (4.4) and (4.5). The transformed strain tensors provide the candidate set $\left[\tilde{\psi}^{\varepsilon}\right]_{cs}$. It is to be noted that $\left[\tilde{\psi}^{\varepsilon}\right]_{cs}$ is a subset of $\left[\tilde{\psi}^{\varepsilon}\right]$.

5.3 D-optimal Design

Since it is not possible to measure strains at all the possible locations on a structure, to obtain an approximate solution to Eqn. (5.4), a subset of the candidate set $\left[\tilde{\psi}^{\varepsilon}\right]_{cs}$ needs to be identified. In terms of a randomly selected subset $\left[\tilde{\tilde{\psi}}^{\varepsilon}\right]$, the approximate solution to Eqn. (5.4) can be written as:

$$\{\tilde{q}(t)\} \cong \{\tilde{\tilde{q}}(t)\} = \left(\left[\tilde{\tilde{\psi}}^{\varepsilon}\right]^{T}\left[\tilde{\tilde{\psi}}^{\varepsilon}\right]\right)^{-1}\left[\tilde{\tilde{\psi}}^{\varepsilon}\right]^{T}\{\tilde{\varepsilon}(t)\} \tag{5.5}$$

where $\{\tilde{\tilde{q}}(t)\}$ is an approximation to $\{\tilde{q}(t)\}$ and $\{\tilde{\varepsilon}(t)\}$ is strain vector at randomly chosen locations on the structure. Compare Eqn. (5.5) to Eqn. (4.2); it is important to realize here that $\left[\tilde{\tilde{\psi}}^{\varepsilon}\right]$ plays the same role in dynamic load recovery as $[A]$ in static load recovery. As stated previously, $\{\tilde{\varepsilon}(t)\}$ is prone to measurement errors and the inverse problem identified by Eqn. (5.5) tends to be ill-conditioned. The precision with which $\{\tilde{\tilde{q}}(t)\}$ is estimated from measured strain response depends on the number, locations and angular orientations of strain gages on the structure. $\left[\tilde{\tilde{\psi}}^{\varepsilon}\right]$ needs to be such a subset of $\left[\tilde{\psi}^{\varepsilon}\right]_{cs}$ that provides the most precise estimates of $\{\tilde{\tilde{q}}(t)\}$. For a given number of strain gages g, following the D-optimal design algorithm described at length in Sec. 4.1.3, the candidate set $\left[\tilde{\psi}^{\varepsilon}\right]_{cs}$ is searched to determine its optimum subset $[\psi^{\varepsilon}]_{opt}$.

Once $[\psi^{\varepsilon}]_{opt}$ and, in turn, optimum strain gage locations and angular orientations are determined, strain gages are mounted at the identified locations and angular orientations and time varying strain $\{\varepsilon(t)\}_{opt}$ is measured. $\{\tilde{\tilde{q}}(t)\}$, which is an approximation to $\{\tilde{q}(t)\}$, is then estimated using the deterministic form of Eqn. (5.5) as:

$$\{\tilde{q}(t)\} \cong \{\tilde{\tilde{q}}(t)\} = \left([\psi^{\varepsilon}]_{opt}^{T}[\psi^{\varepsilon}]_{opt}\right)^{-1}[\psi^{\varepsilon}]_{opt}^{T}\{\varepsilon(t)\}_{opt} \tag{5.6}$$

Next, $\{x(t)\}$ is generated using Eqn. (3.6), which can then be successively numerically differentiated to yield $\{\dot{x}(t)\}$ and $\{\ddot{x}(t)\}$. The applied load $\{f(t)\}$ can now be computed using Eqn. (3.1). Presented next are few experimental as well as numerical examples demonstrating the proposed approach.

5.4 Example – Cantilevered Beam (Experimental)

A 12 in long, 2 in wide and 1/8 in thick cantilevered aluminum beam was modeled in I-DEAS® and the first five normal modes were retained for analysis. Of the first five retained normal modes, the third mode is a twist mode whereas the other four modes induce lateral vibrations in the beam. A total of 8 gages (arbitrarily selected number > 4) were mounted on the beam and the optimum gage locations and orientations are shown in Fig. 5.1. The beam was clamped at the base and attached to a shaker head (see Fig. 5.2).

Two input base excitations, namely a 28 Hz sine dwell and a 171 Hz sine dwell were input into the shaker head and the fixture to excite the structure. The strains at each drive input were measured and analyzed to arrive at the MPF $\{\tilde{q}(t)\}$. Since the 28 Hz excitation is very close to the fundamental frequency of the beam (28.178 Hz), mode 1 dominates the overall response and overshadows all other modes by close to two orders of magnitude. This is borne out by the results given in Fig. 5.3 and Table 5.1. Fig. 5.3 gives the MPF for the input 28 Hz loading for all normal modes whereas Fig. 5.4 illustrates the recovered participation factors for all modes. The scale of MPF for mode 1 in Fig. 5.4 is one order of magnitude higher than those for modes 2 through 5. The numerical values in Table 5.1 are taken at an instant of time, and give a snapshot of various MPF at the chosen time. It can be seen from the results in Table 5.1 that mode 1 dominates all other modes, and its participation percentage is recovered within 5% of the theoretical value. It may be noted that since mode shapes are known up to a constant, the MPF from finite element analysis and from proposed load recovery procedure cannot be compared directly on a one-to-one basis. To resolve this ambiguity regarding the mode

shapes and MPF, the participation percentages are compared. It is seen from Table 5.1 that the participation percentages of all modes are in good agreement with the theoretical values.

An additional check on the recovery procedure as outlined herein includes correlating the measured and predicted strains in various gages mounted on the beam. Fig. 5.5 shows that the strain in gage 1 is reproduced within 0.56% error whereas for gage 3, the strain error is of the order of 5-10 micro-strains (Fig. 5.6). The error for gage 3 was within the experiment's measurement limit of about 10 micro-strains.

Next, the beam is excited by a 171 Hz sine dwell which is not too far from the second frequency of 176.34 Hz. For this case, mode 2 dominates the overall response because the 171 Hz excitation is closer to the second frequency of the beam of 176.35 Hz. The mode participation factors $\{\tilde{q}(t)\}$ for all modes were computed and numerical values at a particular instant in time are given in Table 5.2. It was seen that MPF are recovered reasonably accurately. With $\{\tilde{q}(t)\}$ known, $\{x(t)\}$ can be computed using Eqn. (3.6), which can then be successively numerically differentiated to yield $\{\dot{x}(t)\}$ and $\{\ddot{x}(t)\}$. The applied load $\{f(t)\}$ can then be reconstructed using Eqn. (3.1).

The example illustrates the effectiveness of the proposed approach in recovering the mode participation factors due to applied loads that induce significant level of vibration in the structure.

5.5 Example – Cantilevered Beam (Numerical)

The dynamic load estimation method is also illustrated through numerical simulation on a cantilevered beam where a sinusoidal load acting at one end of the beam

needs to be estimated. Without loss of generality, the system is assumed to be undamped.

A finite element model of the beam was developed in ANSYS using SOLID45 elements.

Considering the top and the bottom surfaces of the beam as the regions of potential strain

gage locations, they were meshed using SHELL41 elements so that the surface strain

information is available at all candidate gage locations. The shell elements were given

near zero values for the modulus of elasticity, thickness and density so that the dynamic

characteristics of the model remain unchanged by the addition of the shell elements. The

left end of the beam was fixed in all degrees of freedom. The finite element model of the

beam along with the applied load and boundary conditions is shown in Fig. 5.7. The

beam model consisted of 160 shell elements and 200 unconstrained nodes with 3 degrees

of freedom per node, i.e., the total number of degrees of freedom of the model was 600.

A sinusoidal forcing function $f(t) = 8000\sin(30t)$ is applied at the free end of

the beam. The task is to determine the optimum strain gage locations and angular

orientations and reconstruct the input force based on the strain time response measured at

those locations. Table 5.3 summarizes the relevant problem input data.

A modal analysis was performed on the beam model and the response of the

structure was approximated by retaining 7 normal modes. The modes in the transverse

direction only were considered; they formed the modal matrix $[\phi]$. The $[M]$ and $[K]$

matrices were obtained using finite element method. ANSYS provides data for $[M]$ and

$[K]$ matrices in the Harwell-Boeing file format. A routine was written in MATLAB to

convert them into the matrix format suitable for current application. Each of the retained

modes was applied to the beam model as a displacement load case, one at a time, and

strain tensors were obtained at all the shell elements. All further processing of the strain

data and calculations were performed in MATLAB. The candidate set $[\tilde{\psi}^\varepsilon]_{cs}$ was generated from the surface strains. Since the number of retained normal modes m was 7, the number of strain gages g was arbitrarily selected to be 9. The D-optimality criterion was utilized to obtain $[\psi^\varepsilon]_{opt}$ and, in turn, the optimum gage locations and angular orientations for the given number of strain gages was determined. The shell elements corresponding to the optimum gage locations along with the element coordinate systems are shown in Fig. 5.8.

Next, an undamped transient analysis was performed on the finite element beam model with the applied load $f(t)$. Time dependent strains $\{\varepsilon(t)\}_{opt}$ were obtained at the optimum gage locations and transformed to give strain values along optimum angular orientations. To simulate the real world scenario where strains are measured experimentally, each element in $\{\varepsilon(t)\}_{opt}$ was corrupted with normally distributed random errors with zero mean and standard deviation of 10% of its value. $\{\tilde{q}(t)\}$ for all the 7 retained modes was estimated by solving Eqn. (5.6) at each instant of time. For comparison, the exact MPF for the retained modes were also obtained from the finite element analysis. Comparisons of the recovered MPF for the first, second and sixth retained modes with the corresponding exact MPF are shown in Figs. 5.9 to 5.11 respectively. Even though only three representative modes are shown in Figs. 5.9 to 5.11, it may be noted that the MPF for all 7 retained modes are recovered precisely. Next, $\{x(t)\}$ was generated using Eqn. (3.6), which was then numerically differentiated successively to yield $\{\dot{x}(t)\}$ and $\{\ddot{x}(t)\}$. Finally, the applied sinusoidal load $\{f(t)\}$ was reconstructed using Eqn. (3.1). The applied and the recovered loads are plotted in Fig. 5.12.

The above described approach, though seemingly promising, suffers from an inherent limitation. It can be inferred from the plots that even though the estimation of the MPF of the retained modes is relatively accurate, the estimation of the applied load is poor. This is due to the fact that only 7 out of the 600 possible modes were retained for the analysis which resulted in a large amount of truncation error. Moving from Eqn. (5.2) to Eqn. (5.3) results in truncation error which depends upon the number of modes retained. Acceptable load estimates may only be obtained by retaining a high number of modes in the analysis, which is rarely possible in real world problems. Figure 5.13 shows the load recovery plot with 15 retained modes (g = 17), which indicates sign of improvement in recovered load with increased number of retained modes; the recovered load is still far off from the applied load.

Theoretically, the best load estimate can be obtained by retaining all the possible modes in the analysis; this is governed by the number of strain gages used, which, in turn, is limited by the number of shell elements in the model. In reality, financial and practical constraints place limitations on the number of strain gages utilized and thereby, on the number of modes whose MPF can be estimated from the strain measurements. Following this, the quality of the load estimation gets severely affected owing to the truncation error. To overcome this limitation, a novel approach based on model order reduction is proposed. This approach, when applied to the load recovery procedure, results in significant improvement in the load estimates. The proposed approach is the subject of discussion in the next section.

5.6 Load Estimation Technique using Model Order Reduction

As described in Sec. 3.2, model order reduction methods, also referred to as condensation methods, aim at reducing the number of degrees of freedom in a model without changing its dynamic characteristics significantly. For the reasons mentioned in Sec. 3.2.3, fixed interface CMS, also known as Craig-Bampton model reduction, is chosen to be introduced here in the load identification algorithm so that precise load estimated are obtained.

Having computed $\{x(t)\}$ through Eqn. (3.6), and its derivatives as mentioned in the previous section, Eqns. (3.30) and (3.31) are used to obtain $\begin{Bmatrix} \{x(t)\}_b \\ \{q(t)\}_p \end{Bmatrix}$ and its derivatives. The applied loads can subsequently be estimated using Eqn. (3.1) re-written in reduced form as:

$$[M]_{CB} \begin{Bmatrix} \{\ddot{x}(t)\}_b \\ \{\ddot{q}(t)\}_p \end{Bmatrix} + [C]_{CB} \begin{Bmatrix} \{\dot{x}(t)\}_b \\ \{\dot{q}(t)\}_p \end{Bmatrix} + [K]_{CB} \begin{Bmatrix} \{x(t)\}_b \\ \{q(t)\}_p \end{Bmatrix} = \begin{Bmatrix} \{f(t)\}_b \\ \{f(t)\}_p \end{Bmatrix} \tag{5.7}$$

where the reduced stiffness matrix $[K]_{CB}$, reduced mass matrix $[M]_{CB}$ and reduced damping matrix $[C]_{CB}$ are given by Eqn. (3.32). It is to be noted that the DOFs corresponding to the load application locations must be a subset of the boundary DOFs.

The reason the above mentioned reduction based technique results in improvement of the load estimates can be understood as follows. In the case of full model, the final load identification step can be identified effectively as Eqn. (3.7) which uses few available modes and their participation factors to estimate the applied loads. This results in large degree of error in load estimates since significant amount of dynamic information is lost due to mode truncation. Next, consider the case of reduced model where the number of condensed DOFs is purposely made equal (or nearly equal) to the

number of MPFs available for the full model. In such a case, the number of modes is equal to the number of DOFs of the reduced model, all of whose MPFs are previously estimated. In other words, more dynamic information is condensed into fewer number of modes of the reduced model than the information contained in the same number of modes of the full model. Therefore, Eqn. (5.7) is dynamically more complete and is expected to produce better load estimates than Eqn. (3.1) for the same number of available/retained modes.

Presented next are two numerical examples demonstrating the efficacy of the proposed approach on two problems where it is shown that the applied loads are recovered accurately despite the presence of noise in strain measurements.

5.7 Example Revisited – Cantilevered Beam (Numerical)

The numerical example of cantilevered beam described in Sec. 5.5 was revisited and load identification procedure in conjunction with the Craig-Bampton model reduction was applied. Additional inputs for the load recovery problem are tabulated in Table 5.4. The procedure remains the same until the determination of $\{x(t)\}$ and its derivatives using Eqn. (3.6), following which, Eqns. (3.30) and (3.31) were used to obtain $\begin{Bmatrix} \{x(t)\}_b \\ \{q(t)\}_p \end{Bmatrix}$ and its derivatives. The applied load was finally recovered using Eqn. (5.7). It is to be noted again that the DOFs corresponding to the load application locations must be a subset of the boundary DOFs. The actual applied load and the recovered load using the technique of model reduction are plotted in Fig. 5.14. The rms error using Eqn. (3.33) was calculated to be 3.2%. It can be seen that an excellent agreement is achieved in the applied and the recovered loads when Craig-Bampton model reduction was applied to the

load recovery procedure, with 10% error present in all 9 strain gage readings. The robustness of the method is further examined by re-running the analysis after introducing random error in the mass/stiffness matrix of the model. One such plot is depicted in Fig. 5.15 that shows a comparison between applied and recovered loads with 5% variation in terms in the mass matrix. It can be inferred from the plot that the technique is quite robust to variations in the model also.

5.8 Example – Horn Bracket

The previous example dealt with identification of a single input load. Presented next is a more general numerical example where two mutually perpendicular loads acting on a horn bracket need to be estimated. A finite element model of the bracket was developed in ANSYS using SHELL181 elements. The finite element model of the bracket along with the applied loads and boundary conditions is shown in Fig. 5.16. The two holes were fixed in all degrees of freedom. The model consisted of 198 shell elements and 233 unconstrained nodes with 6 degrees of freedom per node, i.e., the total number of degrees of freedom of the model was 1398.

Two mutually perpendicular forcing functions, $f_1(t) = 5000\sin(60t) + 8000\sin(40t)$ and $f_2(t) = 6000\sin(60t) + 10000\sin(25t)$ are applied as shown in Fig. 5.16. The task again is to determine the optimum strain gage locations and angular orientations and reconstruct the input forces based on the strain time response measured at those locations. Table 5.5 summarizes the relevant problem specific input data.

Load identification procedure in conjunction with the Craig-Bampton model reduction was applied to recover the two applied loads. A procedure similar to the

previous example was followed. The shell elements corresponding to the optimum gage locations along with the element coordinate systems are shown in Fig. 5.17. The numbers next to the elements denote the optimum angular orientations (degree) of strain gages with respect to the x-axes of the element coordinate systems. The applied loads and the recovered loads are plotted in Figs. 5.18 and 5.19. It may be noted that these figures correspond to the case when no error was assumed to be present in strain measurements. Next, to simulate a more realistic scenario where strains are measured experimentally, each element in $\{\varepsilon(t)\}_{opt}$ was corrupted with normally distributed random errors with zero mean and standard deviation of 10% of its value. The applied and recovered loads, with errors in strain measurements, are plotted in Figs. 5.20 and 5.21; the rms errors using Eqn. (3.33) were calculated to be 8.9% and 9.7% respectively. Once again, it can be inferred that the proposed approach is able to recover the applied loads fairly accurately.

5.9 Summary

A computational methodology is presented that allows for indirect measurement of dynamic loads imposed on a component by using the structure itself as a load transducer. This is achieved by placing strain gages on the component such that best possible load estimates are obtained from the measured strain information. A new technique based on the modal model of the structure is developed to identify dynamic loads from the strain response. To improve the precision of load estimates, optimum design of experiment techniques in conjunction with finite element method is used to determine the strain gage locations and orientations. It is observed that the loads

recovered from the unreduced model are highly underestimated due to large amount of truncation errors resulting from few retained modes. The number of strain gages that can be used places a limit on the number of modes that can be retained in the analysis. To overcome this limitation, a novel approach based on model reduction is proposed. Introduction of model reduction in load recovery results in significant improvement in dynamic load estimation. Numerical example results illustrate the effectiveness of the proposed approach in recovering time varying loads which induce significant levels of vibrations in the component. The proposed approach is fairly robust in the sense that the applied loads are recovered accurately even when significant noise (errors) is encountered in strain measurements.

The real interest of the proposed method lies in the case of complicated structures where complex loads are acting. The proposed approach is general and can be applied to any structure without any assumptions regarding the complexity of the structure and/or the applied loads. The robustness of the approach has been demonstrated through two examples wherein the applied loads are recovered accurately despite the presence of simulated measurement errors in strain measurements. Since modal analysis and MPFs form the basis of the approach, care must be taken not to miss any significant modes and make use of engineering judgment when arriving at the MPFs.

Table 5.1 Beam with 28 Hz Base Excitation

28 Hz dwell	Experimental MPF		Theoretical MPF	
Mode	MPF	Particip. %	MPF	Particip. %
1	1.87E-02	94.9	1.16E-01	99.98
2	-5.63E-04	2.8	1.62E-05	0.01
3	-3.28E-04	1.7	-2.42E-14	0.00
4	4.77E-06	0.0	-5.00E-19	0.00
5	9.78E-05	0.5	1.14E-06	0.00

Table 5.2 Beam with 171 Hz Base Excitation

171 Hz dwell	Experimental MPF		Theoretical MPF	
Mode	MPF	Particip. %	MPF	Particip. %
1	-6.50E-04	6.4	-5.60E-03	11.03
2	-8.80E-03	87.0	4.49E-02	88.40
3	3.06E-04	3.0	-6.50E-12	0.00
4	-2.12E-05	0.2	-1.14E-16	0.00
5	3.25E-04	3.0	2.51E-04	0.49

Table 5.3 Input Data for Cantilevered Beam Example

Variable	Value	Variable	Value
n	600	c	160
m	7	g	9

Table 5.4 Input Data for Cantilevered Beam Example with CB Reduction

Variable	Value	Variable	Value	Variable	Value
n	600	c	160	g	9
m	7	b	395, 425, 469, 486	p	3

Table 5.5 Input Data for Horn Bracket Example with CB Reduction

Variable	Value	Variable	Value	Variable	Value
n	1398	c	198	g	7
m	5	b	284, 424, 848, 1293	p	2
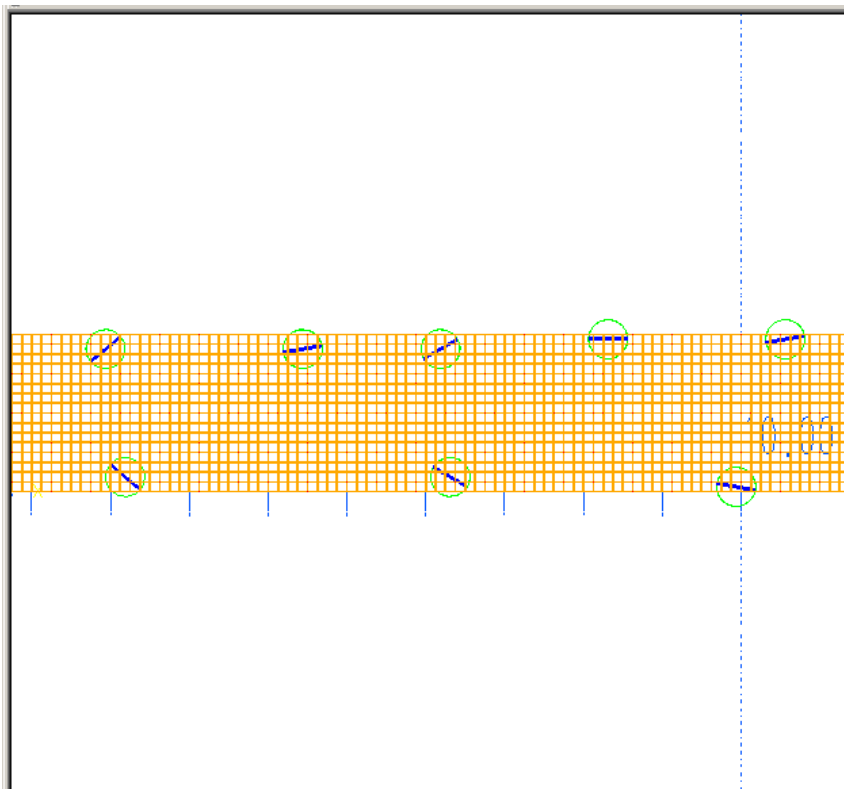
Figure 5.1 Cantilevered Beam with Optimum Gage Placement
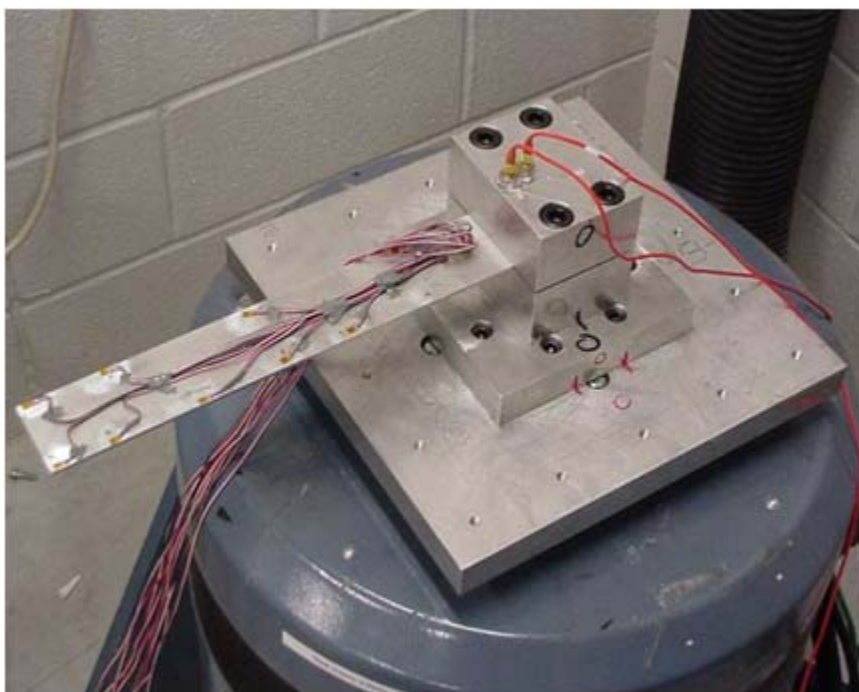
Figure 5.2 Clamped Cantilevered Beam Mounted on Shaker
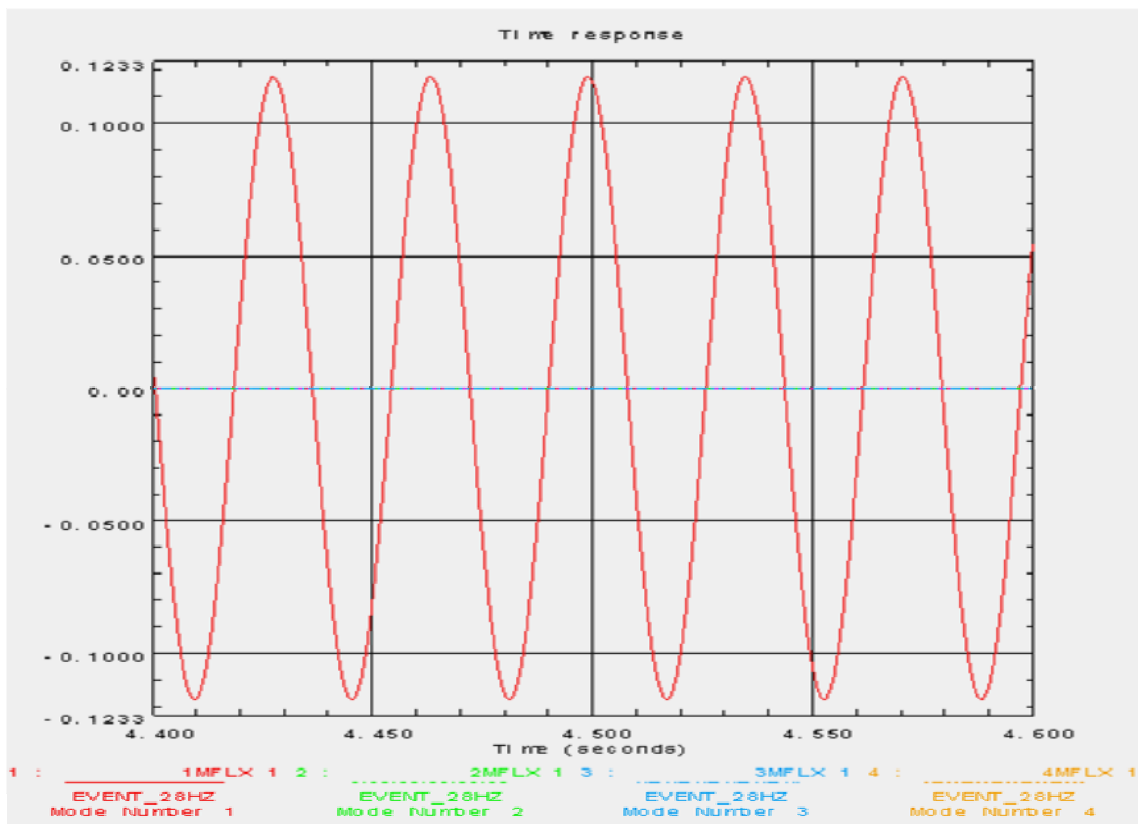
Figure 5.3 MPF for 28 Hz Base Excitation
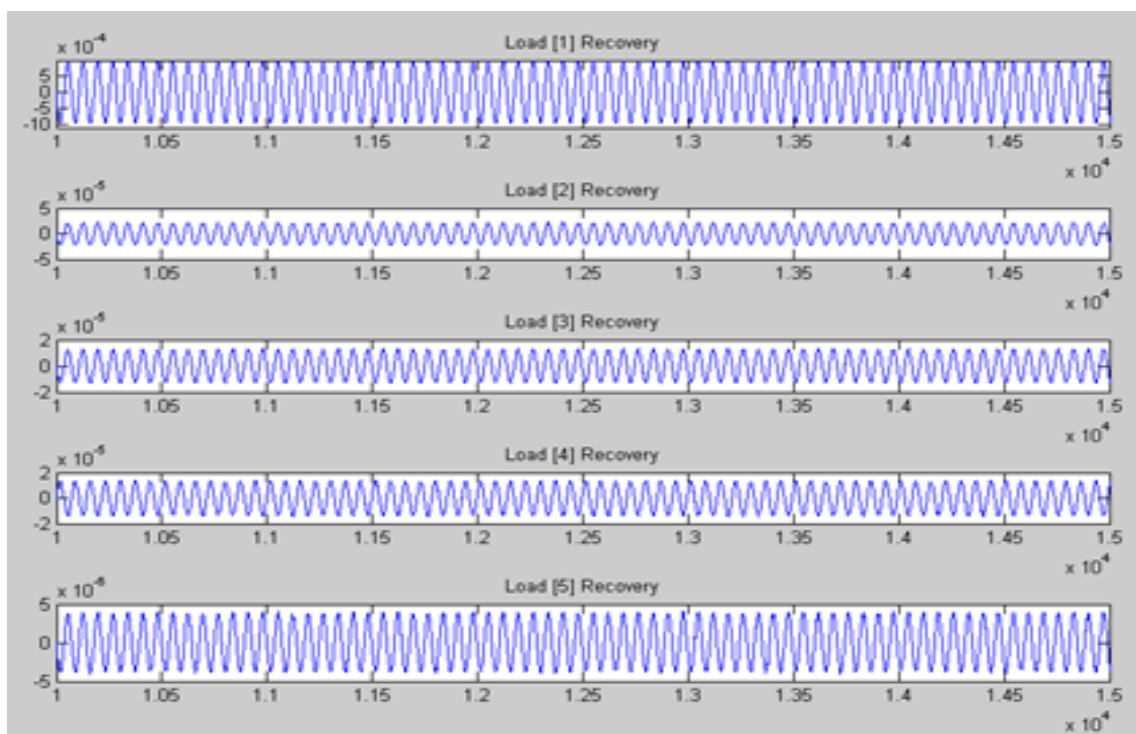
Figure 5.4 Recovered MPF for 28 Hz Input
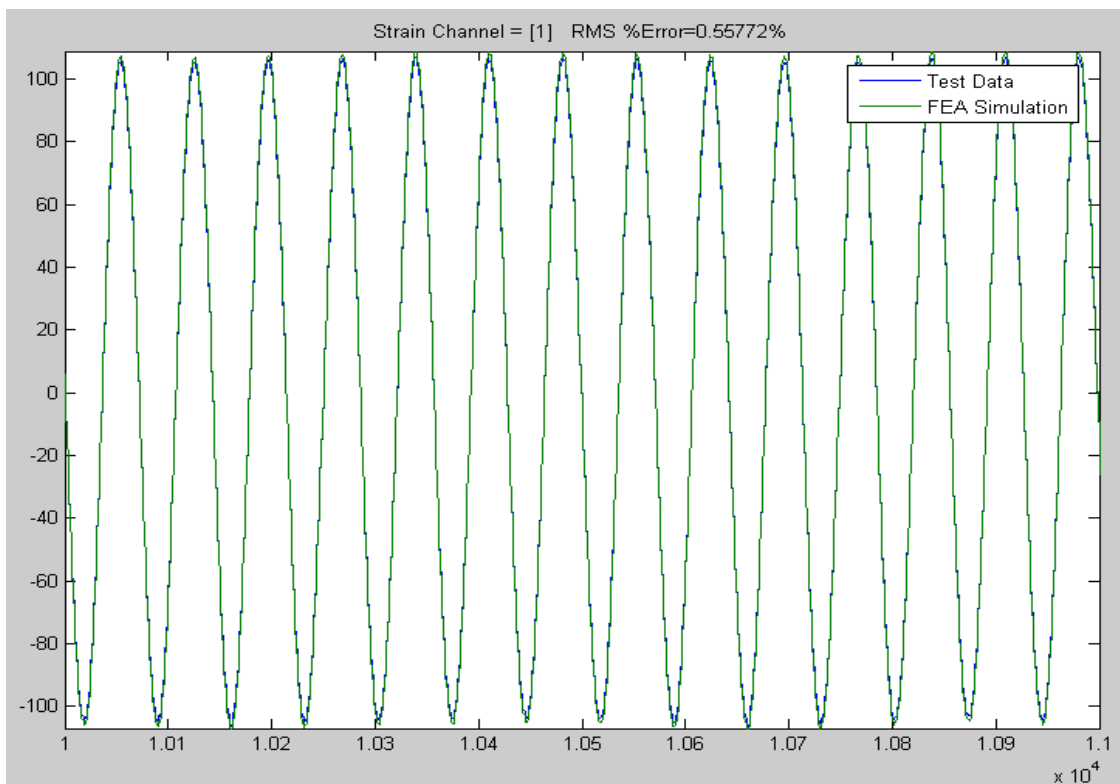
Figure 5.5 Actual and Reconstructed Strains in Gage 1
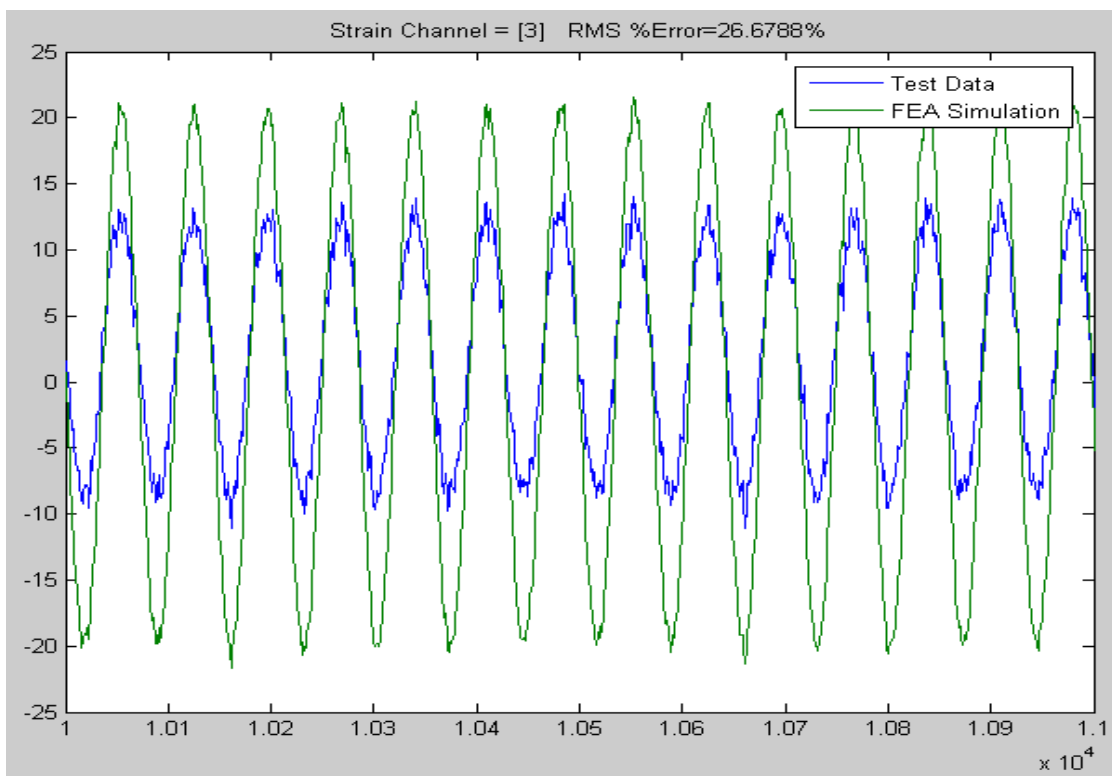
Figure 5.6 Actual and Reconstructed Strains in Gage 3
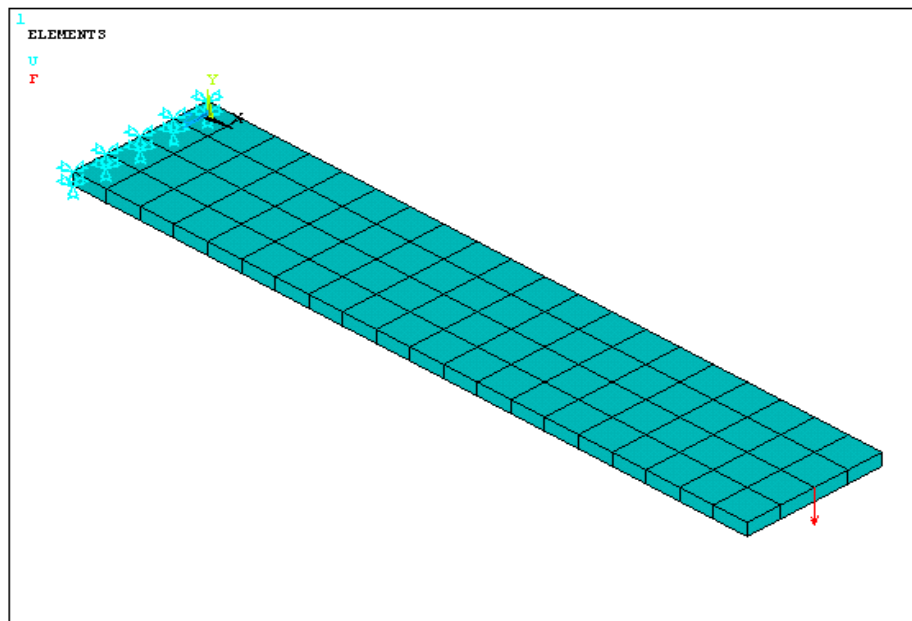
Figure 5.7 Finite Element Model of Cantilevered Beam with Applied Load
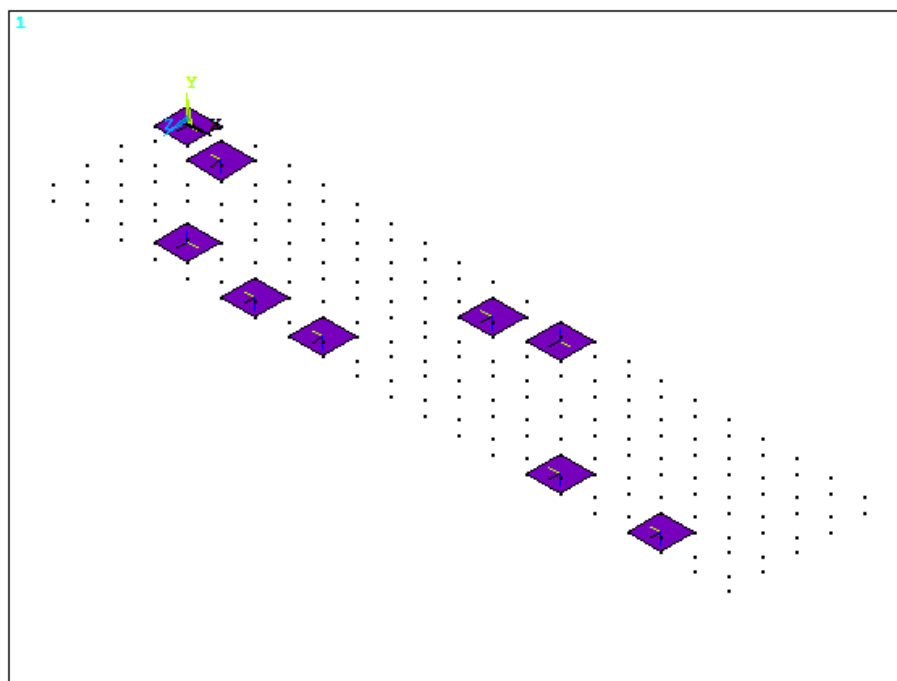
Figure 5.8 Shell Elements Corresponding to Optimum Gage Locations
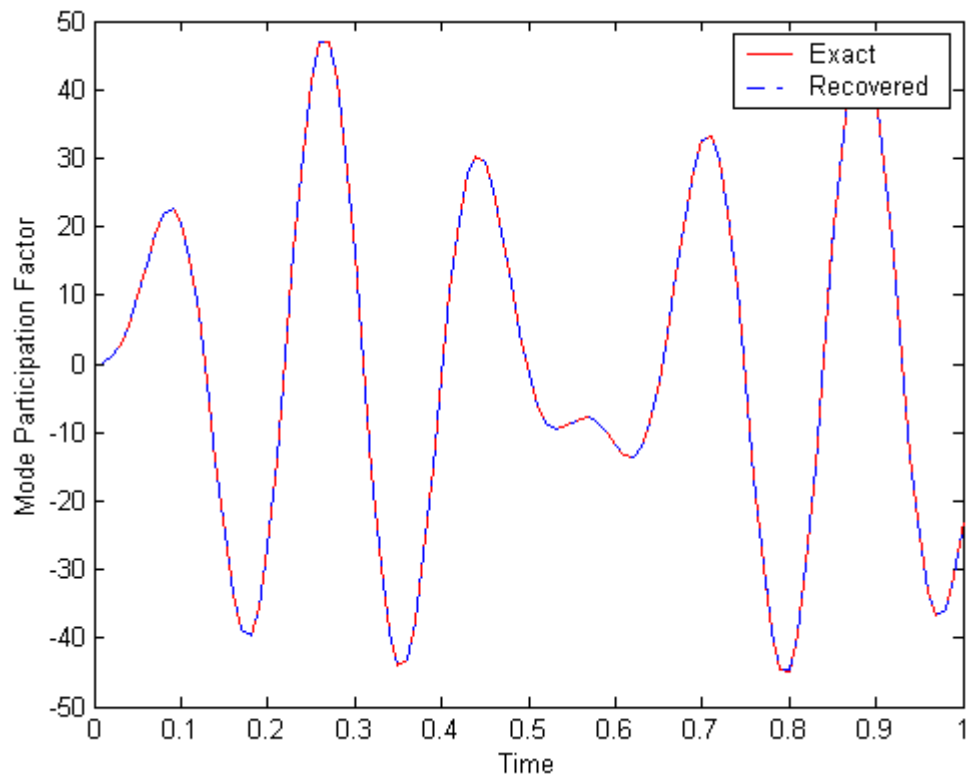
Figure 5.9 MPF for First Mode
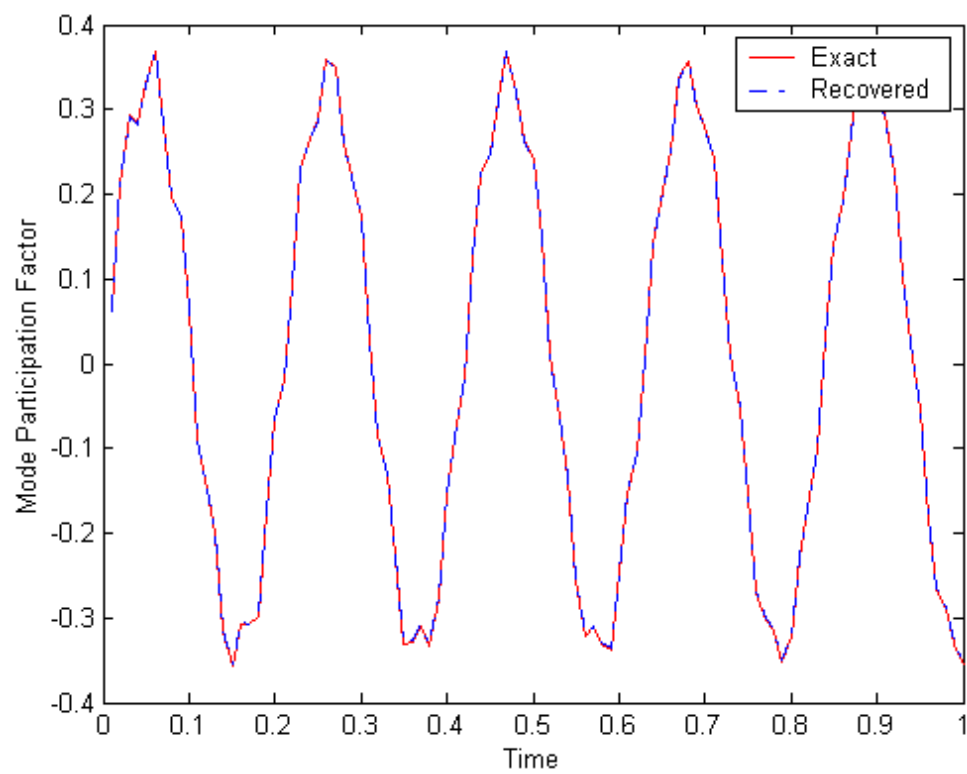
Figure 5.10 MPF for Second Mode
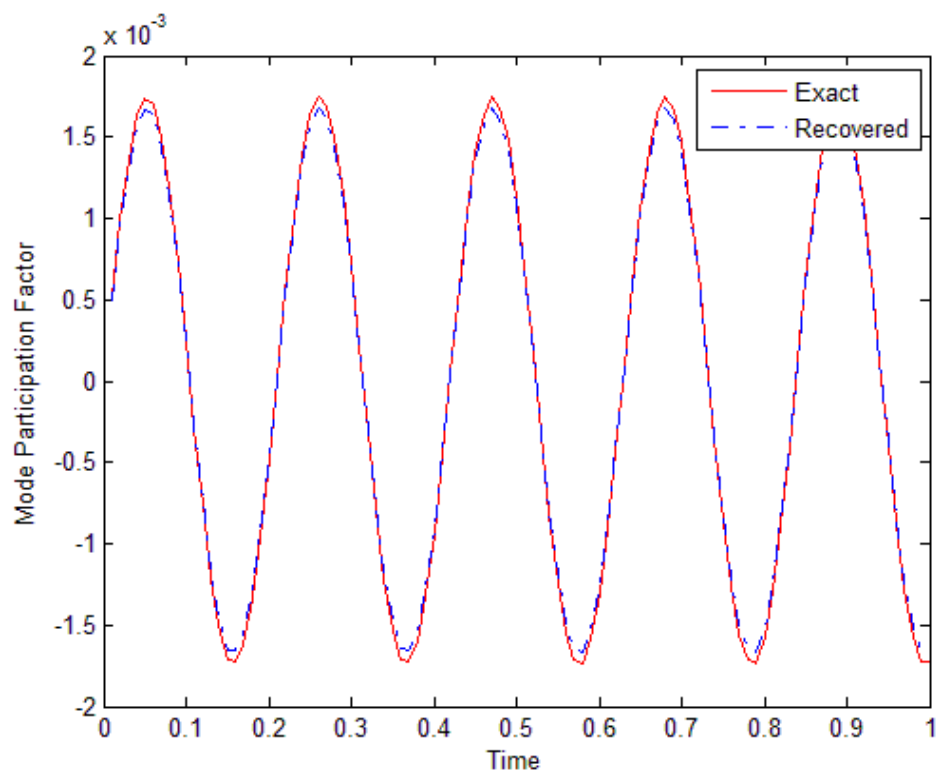
Figure 5.11 MPF for Sixth Mode
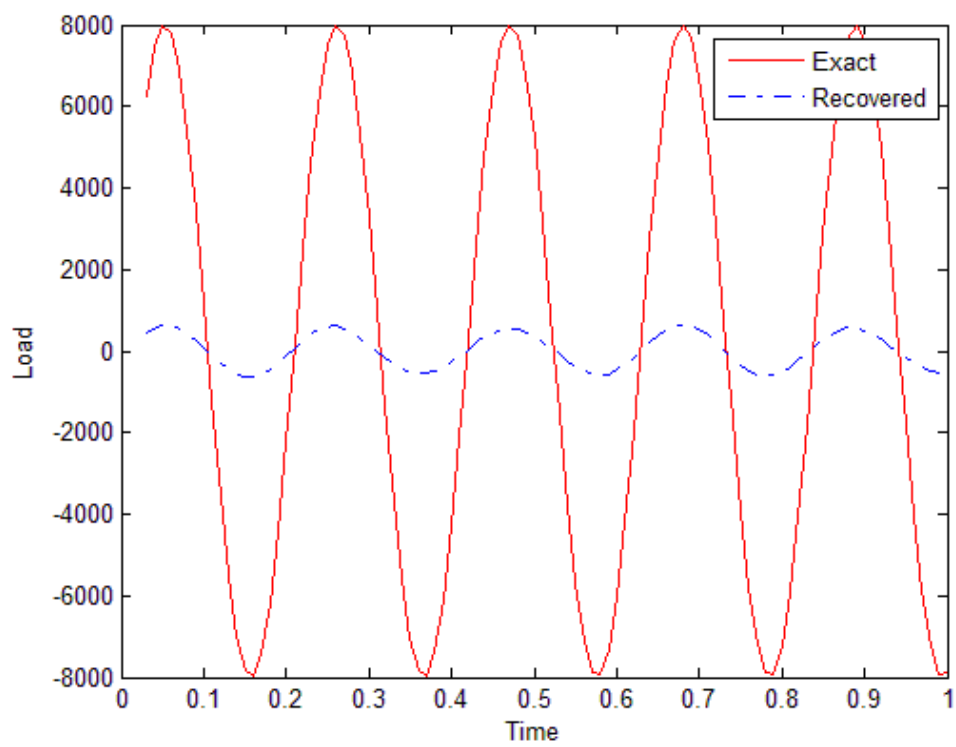
Figure 5.12 Recovered Load with 7 Retained Modes
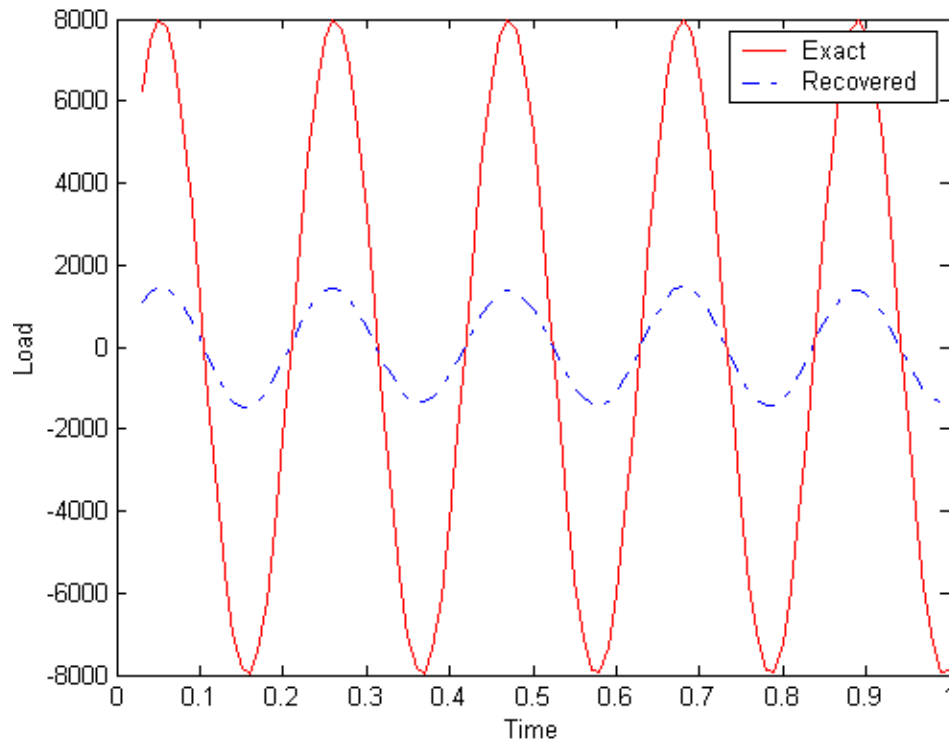
Figure 5.13 Recovered Load with 15 Retained Modes
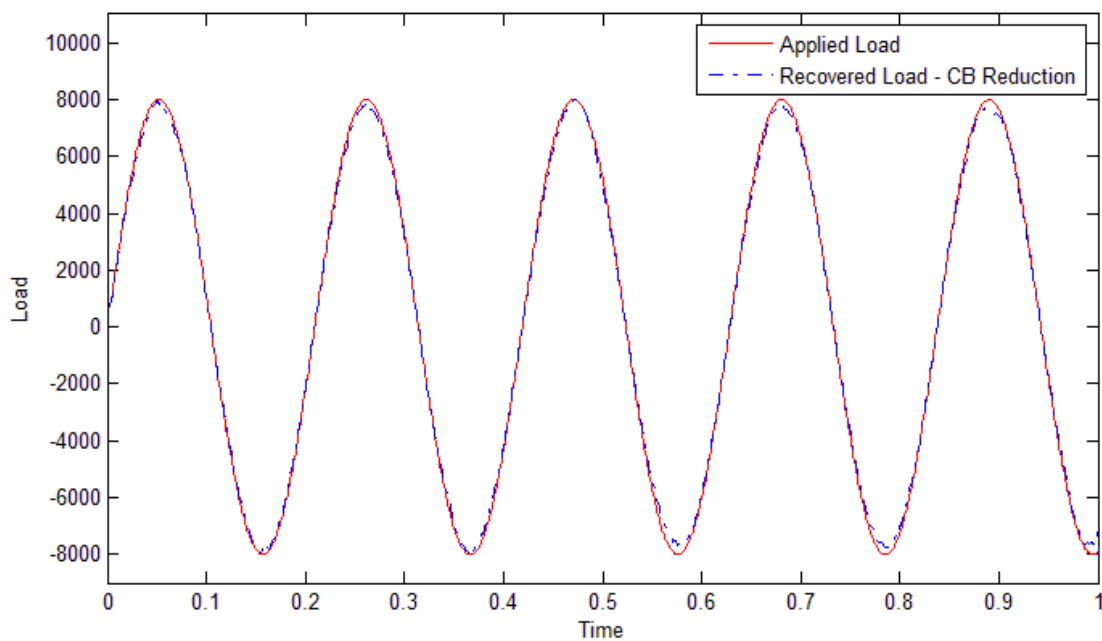
Figure 5.14 Recovered Load with 7 Retained Modes utilizing Model Reduction
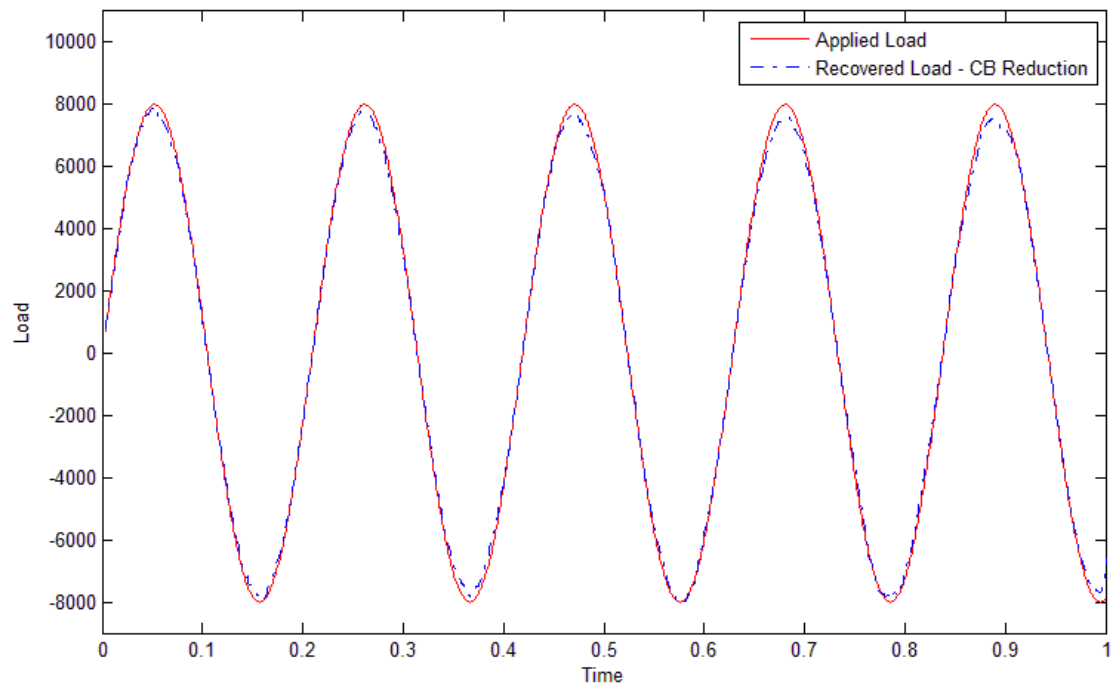
Figure 5.15 Recovered Load with 7 Retained Modes utilizing Model Reduction
and 5% Variation in Mass Matrix
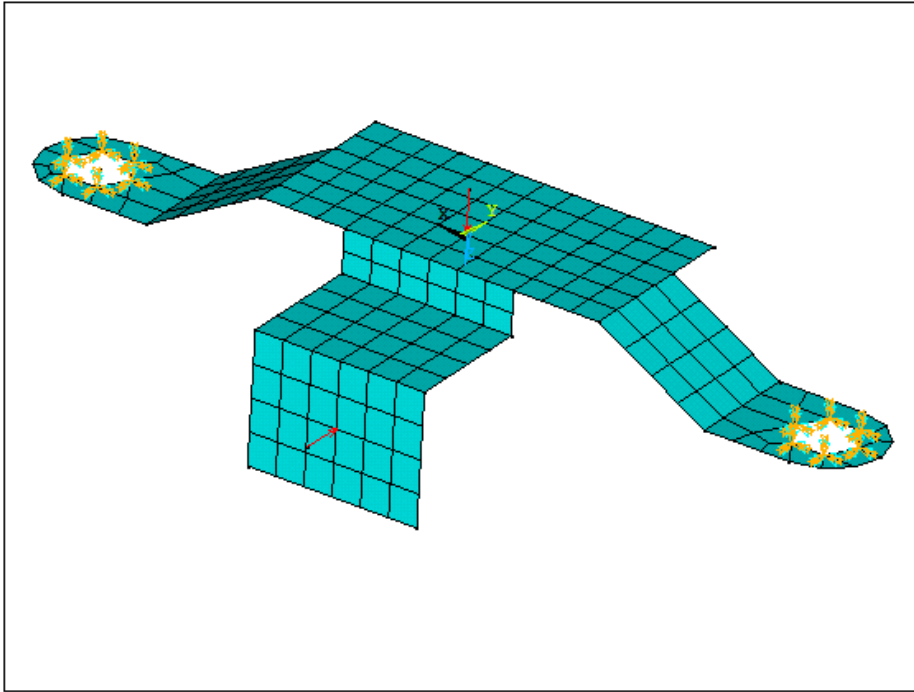
Figure 5.16 Finite Element Model of Horn Bracket with Applied Loads
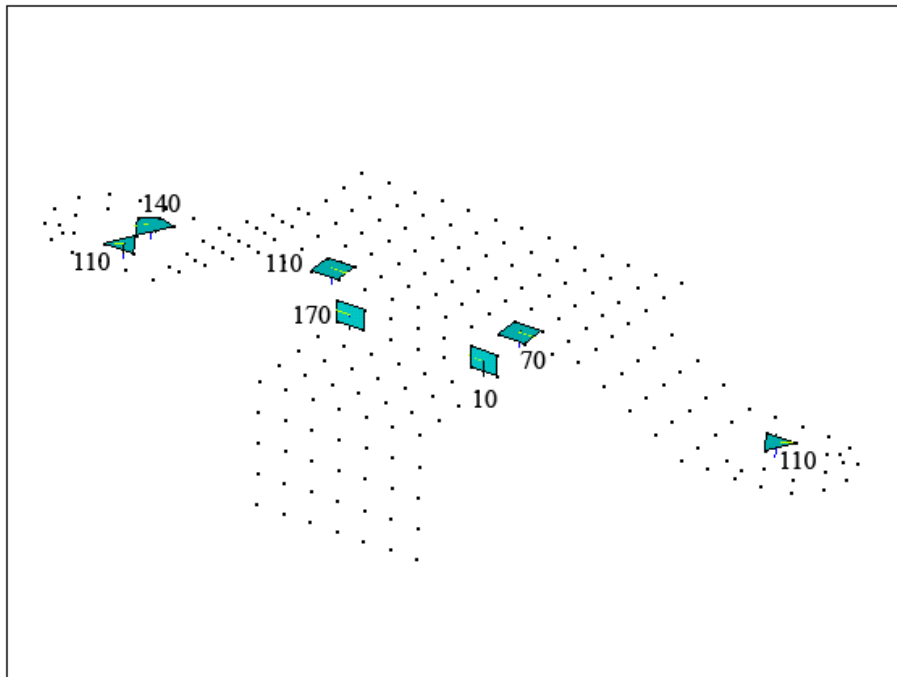
Figure 5.17 Shell Elements Corresponding to Optimum Gage Locations with Angular Orientations
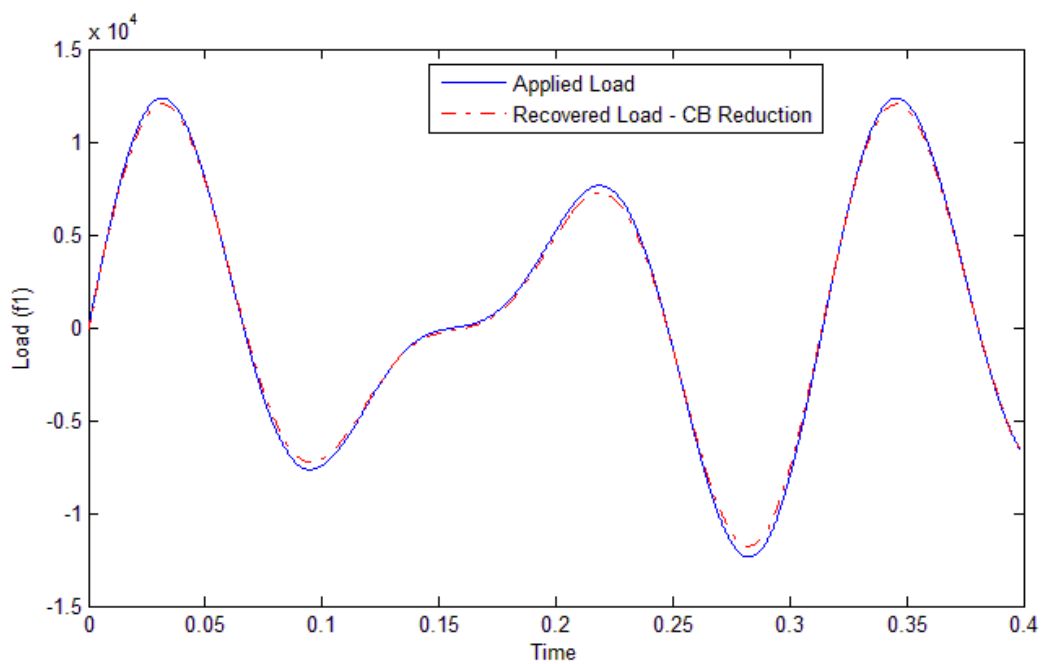
Figure 5.18 Applied and Recovered Load (f_1)
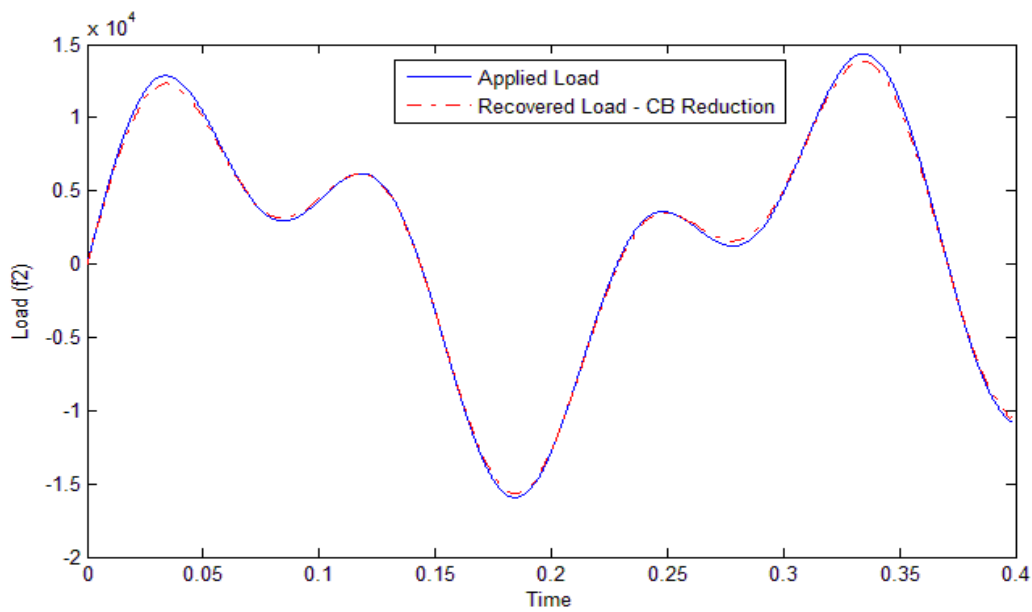
Figure 5.19 Applied and Recovered Load (f_2)
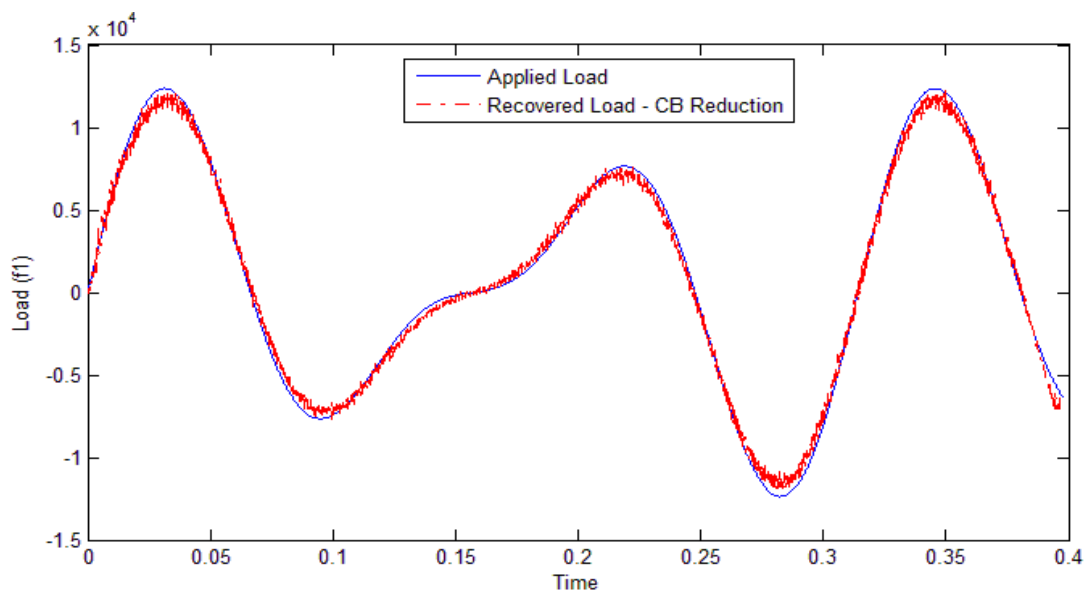
Figure 5.20 Applied and Recovered Load (f_1) with Strain Errors
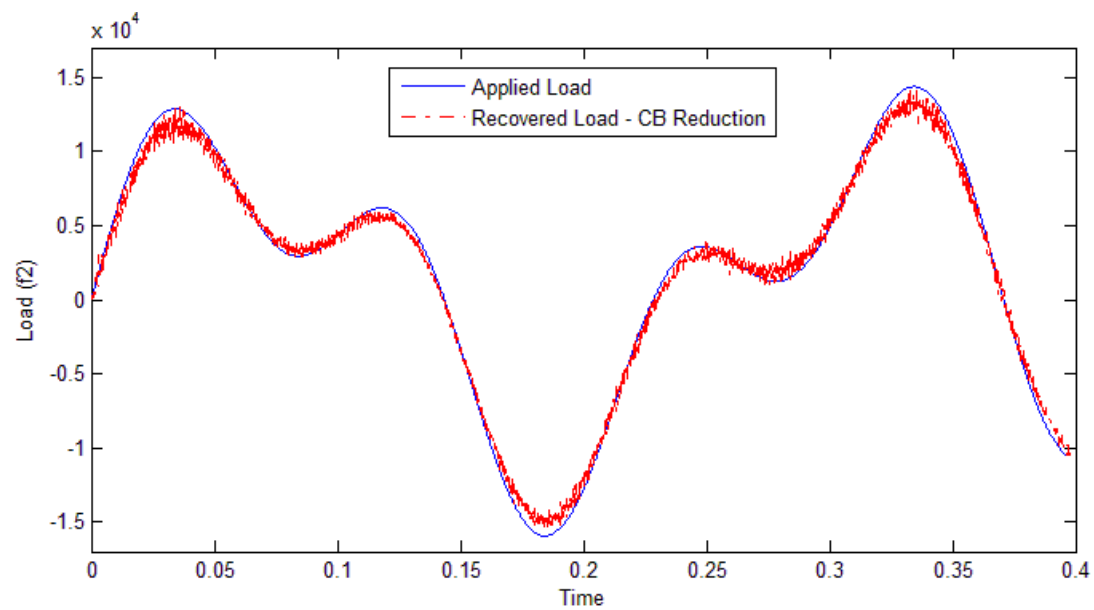
Figure 5.21 Applied and Recovered Load (f_2) with Strain Errors

Chapter 6 -   Dynamic Load Identification from Acceleration Measurements

A detailed treatment of the load identification problem using strain measurements has been presented in the previous two chapters. Apart from load identification based on strain measurements, a significant consideration has also been given by research community to acceleration measurements (Ewins, 2000). Carne *et al.* (1992) proposed a technique referred to as the Sum of Weighted Acceleration Technique (SWAT) that estimates the input forces by summing the weight-scaled measured accelerations. Genaro and Rade (1998) developed a technique based on identified eigen-solutions to reconstruct input forces from acceleration response. Kammer (1998) used acceleration measurements to identify input loads based on inverse Markov parameters. In all these works, it is assumed that the accelerometers are collocated with the forces, which is not always feasible.

In light of the above discussion, it can be concluded that even though significant amount of research has been dedicated towards identifying optimum strain gage locations on the structure for precise load estimation, the idea of determining optimum accelerometer locations has received very little attention. It is recognized (Hansen and Starkey, 1990) that accelerometer placement has a significant influence on the overall quality of results. To overcome the above mentioned shortcomings, this chapter outlines two different algorithms for estimating time-varying loads exciting a structure by measuring acceleration time response at finite number of optimum locations on the

structure. The accuracy of the load estimates is dependent on the locations of the accelerometers.

6.1 Algorithm Based on Sparse Nature of [*M*], [*C*] and [*K*]

In this section, an algorithm based upon the sparse nature of the mass, damping and stiffness matrices is proposed to help select the optimum locations of the accelerometers such that precise load estimates are obtained. An example dealing with numerical validation of the proposed approach is presented to illustrate the technique.

6.1.1 Theoretical Development

Consider the spatially discretized linear second-order ordinary differential equation (ODE) of an *n* degrees of freedom (DOFs) structural system in the matrix form given by Eqn. (3.1); the equation can be re-written with subscripts denoting the size of the matrices as:

$$[M]_{n\times n}\{\ddot{x}(t)\}_{n\times 1} + [C]_{n\times n}\{\dot{x}(t)\}_{n\times 1} + [K]_{n\times n}\{x(t)\}_{n\times 1} = \{f(t)\}_{n\times 1} \tag{6.1}$$

For simple systems, the $[M]$, $[C]$ and $[K]$ matrices may be obtained by writing the system equations of motion; for complex structures they can be obtained from the finite element model of the structure. The vector $\{\ddot{x}(t)\}$ is obtained from experimental acceleration measurements whereby the vectors $\{\dot{x}(t)\}$ and $\{x(t)\}$ can be obtained upon successive numerical integration of $\{\ddot{x}(t)\}$. Given the terms on the left-hand-side, they can be used to estimate the dynamic loads $\{f(t)\}$ acting on the structure through Eqn. (6.1).

It is assumed at this point that the locations of the applied loads are known beforehand. This is a reasonable assumption to make as the locations where the load

transferring body is applying loads to the structure in question are known upfront in most cases. With the knowledge of the locations of the applied loads, only the relevant rows of matrices in Eqn. (6.1) now need to be retained and the remaining rows may be ignored altogether. If j is the number of applied loads, then Eqn. (6.1) can be rewritten as:

$$[M_{rt}]_{j \times n} \{\ddot{x}(t)\}_{n \times 1} + [C_{rt}]_{j \times n} \{\dot{x}(t)\}_{n \times 1} + [K_{rt}]_{j \times n} \{x(t)\}_{n \times 1} = \{f_{rt}(t)\}_{j \times 1} \qquad (6.2)$$

where the subscript 'rt' stands for 'rows truncated'. Here, the rows of the $[M]$, $[C]$ and $[K]$ matrices, corresponding to the degrees of freedom where the loads are applied, are retained.

For measurement of acceleration response, there can be a large number of potential locations on the structure where the accelerometers can be mounted. The accuracy of the identified loads depends on the number of accelerometers used and their locations on the structure. Theoretically, the best load estimates may be obtained when the information on the response is available at the maximum possible number of locations. Practically, although a non-zero response is present over most of the structure, they can only be measured at a finite number of selected locations, with the response at the rest of the locations left untapped. Discussed next is the idea of sparse nature of the $[M]$, $[C]$ and $[K]$ matrices that will be used to determine the optimum locations of accelerometers on the structure.

As stated earlier, the $[M]$, $[C]$ and $[K]$ matrices can be obtained for complex structures using finite element method. The two approaches used extensively in finite element approach to derive the mass matrix are the lumped mass approach and the consistent mass approach. Of the two, the lumped mass matrix is of simpler form and is obtained by placing concentrated masses at the nodes in the directions of the

displacement degrees of freedom. The concentrated masses are obtained based on the assumption that the material within the mean location on either side of a particular node behaves like a rigid body while the remainder of the element does not participate in the motion. This assumption leads to the exclusion of the dynamic coupling that exists between the degrees of freedom and, therefore, the lumped mass matrix is purely diagonal. The consistent mass matrix, on the other hand, is obtained by utilizing the same displacement model that is used for the derivation of the stiffness matrix. This makes the consistent mass matrix non-diagonal, but still, most of its elements are zero. The bottom line of this discussion is that irrespective of the method used to derive the mass matrix, it is always sparse.

The global stiffness matrix of any structure is obtained by assembling the element stiffness matrices together. Its density (number of non-zero elements) depends on the number of elements sharing a particular node. Spatially, there can only be a few elements common to a particular node. This would make the global stiffness matrix sparse, as majority of its elements would become zero upon assembly. The same argument applies to damping matrix, leading to its sparse nature.

Presented next is an algorithm based on sparse nature of the $[M]$, $[C]$ and $[K]$ matrices in conjunction with elimination that will allow for precise load identification through optimal placement of accelerometers at finite number of locations on the structure. To make the idea clear, it is convenient here to define the following terms:

$$\{f_I(t)\}_{j\times 1} = [M_{rt}]_{j\times n}\{\ddot{x}(t)\}_{n\times 1} \tag{6.3}$$

$$\{f_D(t)\}_{j\times 1} = [C_{rt}]_{j\times n}\{\dot{x}(t)\}_{n\times 1} \tag{6.4}$$

$$\{f_E(t)\}_{j\times 1} = [K_{rt}]_{j\times n}\{x(t)\}_{n\times 1} \tag{6.5}$$

Thus, from Eqn. (6.2), it is clear that:

$$\{f_I(t)\} + \{f_D(t)\} + \{f_E(t)\} = \{f_{rt}(t)\} \qquad (6.6)$$

Next, consider Eqn. (6.3); it is important here to note that each row in $\{\ddot{x}(t)\}$ corresponds to a potential accelerometer location on the structure. Having realized that the $[M]$, $[C]$ and $[K]$ matrices are sparse in nature, it is easy to recognize that majority of the elements in each row of $[M_{rt}]$ in Eqn. (6.3) are zero. These zero elements, when multiplied by the corresponding elements in $\{\ddot{x}(t)\}$, do not contribute to load calculation. Therefore, the non-zero elements in each row of $[M_{rt}]$ can be identified and the corresponding row indices in $\{\ddot{x}(t)\}$ be retained as a set. Similar sets may be obtained for all the rows of $[M_{rt}]$. A union of all the sets so obtained (say A) will contain row indices of all those elements in $\{\ddot{x}(t)\}$ that multiply with at least one non-zero element in $[M_{rt}]$.

A similar treatment, as discussed in the previous paragraph, can be given to Eqns. (6.4) and (6.5), and two more sets (say B and C) can be obtained. Next, define set L as:

$$L = A \cup B \cup C \qquad (6.7)$$

where $\cup$ denotes union of sets. The elements of set L denote the row indices of each of the vectors $\{\ddot{x}(t)\}$, $\{\dot{x}(t)\}$ and $\{x(t)\}$ that must be retained in the analysis, and the rest of the rows be eliminated. In other words, the elements of set L provide information on the optimum accelerometer locations on the structure. Let a be the cardinal number of set L; a determines the number of accelerometers that must be used in the analysis.

Accelerometers can then be mounted at determined optimum locations on the structure and acceleration response $\{\ddot{x}(t)\}$ measured, which is numerically integrated successively to yield $\{\dot{x}(t)\}$ and $\{x(t)\}$. Next, only those columns of the $[M_{rt}]$, $[C_{rt}]$ and $[K_{rt}]$ matrices whose indices correspond to the elements in the set L need to be retained

and the remaining columns can be eliminated as their participation does not affect the load calculation process. Equation (6.2) then becomes:

$$[M_{rct}]_{j\times a}\{\ddot{x}(t)\}_{a\times 1} + [C_{rct}]_{j\times a}\{\dot{x}(t)\}_{a\times 1} + [K_{crt}]_{j\times a}\{x(t)\}_{a\times 1} = \{f_{rt}(t)\}_{j\times 1} \qquad (6.8)$$

where the subscript 'rct' stands for 'rows and columns truncated'. The left-hand-side of Eqn. (6.8) is determined fully which can then be used to identify the unknown loads exciting the structure.

Almost all of the load identification techniques that have been proposed historically (refer to Chapter 1) are based on inverse analysis that rely on matrix inversion at some step in the process of load recovery. The ill-conditioning of such matrices poses several challenges and is the major source of errors in the analysis due to noise magnification. The technique described in this section does not depend on any matrix inversion at any step and therefore, errors in acceleration measurements do not get magnified and remain bounded. This leads to precise load identification.

6.1.2 Solution Procedure

An outline of the solution procedure is presented next that will allow for the estimation of time varying loads $\{f(t)\}$ acting on a structure by measuring accelerations at a finite number of optimally placed accelerometers on the structure.

(i)   Obtain the $[M]$, $[C]$ and $[K]$ matrices either analytically or through finite element analysis of the structure.

(ii) Identify the locations (degrees of freedom) at which the unknown loads are applied. Retain only those rows of $[M]$, $[C]$ and $[K]$ matrices that correspond to

the identified degrees of freedom and eliminate the remaining rows. This forms

the matrices $[M_{rt}]$, $[C_{rt}]$ and $[K_{rt}]$.

(iii) Consider the first row of the matrix $[M_{rt}]$; obtain a set consisting of column

indices of all the non-zero elements in that row. Repeat the procedure taking into

account each row one by one, and obtain as many sets as the number of rows.

(iv) Construct a set A by the union of all the sets obtained in step (iii).

(v) Repeat steps (iii) and (iv) for $[C_{rt}]$ and $[K_{rt}]$ to obtain sets B and C respectively.

(vi) Construct set $L = A \cup B \cup C$. The elements of set L denote the optimum

accelerometer locations (degrees of freedom) and its cardinal number determines

the number of accelerometers to be used.

(vii) Mount the accelerometers at the determined optimal locations and measure the

acceleration response $\{\ddot{x}(t)\}$. Numerically integrate it successively to yield $\{\dot{x}(t)\}$

and $\{x(t)\}$.

(viii) Retain only those columns of the $[M_{rt}]$, $[C_{rt}]$ and $[K_{rt}]$ matrices whose indices

correspond to the elements in the set L and eliminate the remaining columns. This

provides the $[M_{rct}]$, $[C_{rct}]$ and $[K_{rct}]$ matrices.

(ix) Identify the unknown applied loads using Eqn. (6.8).

6.1.3 Example: 15-DOF Spring-Mass System

The dynamic load estimation method discussed above is illustrated with the help

of a numerical simulation comprising of a 15 degrees of freedom chain like spring-mass

system as depicted in Fig. 6.1. Without any loss of generality, the system is assumed to

be undamped. Masses m_1 and m_{15} are connected to fixed boundary. Starting from left to

right, the masses are arbitrarily assigned values ranging from 20 to 160 in increments of

10. Similarly, starting from left to right, the springs are arbitrarily assigned stiffness

values ranging from 1×10^8 to 8×10^8 in increments of 0.5×10^8. A sinusoidal forcing

function $f_7(t) = 500\sin(300\pi t) + 350\cos(150\pi t)$ is applied to mass m_7. The task was

to determine the optimum accelerometer locations and reconstruct the input force based

on the acceleration time response at those locations. The $[M]$, $[C]$ and $[K]$ matrices

(15×15) were obtained by writing the equations of motion for the system. In absence of

any experimental data, the acceleration time responses at the relevant degrees of freedom

were calculated by analytical means.

Before applying the solution procedure described in this work, for comparison

purpose, two attempts for reconstructing the applied load were made based on randomly

selected accelerometer locations. The first attempt was made by arbitrarily assuming the

number of accelerometers to be 4. Four uniformly distributed positive integer random

numbers ≤ 15 were generated to simulate the random locations of the accelerometers. The

randomly generated locations were at masses 2, 7, 10 and 14. Analytical acceleration

time responses were calculated at these locations to simulate the accelerometer

measurements, which were then numerically integrated successively to obtain the

velocity and displacement responses. The input force was reconstructed using Eqn. (6.8).

The applied and reconstructed forces are plotted in Fig. 6.2. Similar attempt was made by

increasing the number of accelerometers to 5 in anticipation of better degree of load

identification. The randomly generated accelerometer locations for this case were at

masses 3, 6, 7, 9 and 14. Again, the applied and reconstructed forces are plotted in Fig.

6.3. It can be inferred from both the plots that the load identification based on randomly selected accelerometer locations is very poor and does not yield acceptable results.

Next, load identification solution procedure described in this work was applied to the given problem. Since the load was applied to mass m_7, only row 7 in each of the matrices $[M]$, $[C]$ and $[K]$ was retained. This formed the matrices $[M_{rt}]_{1\times15}$, $[C_{rt}]_{1\times15}$ and $[K_{rt}]_{1\times15}$. In matrix $[M_{rt}]_{1\times15}$, all elements but the element in column 7 were zero; therefore, set $A = \{7\}$. Since the system was assumed to be undamped, all the elements in the matrix $[C_{rt}]_{1\times15}$ were zero, which led to set $B = \{\emptyset\}$. The elements in columns 6, 7 and 8 in matrix $[K_{rt}]_{1\times15}$ were non-zero, which implied that set $C = \{6,7,8\}$. Having obtained sets A, B and C, set $L = A \cup B \cup C = \{6,7,8\}$ was constructed per Eqn. (6.7). Thus, the optimum number of accelerometers is 3, which is equal to the cardinal number of L, with accelerometer locations at masses 6, 7 and 8. Only those columns of the $[M_{rt}]$, $[C_{rt}]$ and $[K_{rt}]$ matrices, whose indices correspond to the elements in the set L, were retained and the remaining columns were eliminated. This provided the matrices $[M_{rct}]_{1\times3}$, $[C_{rct}]_{1\times3}$ and $[K_{rct}]_{1\times3}$. Next, acceleration response $\{\ddot{x}(t)\}$ at masses 6, 7 and 8 were obtained analytically and numerically integrated successively to yield $\{\dot{x}(t)\}$ and $\{x(t)\}$. Based on the response data at the optimal accelerometer locations, the applied load was reconstructed using Eqn. (6.8). The applied and reconstructed forces are plotted in Fig. 6.4, which shows an excellent agreement between the two sets of force values.

6.2 Algorithm Based on D-optimal Design and Reduced Modal Parameter

The load identification algorithm presented in Sec. 6.1 has an inherent limitation - the accelerometers must be collocated with the force locations. In many applications, the force input locations may not be accessible to mount sensors. To overcome this limitation, this section presents a time domain technique for estimating dynamic loads acting on a structure from acceleration time response measured experimentally at a finite number of optimally placed non-collocated accelerometers on the structure. The approach is based on the standard equilibrium equations of motion in modal coordinates. The modal parameters of a system, natural frequencies, mode shapes and damping factors can be estimated experimentally from measured data, analytically for simple problems, or using finite element method. For measurement of the acceleration response, there can be a large number of locations on the structure where the accelerometers can be mounted, and the precision with which the applied loads are estimated from measured acceleration response may be strongly influenced by the locations selected for accelerometer placements. A solution approach, based on the construction of D-optimal designs, is presented to determine the number and optimum locations of accelerometers that will provide the most precise load estimates. An improvement in the algorithm, based on reduced modal matrix, is further proposed to reconstruct the input forces accurately. Two examples dealing with numerical validation of the proposed approach are presented to illustrate the effectiveness of the proposed technique.

6.2.1 Problem Formulation

Consider again the spatially discretized linear second-order ordinary differential equation (ODE) of a structural system in the matrix form given by Eqn. (3.1). For simple systems, $[M]$, $[C]$ and $[K]$ may be obtained by writing the system equations of motion; for complex systems they can be generated from the finite element model of the structure. Assuming that $\{\ddot{x}(t)\}$ is available, which will be discussed later, $\{\dot{x}(t)\}$ and $\{x(t)\}$ can be obtained upon successive numerical integration of $\{\ddot{x}(t)\}$. Given all the terms on the left-hand-side in Eqn. (3.1), they can be used to estimate the dynamic loads $\{f(t)\}$ exciting the structure. There are a number of problems associated with obtaining $\{\ddot{x}(t)\}$, to name a few:

- Each element in the vector $\{\ddot{x}(t)\}$ corresponds to a unique DOF in the structure. It is not possible to place accelerometers at all the DOFs of the structure to obtain $\{\ddot{x}(t)\}$ in full.

- Some means needs to be devised that allows for approximating $\{\ddot{x}(t)\}$ in full by taking acceleration measurements at few finite number of locations on the structure.

- Since the force input locations may not be accessible to mount accelerometers, the acceleration measurements cannot be taken at or around those locations.

- Since there can be a large number of locations on the structure where the accelerometers can potentially be mounted, a natural question arises: if finite number of accelerometers are to be used, where all should they be mounted on the structure such that precise load estimates are obtained.

The following sections present an approach to deal with the above mentioned problems.

6.2.2 Modal Model

Consider Eqn. (3.7) which is basically Eqn. (3.1) transformed into modal coordinates using the following modal transformations:

$$\{\ddot{x}(t)\} = [\phi]\{\ddot{q}(t)\}$$

$$\{\dot{x}(t)\} = [\phi]\{\dot{q}(t)\} \tag{6.9}$$

$$\{x(t)\} = [\phi]\{q(t)\}$$

where $[\phi]$ is the modal matrix and $\{q(t)\}$ is the vector of Modal Participation Factors (MPF). Since, in real world applications, seldom is the case when all the modes in $[\phi]$ are available, one generally has a reduced number of modes m available either from experimental modal analysis or finite element modal analysis, leading to $[\tilde{\phi}]$. Equation (3.7) then gets approximated as:

$$[M][\tilde{\phi}]\{\ddot{\tilde{q}}(t)\} + [C][\tilde{\phi}]\{\dot{\tilde{q}}(t)\} + [K][\tilde{\phi}]\{\tilde{q}(t)\} = \{f(t)\} \tag{6.10}$$

such that

$$\{\ddot{x}(t)\} \cong \{\ddot{\tilde{x}}(t)\} = [\tilde{\phi}]\{\ddot{\tilde{q}}(t)\}$$

$$\{\dot{x}(t)\} \cong \{\dot{\tilde{x}}(t)\} = [\tilde{\phi}]\{\dot{\tilde{q}}(t)\} \tag{6.11}$$

$$\{x(t)\} \cong \{\tilde{x}(t)\} = [\tilde{\phi}]\{\tilde{q}(t)\}$$

where $\{\tilde{q}(t)\}$ is the mode participation factor for the retained modes and $\{\tilde{x}(t)\}$ is the approximate reconstructed displacement vector. As will be made clear in due course of this chapter, it is desired to determine $\{\ddot{\tilde{q}}(t)\}$ at this point. The least-squares estimate of $\{\ddot{\tilde{q}}(t)\}$ is given by:

$$\{\ddot{\tilde{q}}(t)\} = \left([\tilde{\phi}]^T[\tilde{\phi}]\right)^{-1}[\tilde{\phi}]^T\{\ddot{\tilde{x}}(t)\} \tag{6.12}$$

As already stated, since it is not feasible to place accelerometers at all the DOFs on the structure to determine $\{\ddot{x}(t)\}$ completely, the solution to Eqn. (6.12) cannot be fully determined. A methodology is presented next to overcome the identified shortcoming.

6.2.3 Candidate Set

The maximum number of modes obtainable from the finite element model of a structure is equal to the total number of degrees of freedom of the model, which can be a large number. Decision needs to be made on the number of modes m to be retained to approximate the response of the structure; these are the modes whose MPF will be estimated at a later stage from the structure response to applied loads. The fraction of effective modal mass captured by the retained modes can be used to decide upon the number of modes to be retained in the analysis. It has been observed through experience that sufficient number of modes must be retained in the analysis such that the Mass Participation Factor captured by the retained modes is at least 90%.

As more accelerometers are used, the additional information on the accelerations helps to obtain a more precise estimate of $\{\tilde{\tilde{q}}(t)\}$, but practical and financial constraints place limitations on the number of accelerometers that can be used. If the number of mode participation factors to be estimated is m, then the inverse problem defined by Eqn. (6.12) must be over-determined to minimize the error in $\{\tilde{\tilde{q}}(t)\}$ estimates, i.e., the number of accelerometers a must satisfy the criterion $a \geq m$. Further refinement in the number of accelerometers can be made based upon the methodology discussed in Sec. 4.1.2.

Typically, there are a large number of locations on a structure where the accelerometers can potentially be mounted. These locations may exclude inaccessible

locations such as the regions of load application. Let the DOFs associated with all the locations where accelerometers can potentially be mounted be called the candidate degrees of freedom. Define $[\tilde{\phi}]_{cs}$ to be a subset of $[\tilde{\phi}]$ containing rows corresponding to the candidate DOFs only and eliminating the rest. $[\tilde{\phi}]_{cs}$ is called the candidate set.

6.2.4 D-optimal Design

Since it is not possible to measure accelerations at all the possible locations on a structure, to obtain an approximate solution to Eqn. (6.12), a subset of the candidate set $[\tilde{\phi}]_{cs}$ needs to be identified. In terms of a randomly selected subset $[\tilde{\tilde{\phi}}]$, the approximate solution to Eqn. (6.12) can be written as:

$$\{\tilde{q}(t)\} \cong \{\tilde{\tilde{q}}(t)\} = \left([\tilde{\tilde{\phi}}]^{T} [\tilde{\tilde{\phi}}] \right)^{-1} [\tilde{\tilde{\phi}}]^{T} \{\tilde{\tilde{x}}(t)\} \tag{6.13}$$

where $\{\tilde{\tilde{q}}(t)\}$ is an approximation to $\{\tilde{q}(t)\}$ and $\{\tilde{\tilde{x}}(t)\}$ is a random subset of $\{\tilde{x}(t)\}$. Compare Eqn. (6.13) to Eqn. (4.2); it is important to realize here that $[\tilde{\tilde{\phi}}]$ plays the same role in dynamic load recovery as $[A]$ in static load recovery. In practice, $\{\tilde{\tilde{x}}(t)\}$ is prone to measurement errors and the inverse problem identified by Eqn. (6.13) tends to be ill-conditioned. The accuracy of estimated $\{\tilde{\tilde{q}}(t)\}$ from measured acceleration response depends on the number and locations of accelerometers on the structure. $[\tilde{\tilde{\phi}}]$ needs to be such a subset of $[\tilde{\phi}]_{cs}$ that provides the most precise estimates of $\{\tilde{\tilde{q}}(t)\}$. For a given number of accelerometers a, following the D-optimal design algorithm described at

length in Sec. 4.1.3, the candidate set $[\tilde{\phi}]_{cs}$ is searched to determine its optimum subset $[\phi]_{opt}$.

Once $[\phi]_{opt}$ and, in turn, optimum accelerometer locations are determined, accelerometers are mounted at the identified optimum locations and acceleration $\{\ddot{x}(t)\}_{opt}$ is measured, which can then be numerically integrated successively to obtain $\{\dot{x}(t)\}_{opt}$ and $\{x(t)\}_{opt}$. $\left\{\tilde{\ddot{q}}(t)\right\}$, which is an approximation to $\{\ddot{q}(t)\}$, is then estimated using the deterministic form of Eqn. (6.13) as:

$$\{\tilde{\ddot{q}}(t)\} \cong \left\{\tilde{\ddot{q}}(t)\right\} = \left([\phi]_{opt}^{T}[\phi]_{opt}\right)^{-1}[\phi]_{opt}^{T}\{\ddot{x}(t)\}_{opt} \tag{6.14}$$

Similarly, $\{\tilde{\dot{q}}(t)\}$ and $\{\tilde{q}(t)\}$ are estimated from $\{\dot{x}(t)\}_{opt}$ and $\{x(t)\}_{opt}$, respectively. The applied load $\{f(t)\}$ can now be computed using Eqn. (6.10). It is to be noted that in this approach it is not necessary that acceleration measurements be taken at locations where forces are applied.

The above described approach, though seemingly promising, suffers from an inherent limitation. As will be shown in Sec. 6.2.6, the recovered loads get significantly underestimated due to errors associated with the truncation of modes. Moving from Eqn. (5.2) to Eqn. (5.3) results in truncation error which depends upon the number of modes retained. Acceptable load estimates may only be obtained by retaining a high number of modes in the analysis, which is rarely possible in real world problems. To overcome this limitation, a novel approach, which utilizes the technique of model order reduction, is proposed next. The approach, which when applied to the load recovery procedure, results in significant improvement in the load estimation.

6.2.5 Load Estimation Technique using Model Order Reduction

As described in Sec. 3.2, model order reduction methods, also referred to as condensation methods, aim at reducing the number of degrees of freedom in a model without changing its dynamic characteristics significantly. For the reasons mentioned in Sec. 3.2.3, fixed interface CMS, also known as Craig-Bampton model reduction, is used here in the load identification algorithm so that precise load estimated are obtained.

Having computed $\{\tilde{q}(t)\}$ and its derivatives through Eqn. (6.14), Eqns. (6.11), (3.30) and (3.31) are used to obtain $\begin{Bmatrix} \{x(t)\}_b \\ \{q(t)\}_p \end{Bmatrix}$ and its derivatives. The applied loads can subsequently be estimated using Eqn. (5.7). It is to be noted that the DOFs corresponding to the load application locations must be a subset of the boundary DOFs.

6.2.6 Example: 15-DOF Spring-Mass System with One Applied Load

The dynamic load estimation method discussed above is illustrated with the help of a numerical simulation comprising of the 15 degrees of freedom chain like spring-mass system described in Sec. 6.1.3 and shown in Fig. 6.1. A sinusoidal forcing function $f_7(t) = 500\sin(30\pi t) + 350\cos(20\pi t)$ is applied to mass m_7. The task is to determine the optimum accelerometer locations and reconstruct the input force based on the acceleration time response at those locations. Table 6.1 summarizes the relevant assumed inputs.

The system response was approximated using 4 modes. A total of 5 accelerometers were used to measure accelerations of 5 masses. The $[M]$, $[C]$ and $[K]$ matrices were obtained by writing the equations of motion for the system. The modal

matrix $[\phi]$ was obtained by solving the eigen-value problem for the system. In absence of any experimental data, the acceleration time responses at the relevant degrees of freedom were obtained by solving the ordinary differential equations numerically. All numerical computations were performed in a MATLAB programming environment.

All DOFs, except the DOF where the load was applied, were selected to be the locations where accelerometers can potentially be mounted, i.e., the DOF corresponding to the applied load did not form a part of the candidate set. When subjected to the D-optimal design algorithm, the optimum accelerometer locations were found to be at masses m_2, m_6, m_9, m_{10} and m_{13}. Using the acceleration data computed at the optimum accelerometer locations, the input force was recovered through Eqn. (6.10). Next, load identification procedure in conjunction with the Craig-Bampton model reduction was applied and the input force was recovered using Eqn. (5.7). For comparison purpose, static condensation was also utilized to recover the applied load in line with Eqn. (5.7). The actual applied load and the recovered loads using the 3 procedures are plotted in Fig. 6.5. To study the effect of accelerometer locations on the quality of recovered loads, an attempt was made to reconstruct the applied load using randomly selected accelerometer locations. Five uniformly distributed positive integer random numbers ≤ 15 were generated to simulate the random locations of the accelerometers. The randomly generated locations were at masses m_1, m_2, m_{10}, m_{13} and m_{15}. The load identification procedure in conjunction with the Craig-Bampton model reduction was again applied in an attempt to reconstruct the input force using Eqn. (5.7). The applied and reconstructed forces are plotted in Fig. 6.6.

It can be seen from Fig. 6.6 that load identification based on randomly selected accelerometer locations is very poor and does not yield acceptable results. This gives rise to the need for determining the optimal accelerometer locations such that precise load estimates are obtained. Also, as already discussed, it can be inferred from Fig. 6.5 that the recovered load using Eqn. (6.10) is significantly underestimated. This is due to the fact that only 4 out of the 15 possible modes were retained for the analysis which resulted in a large amount of truncation error. Better load estimates can be obtained by increasing the number of retained modes in the analysis, which is not always feasible. Some sign of improvement was detected when static condensation was applied to the load recovery procedure. A significant degree of improvement in recovered loads was observed when Craig-Bampton model reduction was applied to the load recovery procedure. Application of Craig-Bampton reduction to load recovery, though promising, still seems to suffer from the limitation of underestimating the applied loads by a small amount. Introduced next is further improvement in the ongoing load identification algorithm based on reduced modal matrix.

6.2.7 Reduced Modal Parameter Based Algorithm for Load Estimation

Consider the reduced model equation of motion in matrix form given by Eqn. (5.7). A solution to the eigen-value problem for the reduced system yields the Craig-Bampton reduced modal matrix $[\phi]_{CB}$. Since $[M]_{CB}$ and $[K]_{CB}$ are meant to capture the dynamic characteristics of the full model, $[\phi]_{CB}$ also captures the modal information of the full model. Similar to Eqn. (6.9), the reduced model can be transformed to modal coordinates using the following transformation:

$$\begin{Bmatrix} \{\ddot{x}(t)\}_b \\ \{\ddot{q}(t)\}_p \end{Bmatrix} = [\phi]_{CB}\{\ddot{q}(t)\}_{CB} \qquad (6.15)$$

where $\{q(t)\}_{CB}$ is the MPF of the Craig-Bampton reduced normal modes. Pre-multiplying Eqn. (6.15) by $[\psi]_{CB}$ yields:

$$[\psi]_{CB}\begin{Bmatrix} \{\ddot{x}(t)\}_b \\ \{\ddot{q}(t)\}_p \end{Bmatrix} = [\psi]_{CB}[\phi]_{CB}\{\ddot{q}(t)\}_{CB} \qquad (6.16)$$

Using Eqn. (3.30) and substituting $[\phi]_u$ for $[\psi]_{CB}[\phi]_{CB}$ gives:

$$\{\ddot{x}(t)\} = [\phi]_u\{\ddot{q}(t)\}_{CB} \qquad (6.17)$$

Compare Eqn. (6.17) to Eqn. (6.11). It must be noted that $[\phi]_u$ captures the dynamic characteristics of the system better than $[\tilde{\phi}]$ as none of the modes in $[\phi]_u$ have been truncated. Therefore, computation of $\{\ddot{x}(t)\}$ using Eqn. (6.17) is expected to be more accurate than using Eqn. (6.11). Again, similar to Eqns. (6.12) and (6.13), $\{\ddot{q}(t)\}_{CB}$ needs to be determined from Eqn. (6.17) by measuring acceleration at optimum locations on the structure. Following the procedure described in Sec. 6.2.3 and 6.2.4 and treating $[\phi]_{u\_cs}$, a subset of $[\phi]_u$, as the candidate set, optimum subset $[\phi]_{u\_opt}$ of the candidate set is determined by D-optimal design and thereby optimum locations for accelerometer placement are identified.

Next, accelerometers are mounted at the identified optimum locations on the structure and $\{\ddot{x}(t)\}_{opt}$ is measured, which can then be numerically integrated successively to obtain $\{\dot{x}(t)\}_{opt}$ and $\{x(t)\}_{opt}$. $\{\tilde{\tilde{q}}(t)\}_{CB}$, which is an approximation to $\{\ddot{q}(t)\}_{CB}$, is estimated similar to Eqn. (6.14) as:

$$\{\ddot{q}(t)\}_{CB} \cong \{\tilde{\tilde{q}}(t)\}_{CB} = \left([\phi]_{u\_opt}^T[\phi]_{u\_opt}\right)^{-1}[\phi]_{u\_opt}^T\{\ddot{x}(t)\}_{opt} \qquad (6.18)$$

Having computed $\{\ddot{q}(t)\}_{CB}$, $\{\ddot{x}(t)\}$ is determined in full using Eqn. (6.17). Again, Eqns. (3.30) and (3.31) are used to obtain $\begin{Bmatrix} \{x(t)\}_b \\ \{q(t)\}_p \end{Bmatrix}$ and its derivatives. The applied loads can finally be estimated using Eqn. (5.7). It is to be noted again that the DOFs corresponding to the load application locations must be a subset of the boundary DOFs.

6.2.8 Example: Application of the Reduced Modal Parameter Based Algorithm to Load Estimation

The numerical example described in Sec. 6.2.6 was revisited and the problem was solved using the reduced modal matrix based algorithm proposed above. Again, all DOFs, except the DOF where the load was applied, were selected to be the locations where accelerometers can potentially be mounted, i.e., the DOF corresponding to the applied load did not form a part of the candidate set. When subjected to the D-optimal design algorithm, the optimal accelerometer locations were found to be at masses m_2, m_5, m_8, m_{10} and m_{13}. Using the acceleration data computed at the optimal accelerometer locations and following the improved load estimation technique, the input force was recovered through Eqn. (5.7). The actual applied load and the smoothed recovered loads are plotted in Fig. 6.7. Using Eqn. (3.33), the rms error was calculated to be 7.2% in recovered load using Craig-Bampton reduction and 1.3% in recovered load using the reduced modal parameter based algorithm. It can be inferred from the plot that there is almost perfect agreement between the applied and the recovered load. This implies that the reduced modal matrix based algorithm provides a better degree of load recovery than any of the other techniques discussed.

6.2.9 Example: 15-DOF Spring-Mass System with Two Applied Loads

The previous example is extended to the case when two applied loads are present. Loads $f_3(t) = 500\sin(30\pi t) + 350\cos(20\pi t)$ and $f_9(t) = 250\sin(25\pi t) + 450\cos(15\pi t)$ are applied to masses m_3 and m_9, respectively. The task is to determine the optimum accelerometer locations and reconstruct the input forces based on the acceleration time response at those locations. Table 6.2 summarizes the relevant assumed inputs. The number of accelerometers used is increased from 5 to 6 since more number of loads needs to be recovered here. The input loads were reconstructed following the approach discussed in Secs. 6.2.5 and 6.2.7. Using the two approaches, the optimal accelerometer locations were found to be at masses $m_2, m_4, m_7, m_8, m_{12}, m_{13}$ and masses $m_2, m_5, m_7, m_8, m_{11}, m_{13}$, respectively. The applied and recovered loads are plotted in Figs. 6.8 and 6.9. Using Eqn. (3.33), the rms error was calculated to be 5.9% in recovered load $f_3(t)$ using Craig-Bampton reduction and 1.2% in recovered load $f_3(t)$ using the reduced modal parameter based algorithm. The rms error was calculated to be 18.9% in recovered load $f_9(t)$ using Craig-Bampton reduction and 2.3% in recovered load $f_9(t)$ using the reduced modal parameter based algorithm. Once again, it is inferred that the reduced modal matrix based algorithm is more effective than other techniques discussed.

6.2.10 Example: Cantilevered Beam

The numerical example discussed previously dealt with a discrete system. Presented next is a continuous system where the dynamic load estimation technique is illustrated with the help of numerical simulation of a cantilevered beam. A vertical load, $f(t) = 500\sin(30\pi t) + 350\cos(20\pi t)$, acting at free end of the beam is reconstructed

from measured accelerations along the beam. A finite element model of the beam was developed similar to Sec. 5.5. The assumed inputs are provided in Table 6.3.

The $[M]$ and $[K]$ matrices were obtained using finite element method. ANSYS provides data on the $[M]$ and $[K]$ matrices in the Harwell-Boeing file format; a routine written in MATLAB was used to convert them into the matrix format suitable for current application. The D-optimal design criterion was utilized to determine the optimum accelerometer locations, following which, the acceleration data at those locations was obtained from the finite element transient analysis of the beam in ANSYS. The optimum accelerometer locations are also shown in Fig. 6.10. The input load was reconstructed following the approach discussed in Sec. 6.2.5 and 6.2.7. The applied and recovered loads are plotted in Fig. 6.11. The rms error using Eqn. (3.33) was calculated to be 1.8%. It can be seen that the applied load is recovered accurately for this 600 DOF system by approximating the complete response using 7 modes and measuring accelerations at 8 optimum locations.

Based on the results for both examples, it can be seen that for discrete as well as continuous systems, the proposed approach is able to accurately estimate the loads acting on a component by measuring the acceleration response at a finite number of optimum locations.

6.3 Summary

In this chapter, two algorithms are presented that allow for indirect identification of vibration inducing dynamic loads applied to a structure. The algorithms are based on acceleration measurements at finite number of optimal locations on the structure such that

best possible load estimates are obtained. In Sec. 6.1, to determine the optimum locations for the accelerometers, the sparse nature of mass, damping and stiffness matrices is utilized. With the aid of a numerical example, it is illustrated that randomly selected accelerometer locations yield poor load estimation. Excellent agreement between the applied and recovered load is observed when acceleration data from optimum locations of accelerometers is used. This approach, however, suffers from the limitation that the accelerometers need to be collocated with the forces, which is not always feasible.

To deal with the aforementioned shortcoming, an alternate algorithm is presented in Sec. 6.2 for estimating dynamic loads exciting the structure from acceleration time response measured experimentally at a finite number of optimally placed non-collocated accelerometers on the structure. D-optimal design technique is used to determine the optimum accelerometer locations such that best possible load estimates are obtained from the measured acceleration data. It is observed that the load recovered from optimally placed accelerometer data and unreduced model is highly underestimated due to large amount of truncation error resulting from few retained modes. Introduction of static condensation in load recovery shows some improvement in the load estimation, but it still underestimates the applied load. Still better load estimates are obtained by utilizing Craig-Bampton model reduction technique. A very good agreement in the applied and the recovered load is observed when the proposed reduced modal matrix based algorithm is utilized in conjunction with optimal accelerometer locations. The numerical examples illustrate the effectiveness of the proposed approach in recovering multiple time varying loads in discrete as well as continuous systems which induce significant level of vibrations in the structure.

Table 6.1 Input Data for Spring-Mass System Example with One Applied Load

Variable	Value	Variable	Value	Variable	Value
n	15	c	14	a	5
m	4	b	7	p	4

Table 6.2 Input Data for Spring-Mass System Example with Two Applied Loads

Variable	Value	Variable	Value	Variable	Value
n	15	c	13	a	6
m	3	b	3, 9	p	4

Table 6.3 Input Data for Cantilevered Beam Example

Variable	Value	Variable	Value	Variable	Value
n	600	c	597	a	8
m	7	b	213, 280, 372, 425	p	2
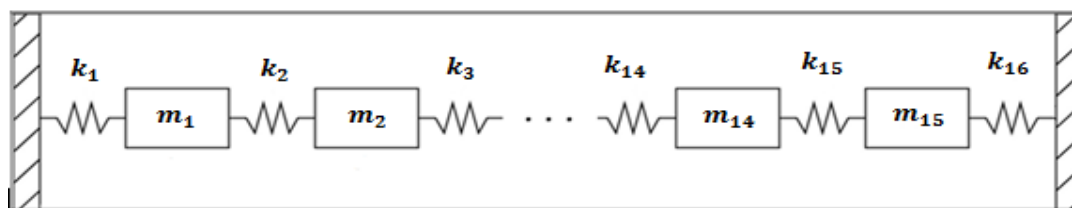
Figure 6.1 15-DOF Spring-Mass System
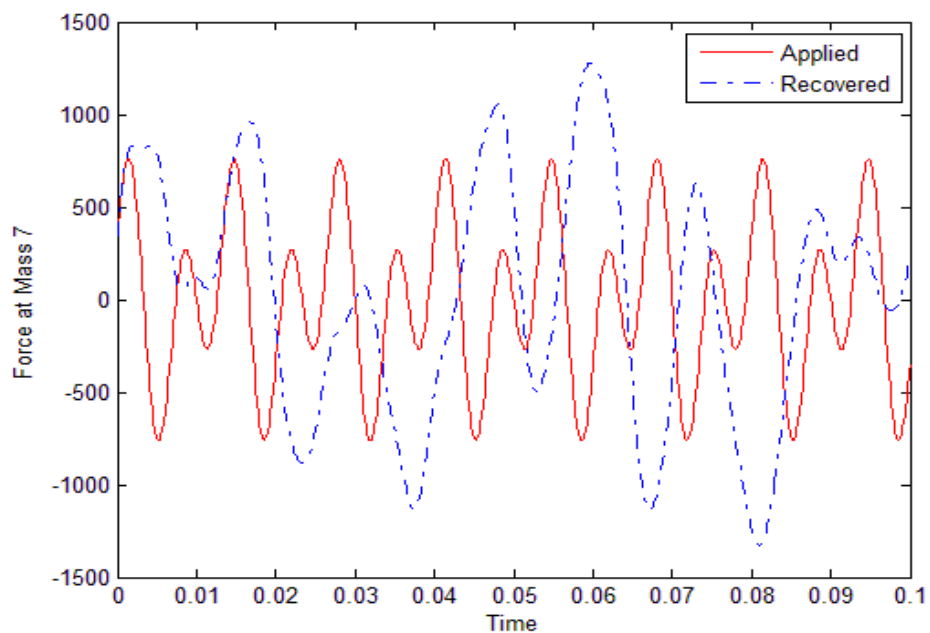
Figure 6.2 Applied and Recovered Force with Random Accelerometer Locations at Masses 2, 7, 10 and 14
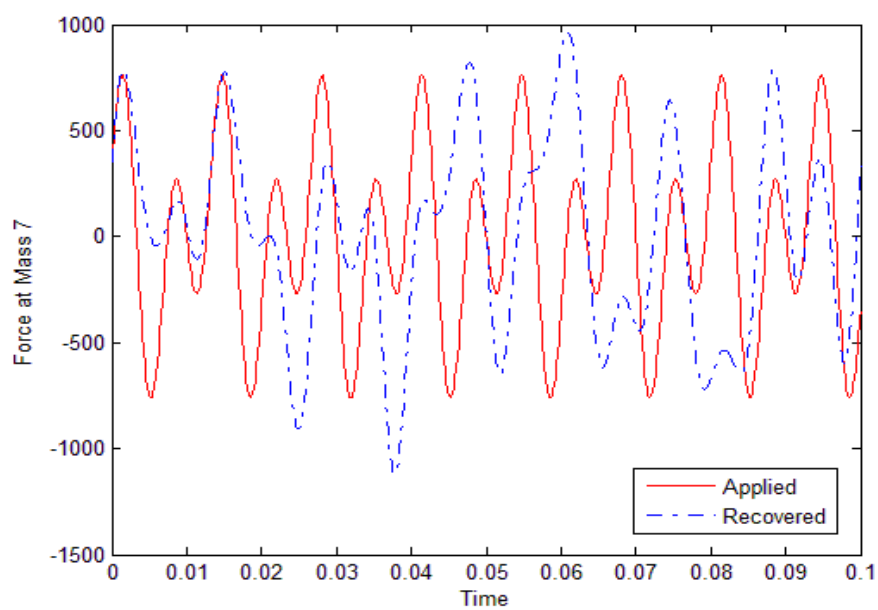
Figure 6.3 Applied and Recovered Force with Random Accelerometer Locations
at Masses 3, 6, 7, 9 and 14
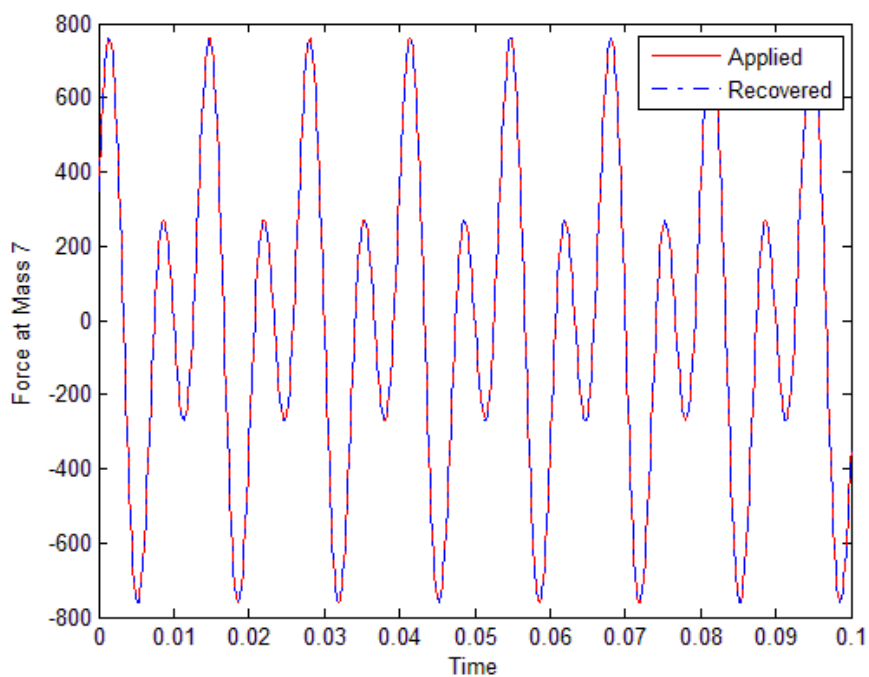
Figure 6.4 Applied and Recovered Force with Optimal Accelerometer Locations at Masses 6, 7 and 8
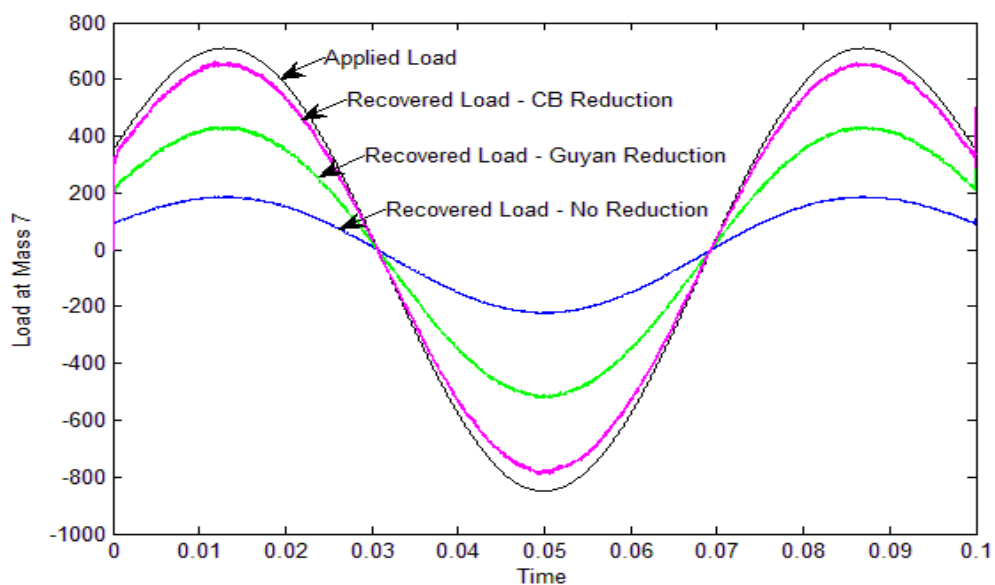
Figure 6.5 Applied and Recovered Loads at Mass 7 with Optimum Accelerometer Placements
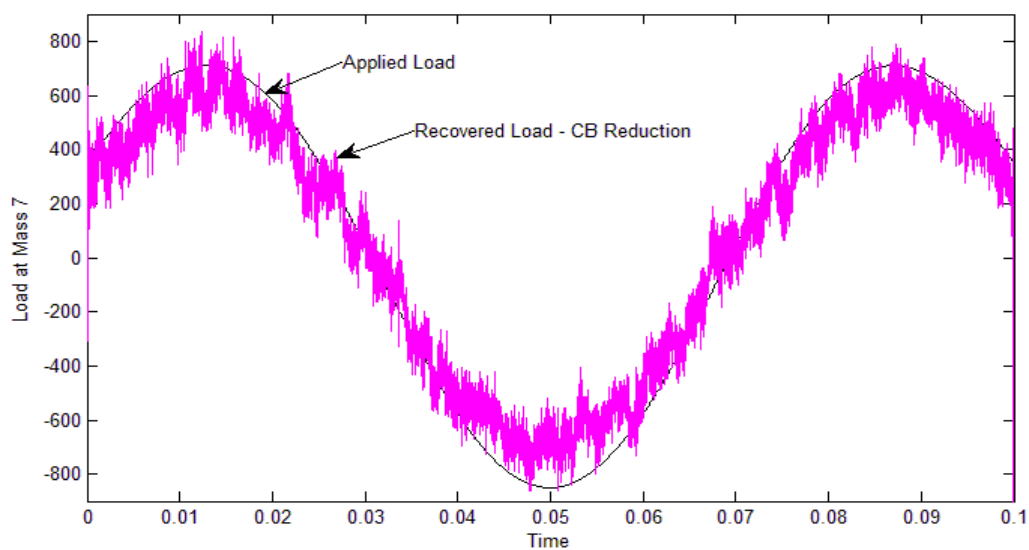
Figure 6.6 Applied and Recovered Load at Mass 7 with Random Accelerometer Placements
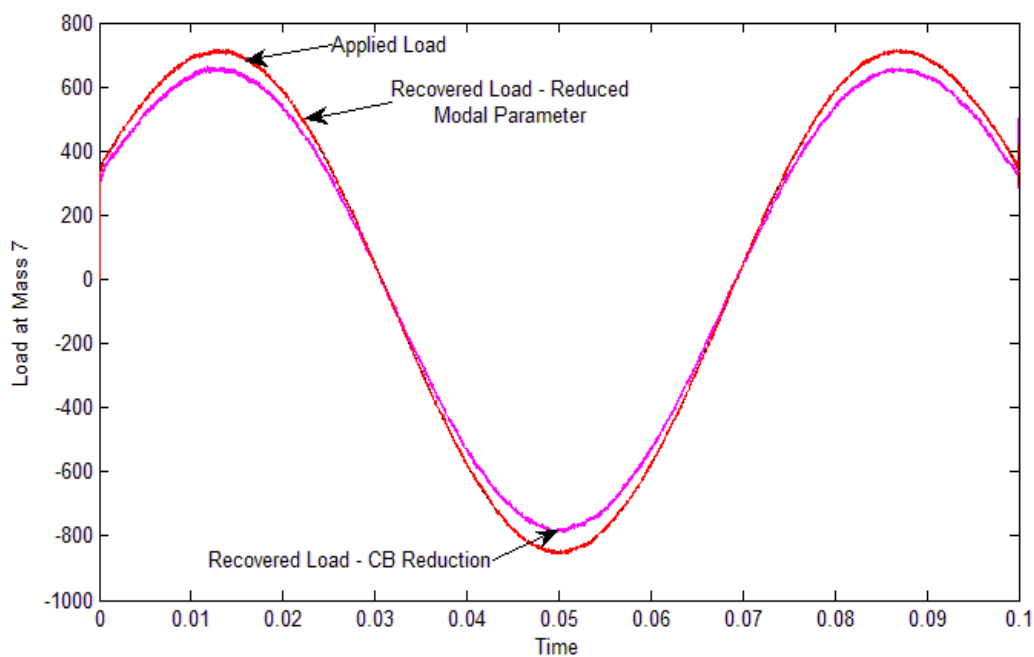
Figure 6.7 Applied and Recovered Loads at Mass 7 with Optimum Accelerometer Placements
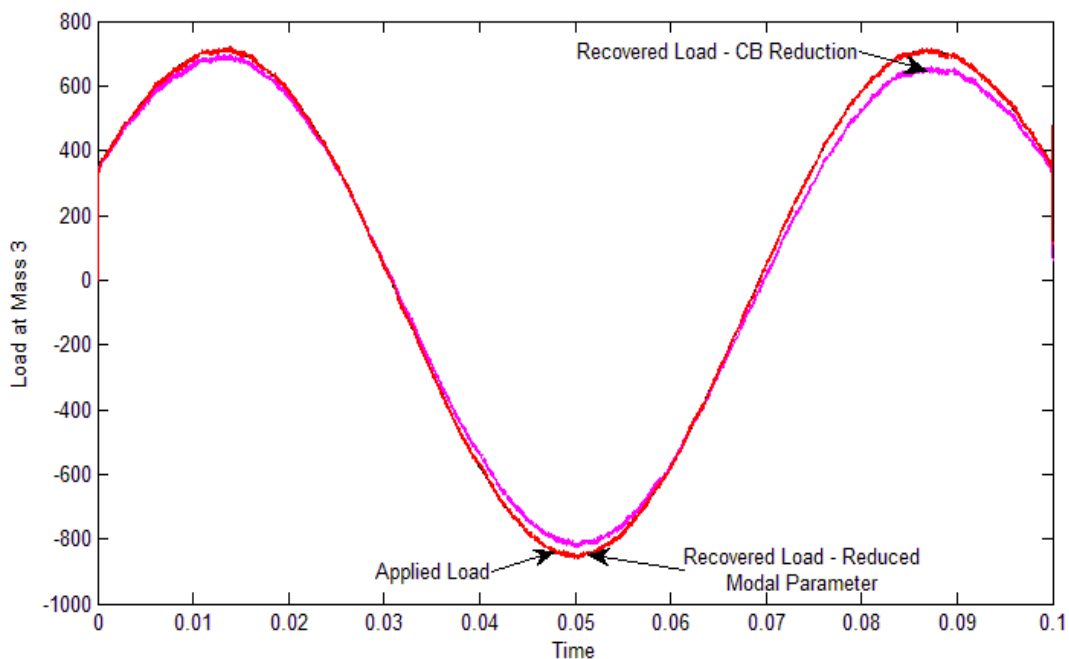
Figure 6.8 Applied and Recovered Loads at Mass 3 with Optimum Accelerometer Placements
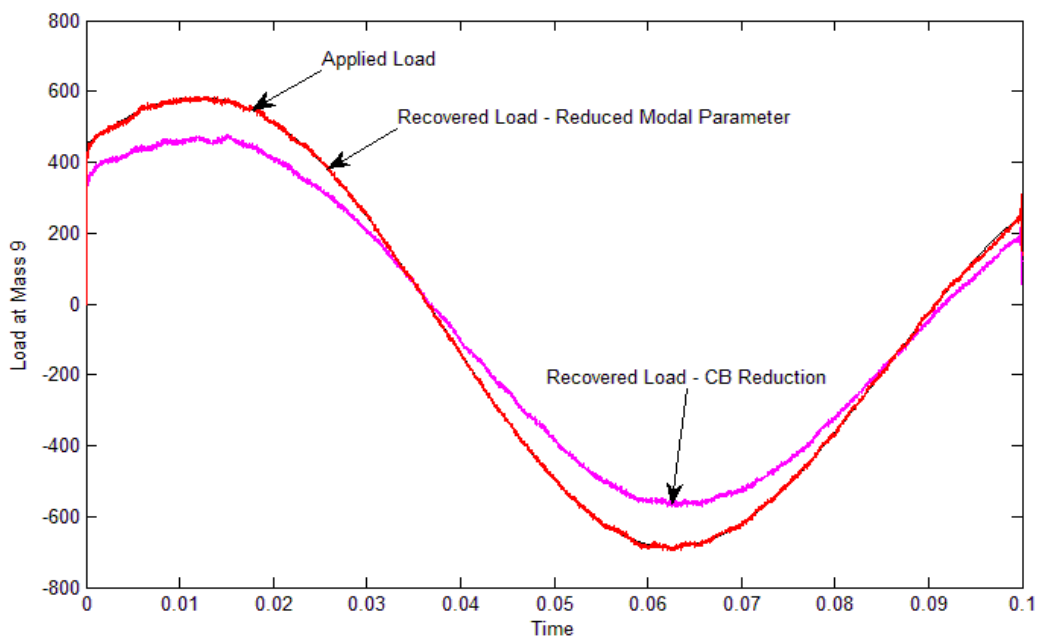
Figure 6.9 Applied and Recovered Loads at Mass 9 with Optimum Accelerometer Placements
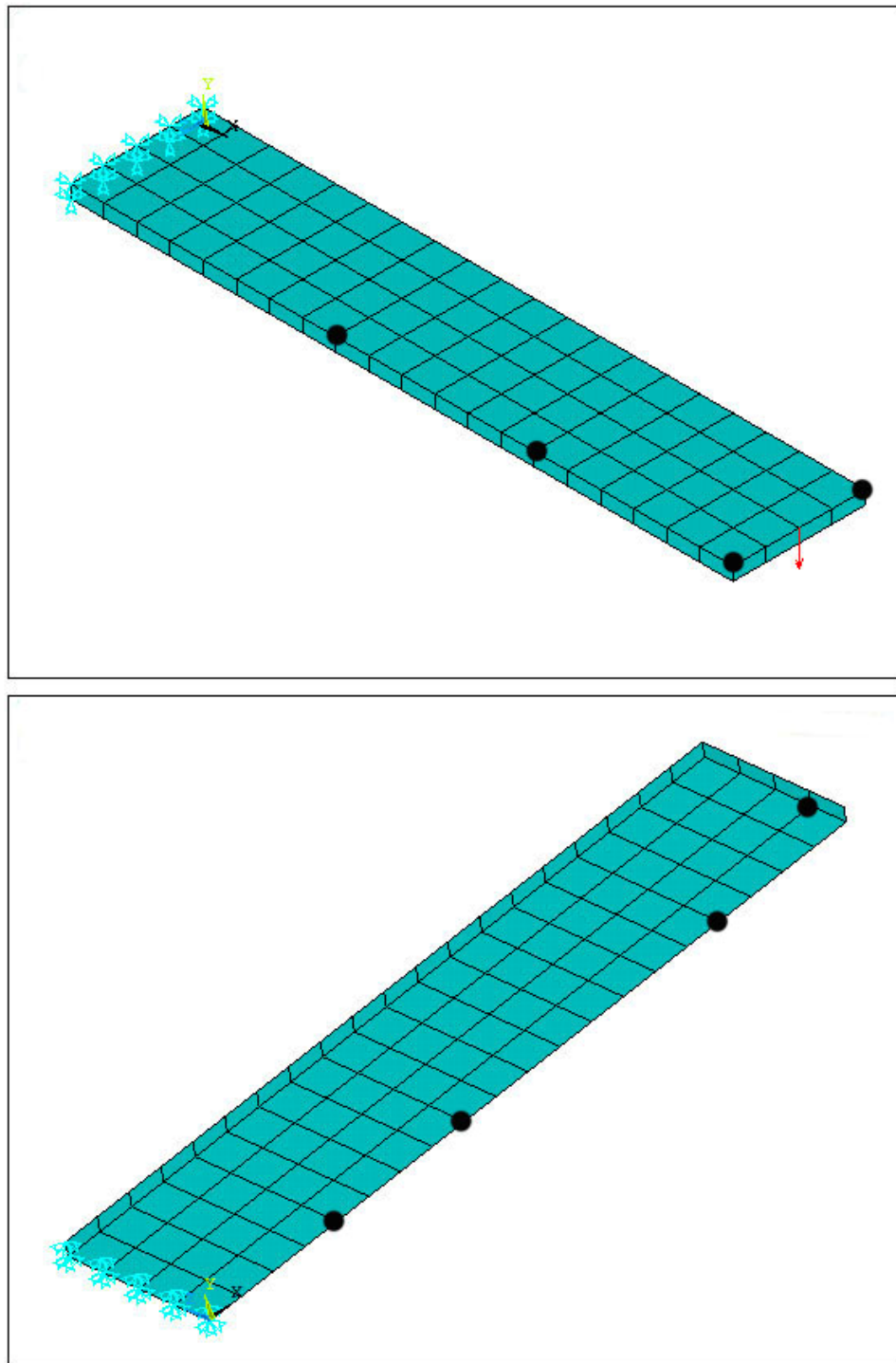
Figure 6.10 Finite Element Model of Cantilever Beam Depicting Applied Load
and Optimum Accelerometer Locations
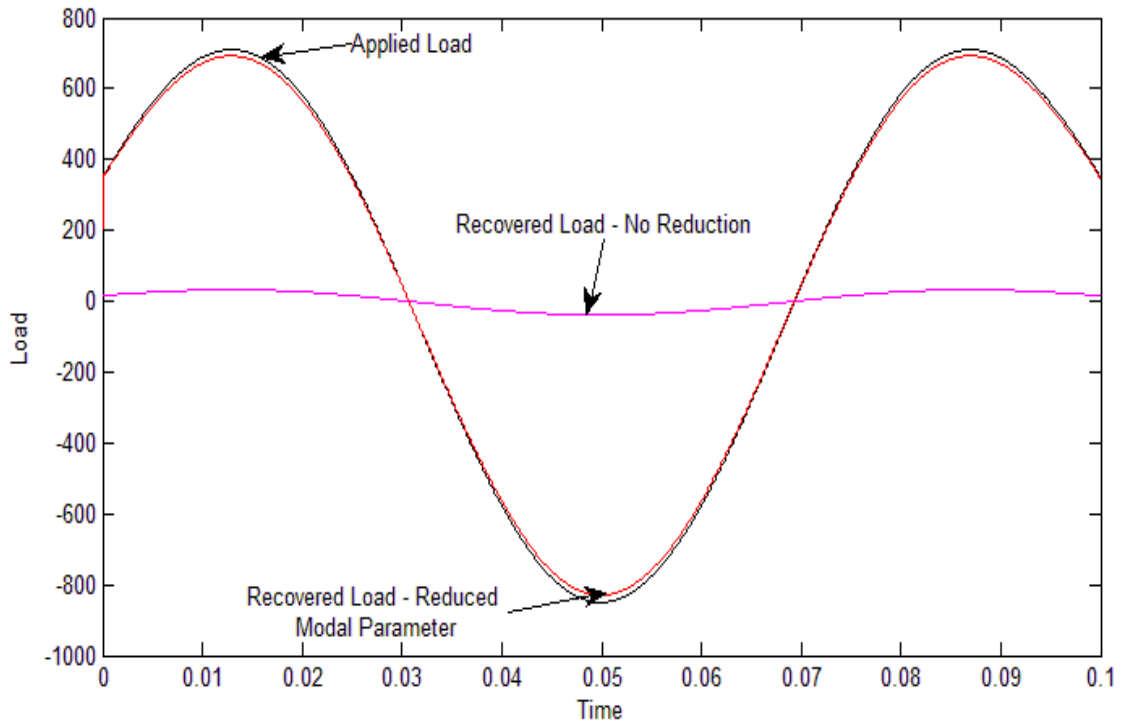
Figure 6.11 Applied and Recovered Loads with Optimum Accelerometer Placements

Chapter 7 - Dynamic Programming Approach to Load Estimation

Apart from the strain and acceleration measurement based techniques developed and described previously in this thesis, there exists another inverse technique developed by Busby and Trujillo (1987) to identify the loads applied to a structure from its experimentally measured response. The technique is based on dynamic programming and consists of a backward (inverse) time sweeping phase followed by a forward time sweeping phase. In the backward sweep, certain matrices and vectors are calculated recursively for all the time steps. These recursive relations are a function of the system parameters and experimental response measurements. The forward sweep then uses these relations to predict the applied loads as well as the structure response. Load estimation problem is cast as a minimization problem of error which is defined as the difference between the measured structural response and the response predicted from the model. Dynamic programming is used to solve the minimization problem.

It has been studied by Hollandsworth and Busby (1989) that the quality of load estimates depends on the locations of sensors on the structure. The technique of D-optimal design algorithm is utilized in this chapter to arrive at optimal sensor placement such that precise load estimates are obtained. One of the disadvantages of the dynamic programming technique is that the computation time increases dramatically as the model order increases. To deal with this shortcoming, a technique based on Craig-Bampton model order reduction is further proposed in this chapter.

7.1 The Dynamic Programming Approach

Consider the discrete linear time-invariant state-space equation given by Eqn. (3.10) that characterizes the input-output behavior of a structural system. In the forward problem, given the system information and the applied load history $\{f\}$, the system responses $\{u\}$ can be solved recursively starting from the known initial conditions. In the inverse problem of interest here, it is desired to solve for the unknown forces $\{f\}$, given the system information and system responses.

Busby and Trujillo (1987) cast the load estimation problem as a minimization problem which can be stated as, "Given the system matrix $[A_d]$, the input matrix $[B_d]$ and the measurements on some of the state variables, find the unknown forces $\{f\}$ that cause the model, Eqn. (3.10), to best match the measurements". Since it is not possible to measure all of the state variables $\{u\}$, it is convenient at this point to introduce the following expression:

$$\{d\}_{ti} \Leftrightarrow [Q]\{u\}_{ti} \tag{7.1}$$

where $\{d\}_{ti}$ is an $(n_s \times 1)$ vector representing the experimental response measurements, n_s is the number of sensors and $[Q]$ is an $(n_s \times 2n)$ transformation matrix describing the locations of sensors. Since the measured response data $\{d\}$ always contains noise or errors, the least-squares sum is the most common method for error quantification. The optimization problem to determine the unknown forces $\{f\}$ is written as a minimization of the least-squares error function stated as:

$$E(u,f) = \sum_{ti=1}^{N} (\{d - Qu\}_{ti}^{T}[W]\{d - Qu\}_{ti})$$

(7.2)

$$\{u\}_{ti+1} = [A_d]\{u\}_{ti} + [B_d]\{f\}_{ti}$$

where $[W]$ is a general weighing diagonal matrix on the data. Unfortunately, this least-squares criterion is not sufficient in the current application because any mathematical solution that will minimize the error function E will end up with the model exactly matching the measured data, a trivial solution. This limitation is overcome by using a method called Tikhonov Regularization, where a regularization term is added to the above least-squares error function as:

$$E(u,f) = \sum_{ti=1}^{N} (\{d - Qu\}_{ti}^{T}[W]\{d - Qu\}_{ti} + \{f\}_{ti}^{T}[H]\{f\}_{ti})$$

(7.3)

$$\{u\}_{ti+1} = [A_d]\{u\}_{ti} + [B_d]\{f\}_{ti}$$

Essentially, it is desired to find the input forces $\{f\}$ that cause the model $[Q]\{u\}$ to match the measured response data $\{d\}$ as closely as possible. In other words, the problem is to minimize the least-squares error function E over the sequence of forcing vectors $\{f\}_{ti}$. The minimization problem can be solved by using the structure of dynamic programming and Bellman's Principle of Optimality. A full derivation of the solution is not presented here; its details can be found in Trujillo and Busby (1997). The solution to the above minimization problem is given by the following recurrence relations:

$$\{f^*\}_{ti} = -[D]_{ti+1}(2[B_d]^{T}[R]_{ti+1}^{T}[A_d]\{u\}_{ti} - [B_d]^{T}[S]_{ti+1})$$

(7.4)

$$\{u\}_{ti+1} = [A_d]\{u\}_{ti} + [B_d]\{f\}_{ti}$$

where

$$[D]_{ti} = \left[2[H] + 2[B_a]^T[R]_{ti}[B_a]\right]^{-1}$$

$$[R]_{ti-1} = [Q]^T[W][Q] + [A_a]^T([R]_{ti} - 2[R]_{ti}[B_a][D]_{ti}[B_a]^T[R]_{ti})[A_a] \qquad (7.5)$$

$$[S]_{ti-1} = -2[Q]^T[W]\{d\}_{ti-1} + [A_a]^T([I] - 2[R]_{ti}[B_a][D]_{ti}[B_a]^T)[S]_{ti}$$

The complete sequence of operations is as follows:

- The backward sweep: Solve Eqn. (7.5) backward and store $[D]$, $[R]$ and $[S]$ starting with the following initial conditions:

$$[R]_N = [Q]^T[W][Q]$$

$$[S]_N = -2[Q]^T[W]\{d\}_N$$

$$(7.6)$$

- The forward sweep: Starting with the initial condition for $\{u\}$, compute the optimal $\{f^*\}$ using Eqn. (7.4) and keep updating $\{u\}$.

As mentioned earlier, there can be a large number of locations on the structure where the sensors can potentially be mounted, and the quality of the load estimates depends on the locations of sensors on the structure. In the procedure described above, the sensor locations are described by the variable $[Q]$ that maps the state variables to the sensor locations. Discussed next is the procedure to obtain optimum sensor locations, and hence $[Q]_{opt}$, such that the loads are estimated precisely.

7.2 Candidate Set and D-optimal Design

It can be observed in the load identification procedure described above that there exists a matrix inversion step – the computation of $[D]_{ti}$ in Eqn. (7.5) – which is similar to the matrix inversion for the computation of $\{f\}$ in Eqn. (4.2). The computation of $[D]$ depends on three matrices – $[H]$, $[R]$ and $[B_a]$. Out of the three matrices, $[H]$ and $[R]$ are generally well-conditioned. It may also be noted that $[R]$ varies with time; therefore, it is

rather infeasible to consider it as a candidate for optimization towards further well-conditioning, even if so desired. The remaining matrix $[B_d]$ can be identified as the one that poses potential ill-conditioning in the computation of $[D]$. Similar to Eqn. (4.3), the variance in $[D]$ depends on $[B_d]$. It may further be assessed through Eqn. (7.4) that the estimation of load $\{f^*\}$ depends directly on $[D]$. Therefore, optimal selection of sensor locations, and hence the optimum matrix $[B_d]$, leads to increased accuracy in the estimation of load $\{f^*\}$.

It must be noted that half of the rows in $[B_d]$ corresponds to state variables and the other half corresponds to their derivatives. To form a candidate set for optimization, first of all, only that half of the rows in $[B_d]$ needs to be retained that corresponds to the measured quantity (state variables or their derivatives). From the subset so obtained, the DOFs (rows) corresponding to force locations and other inaccessible locations for sensor placement are ignored; the subset so obtained is the candidate set $[B_d]_{cs}$.

As more sensors are used, the additional information helps to obtain a more precise estimate of $\{f^*\}$, but practical and financial constraints place limitations on the number of sensors that can be used. If the number of forces to be estimated is n_f, then in order to minimize the error in $\{f^*\}$ estimates, the number of sensors a must satisfy the criterion $a \geq n_f$. Further refinement in the number of sensors can be made based upon the methodology discussed in Sec. 4.1.2.

Having obtained the candidate set $[B_d]_{cs}$, for a given number of sensors, the D-optimal design algorithm described in Sec. 4.1.3 is followed to search $[B_d]_{cs}$ to determine the optimum sensor locations. Once the optimal locations for sensors is determined, $[Q]_{opt}$ is obtained which consists of 1's at the locations corresponding to

optimum sensor locations and the 0's at the remaining locations. Equations (7.4) – (7.6) are then utilized to compute the input forces $\{f^*\}$.

7.3 Example: 15-DOF Spring-Mass System

The above described procedure was applied numerically to the 15 degrees of freedom chain like spring-mass system described in Sec. 6.1.3 and depicted in Fig. 6.1. A sinusoidal forcing function $f_7(t) = 1000\sin(55\pi t) + 600\cos(35\pi t)$ is applied to mass m_7. The task is to determine the optimum accelerometer locations and reconstruct the input force based on the acceleration time response at those locations.

A total of 2 accelerometers were used to measure accelerations of 2 masses. The $[M]$, $[C]$ and $[K]$ matrices were obtained by writing the equations of motion for the system. Continuous time-invariant state-space form of the system was obtained using the equations described in Sec. 3.1.3. In absence of any experimental data, the acceleration time response at the optimum locations were obtained by solving the ordinary differential equations numerically. All DOFs, except the DOF where the load was applied, were selected to be the locations where accelerometers can potentially be mounted, i.e., the DOF corresponding to the applied load did not form a part of the candidate set. All numerical computations were performed in a MATLAB programming environment.

When subjected to the D-optimal design algorithm as described in Sec. 7.2, the optimum accelerometer locations were found to be at masses m_6 and m_8. Using the acceleration data computed at the optimum accelerometer locations, the input force was recovered using Eqns. (7.4) – (7.6). The applied and the recovered loads are plotted in Fig. 7.1. It can be inferred from the plot that the applied load is recovered accurately.

7.4 Example: Crane Load Block

The previous example dealt with a simple spring-mass system. Presented next is a more general numerical example where a vertical dynamic load acting on a crane hoist load block, through a load suspended on its hook, needs to be estimated. An overhead crane along with its trolley is shown in Fig. 7.2. A more detailed image of the trolley and the load block is given in Fig. 7.3. A sinusoidal input vertical forcing function $f(t) = 750\sin(60t) + 900\cos(75t)$ is assumed to be applied to the load block. The problem is to determine the optimum accelerometer locations and reconstruct the input force based on the acceleration time response at those locations.

A finite element model of the load block was developed in ANSYS using SHELL181 elements. The finite element model of the load block along with the applied load and boundary conditions is shown in Fig. 7.4. The model was simplified and all holes were eliminated in order to enable generation of quad-mesh. The model consisted of 272 shell elements and 321 unconstrained nodes with 3 degrees of freedom per node (the rotational degrees of freedom were ignored), i.e., the total number of degrees of freedom of the model was 963.

The $[M]$ and $[K]$ matrices were obtained using finite element method. ANSYS provides data for $[M]$ and $[K]$ matrices in the Harwell-Boeing file format. A routine was written in MATLAB to convert them into the matrix format suitable for current application. The damping $[C]$ was assumed to be 0.01% of $[K]$. All further calculations were performed in MATLAB. Continuous time-invariant state-space form of the system is obtained using the equations described in Sec. 3.1.3. In absence of any experimental

data, the acceleration time response at the optimum locations were obtained by solving the ordinary differential equations numerically.

Load identification solution procedure based on optimal accelerometer locations was applied to the given problem. All DOFs, except the DOF where the load was applied, were selected to be the locations where accelerometers can potentially be mounted, i.e., the DOF corresponding to the applied load did not form a part of the candidate set. The number of accelerometers was arbitrarily assumed to be 5. After determining the optimal accelerometer locations based on the procedure described in Sec. 7.2, the input force was reconstructed using Eqns. (7.4) – (7.6). The applied and reconstructed forces are plotted in Fig. 7.5. It can be inferred that they are in good mutual agreement.

7.5 Load Estimation Technique using Model Order Reduction

The load block example discussed in the previous section took a while to execute and produce results. Application of the dynamic programming technique is limited since the computation time increases dramatically as the order of the model increases. The number of DOF in the load block example is 963. For complex structures, the number of degrees of freedom can be quite large; therefore, the enormous amount of time taken by the dynamic programming technique to yield meaningful results may render the procedure unworthy of application. To deal with this shortcoming, a technique based on Craig-Bampton model order reduction is proposed to reduce the computational burden.

The full model of the system is taken into consideration in order to determine the optimum sensor locations based on the technique described in Sec. 7.2. The full model matrices $[M]$, $[C]$ and $[K]$ are subjected to Craig-Bampton model order reduction method

described in Sec. 3.2.3 to yield the Craig-Bampton reduced matrices $[M]_{CB}$, $[C]_{CB}$ and $[K]_{CB}$ per Eqn. 3.32. The reduced matrices are then used to transform the model into discrete time-invariant state-space model per Eqn. (3.10). The applied load $\{f^*\}$ can then be reconstructed using the technique described in Sec. 7.1 and Eqns. (7.4) – (7.6).

7.6 Example Revisited: Crane Load Block

The load block example described in Sec. 7.4 was revisited and load identification procedure in conjunction with the Craig-Bampton model reduction explained in Sec. 7.5 was applied. The 963 DOF system was reduced to 36 DOF system and the input load was reconstructed following the procedure similar to Sec. 7.4. The applied and recovered loads are plotted in Fig. 7.6. After the structure response from optimal accelerometer locations are obtained, a comparison of computation time elapsed in reconstructing the applied loads was made. The computation time for the full model was observed to be 258.74 s which decreased to a mere 5.56 s for the reduced model.

It may be noted that Figs. 7.5 and 7.6 correspond to the case when no error was assumed to be present in acceleration measurements. Next, to simulate a more realistic scenario where accelerations are measured experimentally, the acceleration response vector $\{d\}$ was corrupted with normally distributed random errors with zero mean and standard deviation of 10% of its value. The applied and recovered loads, with errors in acceleration measurements, are plotted in Figs. 7.7 and 7.8; the rms errors using Eqn. (3.33) were calculated to be 8.5% and 12.3% respectively. It can be concluded from the plots that the proposed approach is robust in recovering the applied loads precisely even when significant measurement errors are present in the structure response.

7.7 Summary

A computational technique is studied where load estimation problem is cast as a minimization problem of error which is defined as the difference between the measured structural response and the response predicted from the model. Dynamic programming is used to solve the minimization problem. The quality of load estimates depends on the locations of sensors on the structure. To improve the precision of load estimates, the technique of D-optimal design in conjunction with finite element analysis is utilized to determine the optimum sensor locations. It is observed that the loads recovered based on accelerations measured from optimally placed accelerometers on the structure are in excellent agreement with the applied loads.

One of the disadvantages of the dynamic programming technique is that the amount of computation increases dramatically as the order of the model increases. To overcome this limitation, a technique based on Craig-Bampton model order reduction is further proposed. It is observed that the load recovered using the reduced model shows a deviation initially, but later follows the applied load closely. For the example considered herein, it is seen that with the introduction of model order reduction, the computation time can be reduced by as much as 98% without compromising on the quality of load estimates. This result deems the dynamic programming technique of load identification, in conjunction with model order reduction, worthy to be applied to higher order problems of increased complexity. The robustness of the approach is demonstrated such that the loads are reconstructed precisely even when errors are present in the measured structure response.
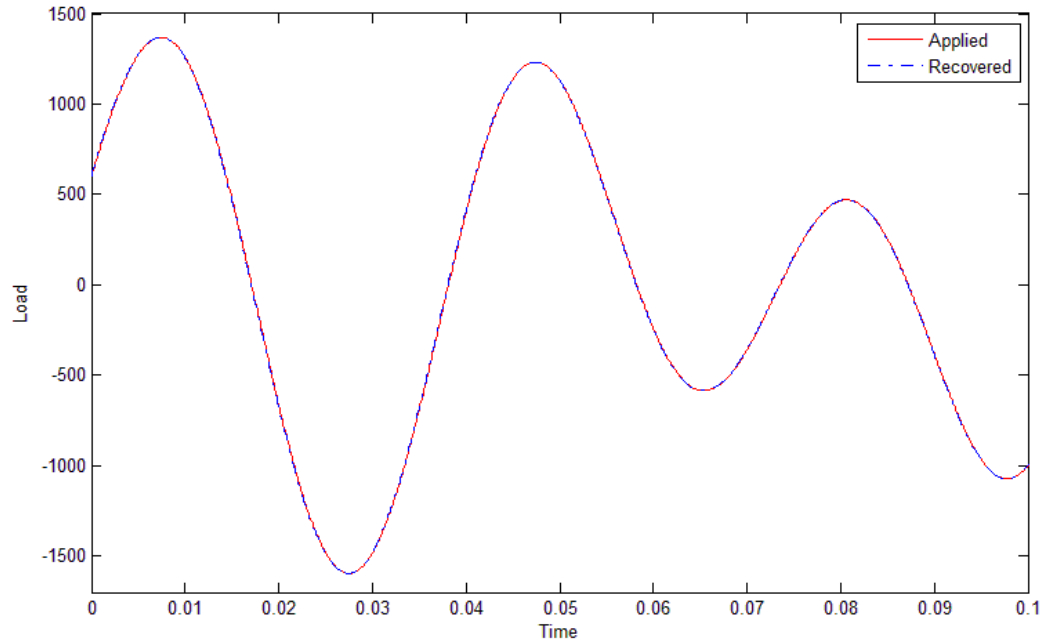
Figure 7.1 Applied and Recovered Load with Optimal Accelerometer Locations at Masses 6 and 8
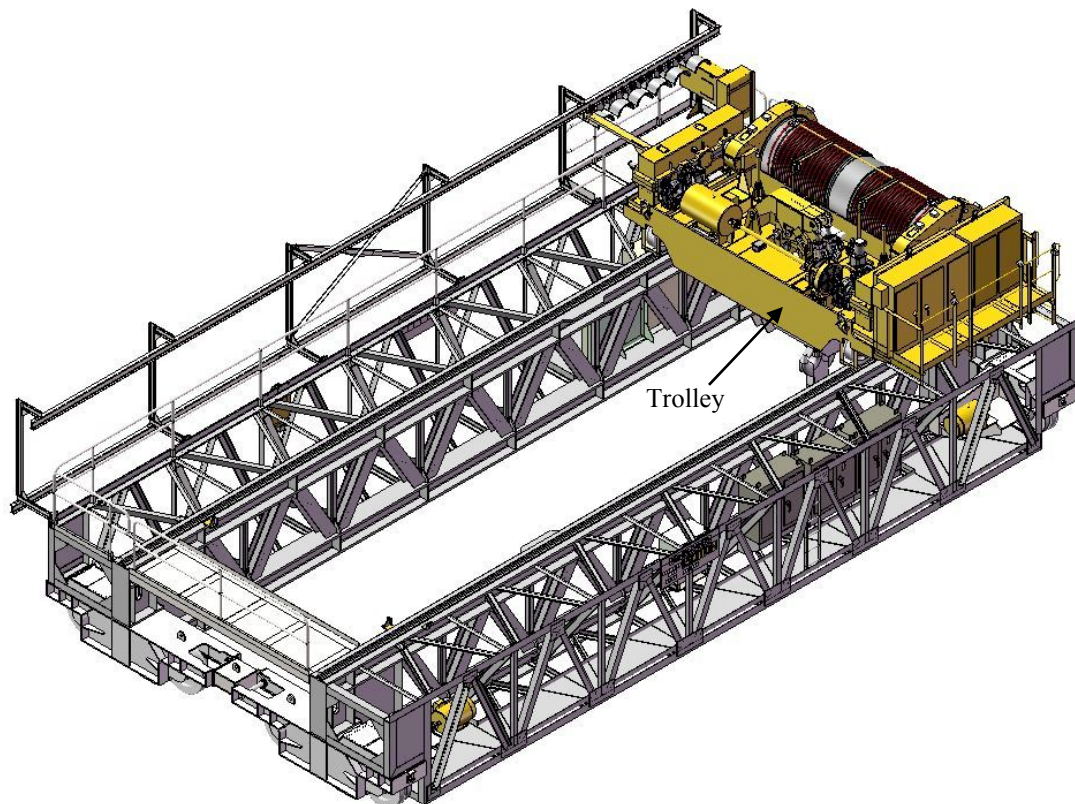
Trolley

Figure 7.2 Overhead Crane
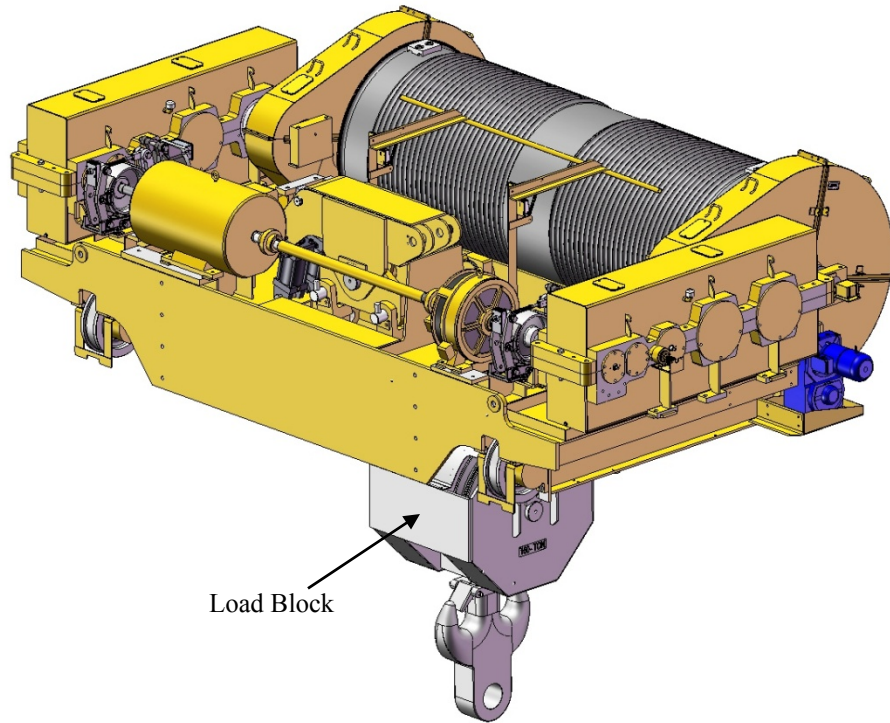
Figure 7.3 Trolley with Load Block
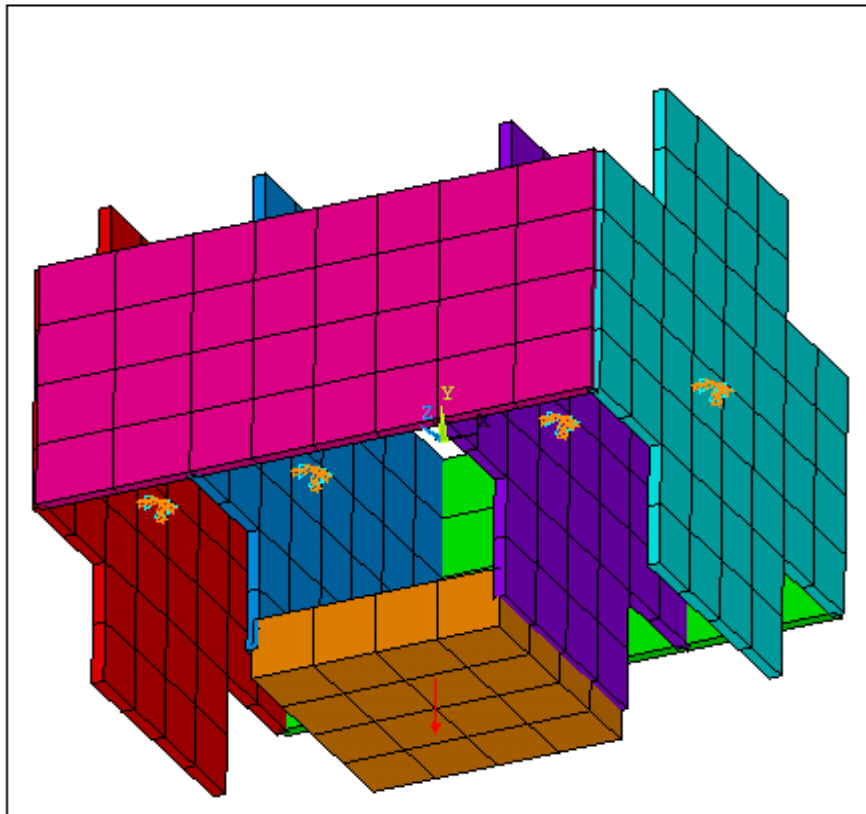
Figure 7.4 Finite Element Model of Load Block with Applied Load
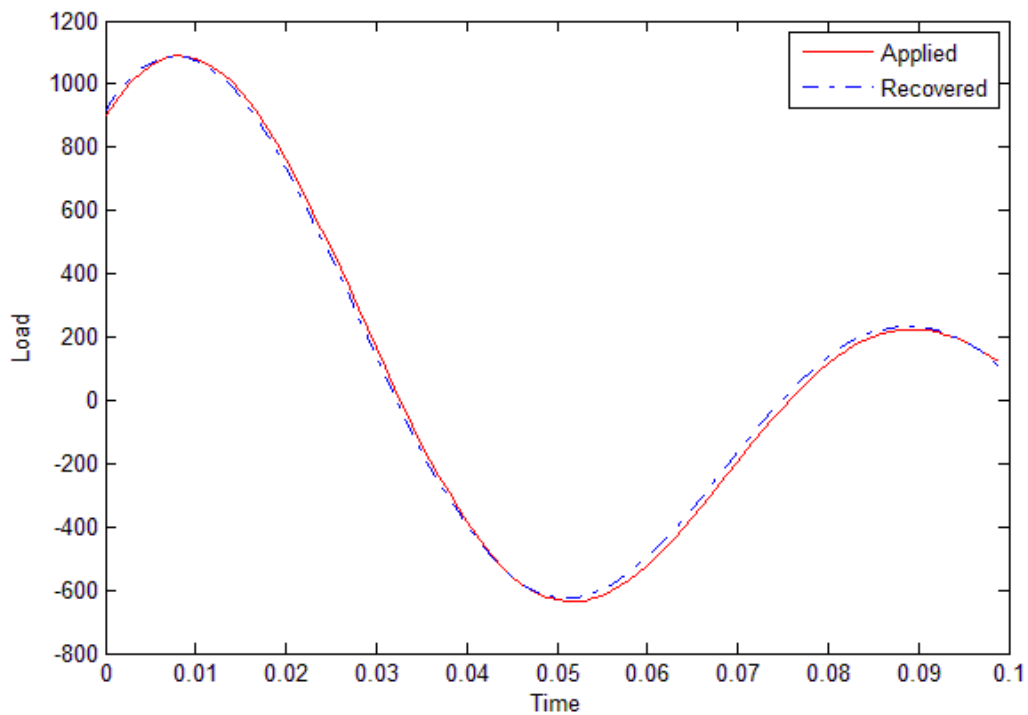
Figure 7.5 Applied and Recovered Load from Full Model
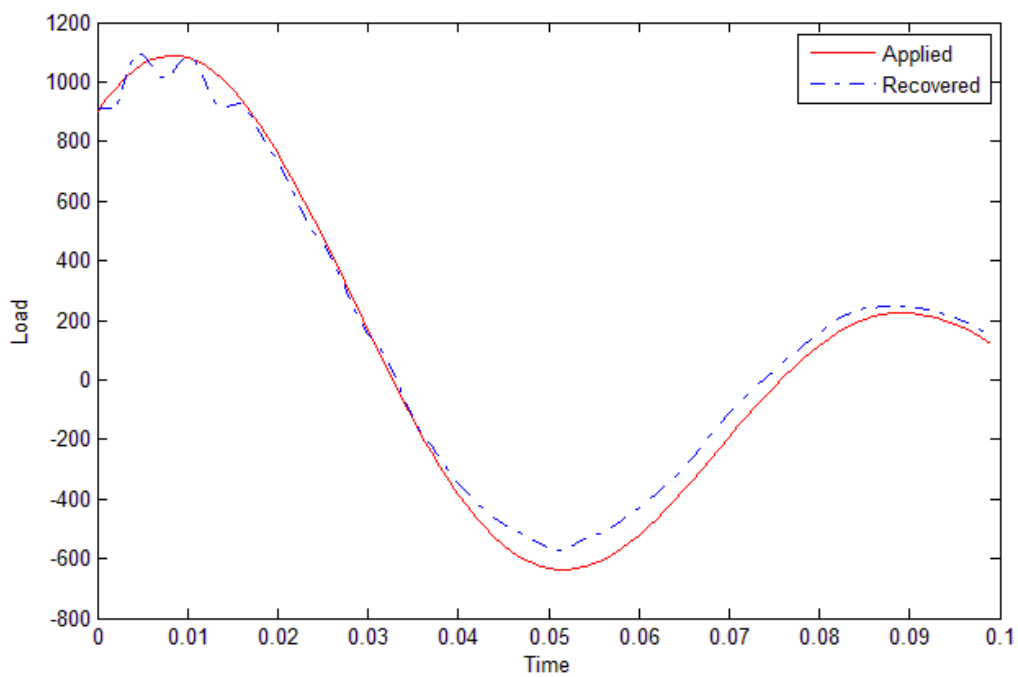
Figure 7.6 Applied and Recovered Load from Reduced Model
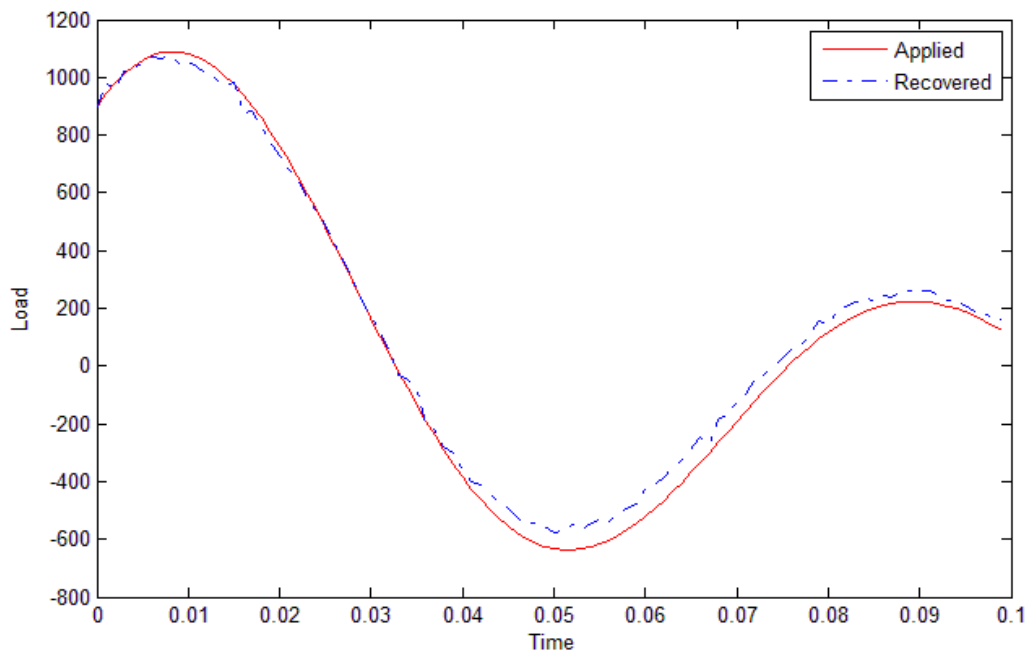
Figure 7.7 Applied and Recovered Load from Full Model with Acceleration Errors
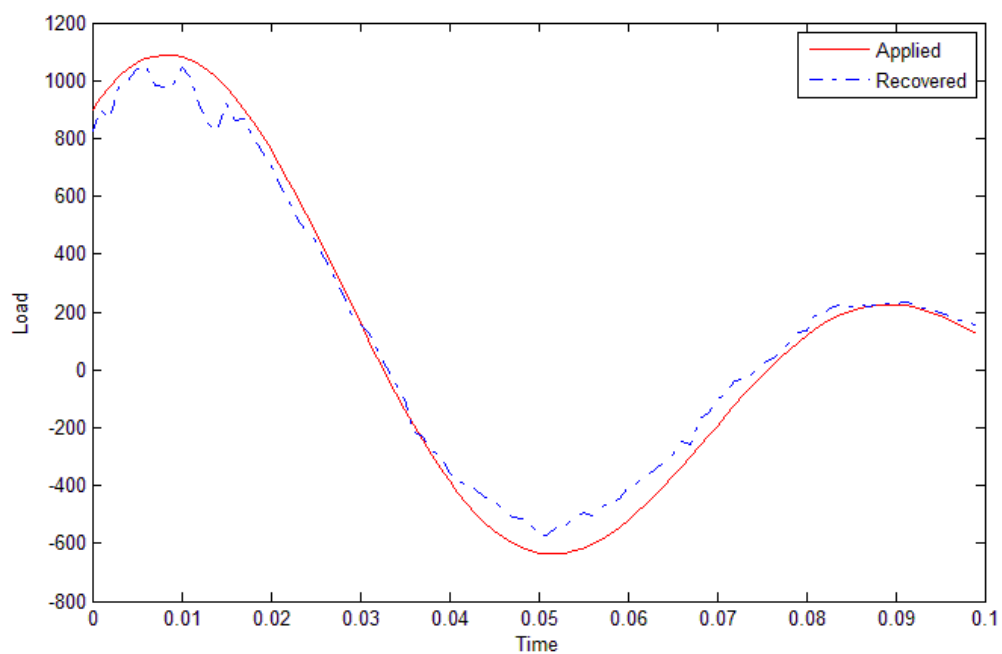
Figure 7.8 Applied and Recovered Load from Reduced Model with Acceleration Errors

Chapter 8 - Force Identification using Markov Parameters

This chapter examines a technique proposed by Kammer (1998) for identifying dynamic loads acting on a structure based upon the impulse response of the structure, also referred to as the system Markov parameters. Inverse Markov parameters are computed from the forward Markov parameters using a linear prediction algorithm, and have the roles of input and output reversed. The applied loads are then reconstructed by convolving the inverse Markov parameters with the system response to the loads.

It has been noted that the computation of inverse Markov parameters, like all the other inverse problems encountered in this dissertation, is ill-conditioned which causes their convolution with the measured response to become quite sensitive to errors in the measurements. The computation of inverse Markov parameters, and thereby the quality of load estimates, depends on the locations of sensors on the structure. To ensure that the computation of inverse Markov parameters is well-conditioned, the technique of D-optimal design algorithm is utilized in this chapter to determine the optimal sensor locations such that precise load estimates are obtained.

8.1 The Markov Parameter Approach

Consider again the discrete linear time-invariant state-space equation given by Eqn. (3.10) that characterizes the input-output behavior of a structural system. The corresponding system output is given by Eqn. (3.12). For zero initial conditions, it has been shown in Sec. 3.1.4 that Eqns. (3.10) and (3.12) can be combined to produce the

output at any time step (see Eqn. (3.14)). In the forward problem, given the system Markov parameters $[H]_i$ and the applied load history $\{f\}$, the system responses $\{u\}$ can be solved recursively starting from the known initial conditions. In the inverse problem of interest here, the objective is to estimate the input forces $\{f\}$, given the forward Markov parameters and system responses.

From Eqn. (3.14), the system response at $ti = 0$ is given by:

$$\{y\}_0 = [H]_0\{f\}_0 \tag{8.1}$$

Assuming the case where the number of sensors used is at least equal to the number of loads, the least-squares estimates of the loads at $ti = 0$ is given as:

$$\{f\}_0 = ([H]_0^T[H]_0)^{-1}[H]_0^T\{y\}_0 \tag{8.2}$$

Similarly, at $ti = 1$, the system response is given by:

$$\{y\}_1 = [H]_0\{f\}_1 + [H]_1\{f\}_0 \tag{8.3}$$

which can again be solved for the loads as:

$$\{f\}_1 = ([H]_0^T[H]_0)^{-1}[H]_0^T(\{y\}_1 - [H]_1\{f\}_0) \tag{8.4}$$

By induction, the loads at time ti can be verified to be:

$$\{f\}_{ti} = ([H]_0^T[H]_0)^{-1}[H]_0^T\left(\{y\}_{ti} - \sum_{i=1}^{ti}[H]_{ti}\,[f]_{ti-i}\right) \tag{8.5}$$

Next, define a discrete inverse system similar to Eqns. (3.10) and (3.12), where the roles of input forces $\{f\}$ and system response $\{y\}$ are reversed, as:

$$\{u\}_{ti+1} = [A_d]_I\{u\}_{ti} + [B_d]_I\{y\}_{ti}$$
$$\{f\}_{ti} = [C_d]_I\{u\}_{ti} + [D_d]_I\{y\}_{ti} \tag{8.6}$$

where the inverse matrices $[A_d]_I$, $[B_d]_I$, $[C_d]_I$ and $[D_d]_I$ are related to the corresponding forward matrices by:

$$[A_a]_I = [A_a] - [B_a]([D_a]^T[D_a])^{-1}[D_a]^T[C_a]$$

$$[B_a]_I = [B_a]([D_a]^T[D_a])^{-1}[D_a]^T$$

$$[C_a]_I = -([D_a]^T[D_a])^{-1}[D_a]^T[C_a] \qquad (8.7)$$

$$[D_a]_I = ([D_a]^T[D_a])^{-1}[D_a]^T$$

Similar to Eqns. (3.13) and (3.14), given the system response, the input forces at any time are given by the convolution relation as:

$$\{f\}_{ti} = \sum_{i=0}^{ti}[h]_i\{y\}_{ti-i} \qquad (8.8)$$

where the matrices $[h]_i$ are known as the inverse Markov parameters. The inverse Markov parameters, similar to the forward Markov parameters, contain the dynamic properties of the inverse system. On comparison of expansions of Eqns. (8.5) and (8.8), it may be ascertained that the inverse Markov parameters $[h]_i$ are related to the forward Markov parameters $[H]_i$ by a linear predictive equation given by:

$$[h]_0 = ([H]_0^T[H]_0)^{-1}[H]_0^T$$

$$[h]_k = -[h]_0\sum_{i=1}^{k}[H]_i[h]_{k-i} \qquad (8.9)$$

There exist cases where $[H]_0$ is zero matrix. In certain other non-minimum phase structural systems, $[H]_0$ is rank deficient and the least-squares inverse in Eqn. (8.9) does not exist. This renders the causal summation in Eqn. (8.8) undefined. To deal with this limitation, the system output (Eqn. (3.12)) is stepped forward in time as:

$$\{y\}_{ti} = [C_a]\{u\}_{ti} + [C_a][B_a]\{f\}_{ti} \qquad (8.10)$$

The inverse system associated with Eqn. (8.10) is non-causal, i.e., the input force estimates at current time become a function of the structural response at future times. In

general, if the first z Markov parameters in Eqn. (3.13) are zero, i.e., $[D_d] = [C_d][B_d] = [C_d][A_d][B_d] = \cdots = [C_d][A_d]^{z-2}[B_d] = [0]$, the non-causal z-lead inverse system can be constructed as:

$$[h]_z = ([H]_z^T[H]_z)^{-1}[H]_z^T$$

$$[h]_{k+z} = -[h]_z \sum_{i=1}^{k}[H]_{i+z}\,[h]_{k-i+z} \tag{8.11}$$

and the corresponding force estimates are given by:

$$\{f\}_{ti} = \sum_{i=0}^{ti}[h]_{i+z}\,\{y\}_{ti-i+z} \tag{8.12}$$

It must be noted in Eqn. (8.12) that the input force estimates $\{f\}$ at current time ti are dependent on the structural response $\{y\}$ at future times $ti - i + z$.

The determination of the inverse Markov parameters from the forward Markov parameters using Eqn. (8.11) is computationally expensive; however, it must be noted that the computation of the inverse Markov parameters needs to be performed only once for any particular system. Once the inverse Markov parameters are computed, the input forces can be predicted from the responses using Eqn. (8.12).

8.2 Candidate Set and D-optimal Design

The load identification technique based on Markov parameters, though different from previously discussed techniques in this thesis, suffers from a similar limitation as all the other techniques – ill-conditioning. The inaccuracies in system modeling translate to errors in forward Markov parameters. The computation of inverse Markov parameters from erroneous forward Markov parameters is ill-conditioned, and the computed inverse

Markov parameters become unbounded. Thus, the convolution of the inverse Markov parameters $[h]$ with the noisy structural response $\{y\}$ given by Eqn. (8.12) is not always a converging sum. The sum becomes numerically unstable due to the intrinsic ill-conditioning of the inverse problem identified by Eqn. (8.11). The precision with which the input loads $\{f\}$ are estimated from measured structural response $\{y\}$, using Eqn. (8.12), depends on the locations of sensors on the structure. There can be a large number of locations on the surface of a structure on which sensors can be mounted. As more sensors are used, the additional information helps to obtain a more precise estimate of $\{f\}$, but practical and financial constraints place limitations on the number of sensors that can be used. If the number of forces to be estimated is n_f, then in order to minimize the error in $\{f\}$ estimates, the number of sensors a must satisfy the criterion $a \geq n_f$. Further refinement in the number of sensors can be made based upon the methodology discussed in Sec. 4.1.2.

It can be inferred from the load identification step in Eqn. (8.12) that the quality of load estimates depends directly on how accurately the inverse Markov parameters are computed. It can further be assessed from Eqn. (8.11) that the zth inverse Markov parameter $[h]_z$ is computed by the least-squares inversion of the zth Markov parameter $[H]_z$. All the other higher order inverse Markov parameters depend on $[h]_z$. Therefore, the accuracy of $[h]_z$ directly dictates the accuracy of all the other higher order inverse Markov parameters. The least-squares estimate of $[h]_z$ in Eqn. (8.11) can be compared to Eqn. (4.2). It must be noted here that $[H]_z$ plays the same role in dynamic load recovery based on Markov parameters as $[A]$ in static load recovery. Therefore, optimal selection

of sensor locations, and hence the optimum matrix $[H]_{z\_opt}$, leads to increased accuracy in the estimation of $\{f\}$.

Each row in $[H]_z$ corresponds to a unique DOF of the system output. To form a candidate set for optimization, the DOFs (rows) corresponding to the force locations and other inaccessible locations for sensor placement are ignored; the subset so obtained is the candidate set $[H]_{z\_cs}$. Having obtained the candidate set $[H]_{z\_cs}$, for a given number of sensors, the D-optimal design algorithm described in Sec. 4.1.3 is followed to search $[H]_{z\_cs}$ to determine the optimum matrix $[H]_{z\_opt}$. Once the optimal locations for sensors are determined, sensors are mounted at the optimum locations and structural response is measured. Equations (8.11) and (8.12) are then utilized to compute the input forces $\{f\}$.

8.3 Example: 15-DOF Spring-Mass System

The above described procedure was applied numerically to the 15 degrees of freedom chain like spring-mass system described in Sec. 6.1.3 and depicted in Fig. 6.1. A sinusoidal forcing function $f_7(t) = 900\sin(50\pi t) + 650\cos(25\pi t)$ is applied to mass m_7. The task is to determine the optimum accelerometer locations and reconstruct the input force based on the acceleration time response at those locations.

A total of 2 accelerometers were used to measure accelerations of 2 masses. The $[M]$, $[C]$ and $[K]$ matrices were obtained by writing the equations of motion for the system. Continuous time-invariant state-space form of the system was obtained using Eqns. (3.9) − (3.12). Forward Markov parameters were computed from the state-space model using Eqn. (3.15). All numerical computations were performed in a MATLAB programming environment.

All DOFs, except the DOF where the load was applied, were selected to be the locations where accelerometers can potentially be mounted, i.e., the DOF corresponding to the applied load did not form a part of the candidate set $[H]_{z\_cs}$. $[H]_{z\_cs}$ was subjected to the D-optimal design algorithm described in Sec. 7.2 to obtain $[H]_{z\_opt}$ whereby the optimum accelerometer locations were found to be at masses m_6 and m_8. Having obtained the optimum accelerometer locations, the inverse Markov parameters were computed using Eqn. (8.11). In absence of any experimental data, the acceleration time response at the optimum locations were obtained by solving the ordinary differential equations numerically. Using the acceleration data $\{y\}$ computed at the optimum accelerometer locations, the input force $\{f\}$ was recovered using Eqn. (8.12). The applied and the recovered loads are plotted in Fig. 8.1. It can be inferred from the plot that the applied load is recovered accurately.

8.4 Example: Overhead Crane Girder

A more general numerical example is presented here where a vertical dynamic load acting on an overhead crane girder, through the trolley wheels (Fig. 7.2), needs to be estimated. For the sake of illustration and simplicity, the number of loads is assumed to be one. A sinusoidal input vertical forcing function $f(t) = 6000\sin(60t) + 10000\cos(25t)$ is assumed to be applied to the girder mid-span. The problem is to determine the optimum accelerometer locations and reconstruct the input force based on the acceleration time response at those locations.

A finite element model of the girder was developed in ANSYS using BEAM188 elements. The finite element model of the girder along with the applied load and

boundary conditions is shown in Fig. 8.2. The model consisted of 50 beam elements and 49 unconstrained nodes with 6 degrees of freedom per node, i.e., the total number of degrees of freedom of the model was 294.

The $[M]$ and $[K]$ matrices were obtained using finite element method. ANSYS provides data for $[M]$ and $[K]$ matrices in the Harwell-Boeing file format. A routine was written in MATLAB to convert them into the matrix format suitable for current application. All further calculations were performed in MATLAB. Continuous time-invariant state-space form of the system was obtained using Eqns. (3.9) – (3.12). Forward Markov parameters were computed from the state-space model using Eqn. (3.15). The number of accelerometers to be used was arbitrarily assumed to be equal to 3. All DOFs, except the DOF where the load was applied, were selected to be the locations where accelerometers can potentially be mounted, i.e., the DOF corresponding to the applied load did not form a part of the candidate set $[H]_{z\_cs}$. $[H]_{z\_cs}$ was subjected to the D-optimal design algorithm described in Sec. 7.2 to obtain $[H]_{z\_opt}$. The optimum accelerometer locations are also depicted in Fig. 8.2. It is observed that the algorithm predicts the optimum sensor locations to be as close to the loads as possible. This should not be considered as a limitation to the application of the proposed technique since if certain locations around the force application points are not available for sensor placement, they can initially be excluded from the candidate set $[H]_{z\_cs}$. Furthermore, if the sensor positions seem to be too congested mutually, additional criteria may be instructed such as if a particular spot is chosen as a potential sensor location, then certain area around that location may be excluded from the candidate set.
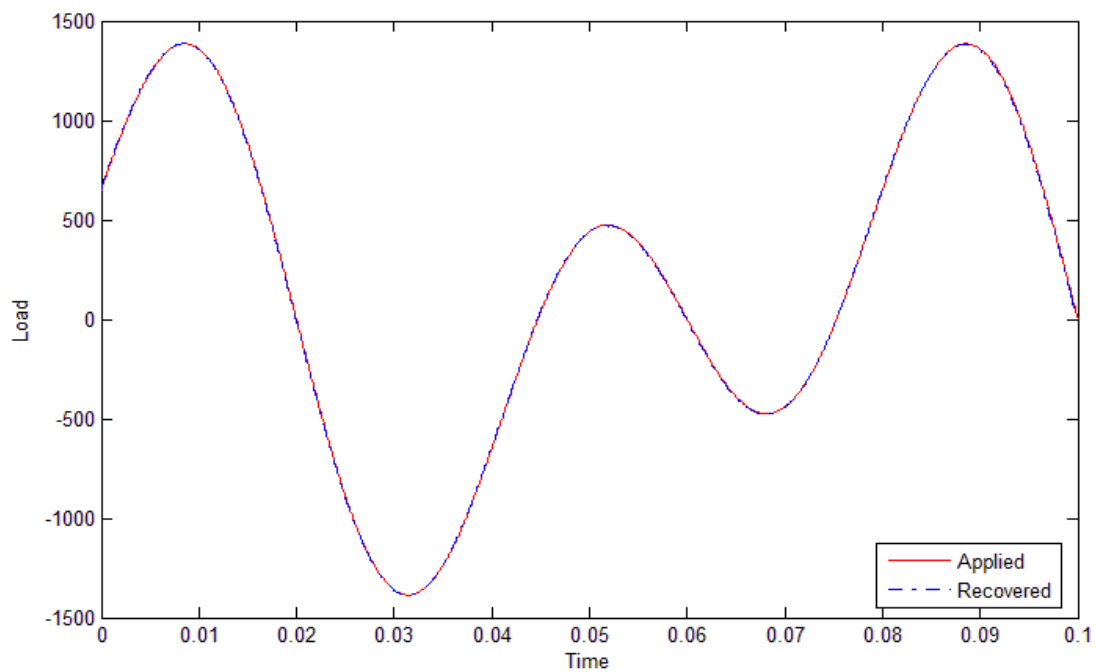
Having obtained the optimum accelerometer locations, the inverse Markov parameters were computed using Eqn. (8.11). In absence of any experimental data, the acceleration time response at the optimum locations were obtained by solving the ordinary differential equations numerically. Using the acceleration data $\{y\}$ computed at the optimum accelerometer locations, the input force $\{f\}$ was recovered using Eqn. (8.12). The applied and the recovered loads are plotted in Fig. 8.3. The rms error using Eqn. (3.33) was calculated to be 0.1%.

Next, to simulate a more realistic scenario where accelerations are measured experimentally, the acceleration data $\{y\}$ was corrupted with normally distributed random errors with zero mean and standard deviation of 10% of its value. The applied and recovered loads, with errors in acceleration measurements, are plotted in Fig. 8.4. The rms error using Eqn. (3.33) was calculated to be 2.3%. It can be inferred from the plots that the proposed approach is able to successfully recover the applied load precisely even when realistic measurement errors are present in the structural response.

8.5 Summary

A computational technique has been studied where the loads exciting a structure are estimated by convolving the structural response with the inverse Markov parameters. The inverse Markov parameters, in turn, are computed from the forward Markov parameters using a linear prediction algorithm. The forward Markov parameters represent the response of the system to applied unit impulse and thus contain the dynamic properties of the system. They can be obtained analytically as well as experimentally.

The computation of the inverse Markov parameters from forward Markov parameters, like all inverse problems, suffers from ill-conditioning. The computed inverse Markov parameters are not always bounded, thus rendering their convolution with the structural response to diverge. The accuracy of the inverse Markov parameters, and thereby the quality of input load estimates, depends on the locations of sensors on the structure. To improve the precision of load estimates, the technique of D-optimal design, in conjunction with finite element method, is utilized to determine the optimum sensor locations. It is observed that the algorithm predicts the optimum sensor locations to be as close to the loads as possible. This should not be considered as a limitation to the application of the proposed technique since if certain locations around the force application points are not available for sensor placement, they can initially be excluded from the candidate set. Furthermore, if the sensor positions seem to be too congested mutually, additional criteria may be instructed such as if a particular spot is chosen as a potential sensor location, then certain area around that location may be excluded from the candidate set. The loads recovered based on accelerations measured from optimally placed accelerometers on the structure are observed to be are in excellent agreement with the applied loads.

Figure 8.1 Applied and Recovered Load with Optimal Accelerometer Locations at Masses 6 and 8
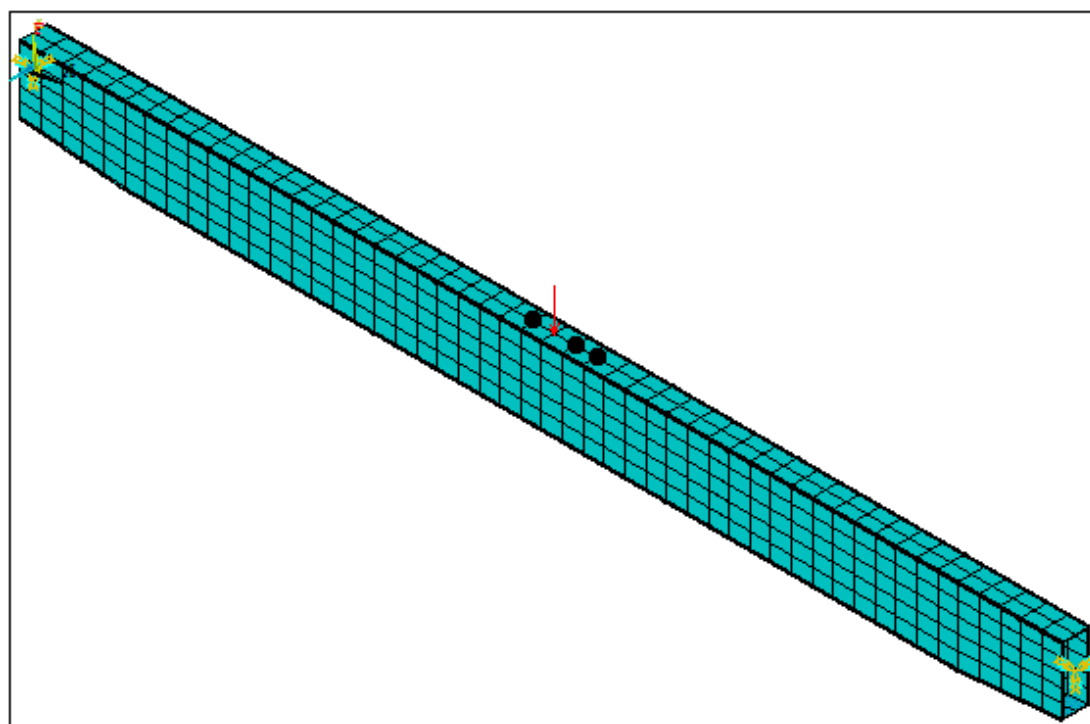
Figure 8.2 Finite Element Model of Girder with Applied Load and Optimum Accelerometer Locations
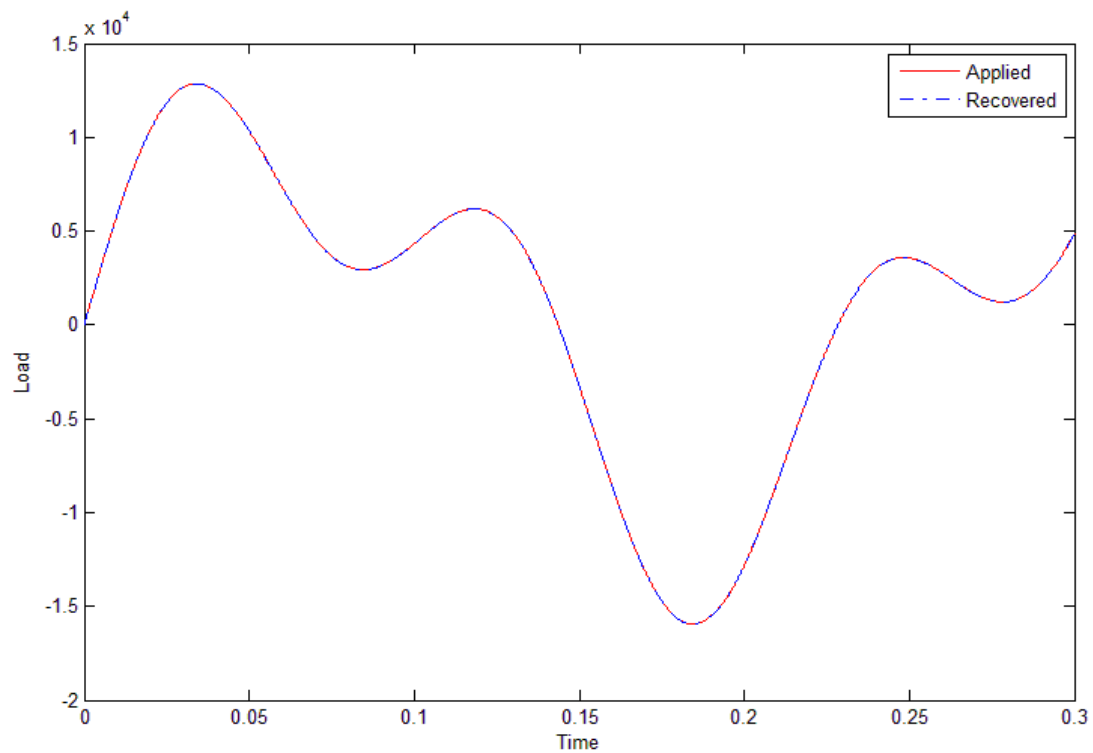
Figure 8.3 Applied and Recovered Load with No Acceleration Errors

Figure 8.4 Applied and Recovered Load with Acceleration Errors

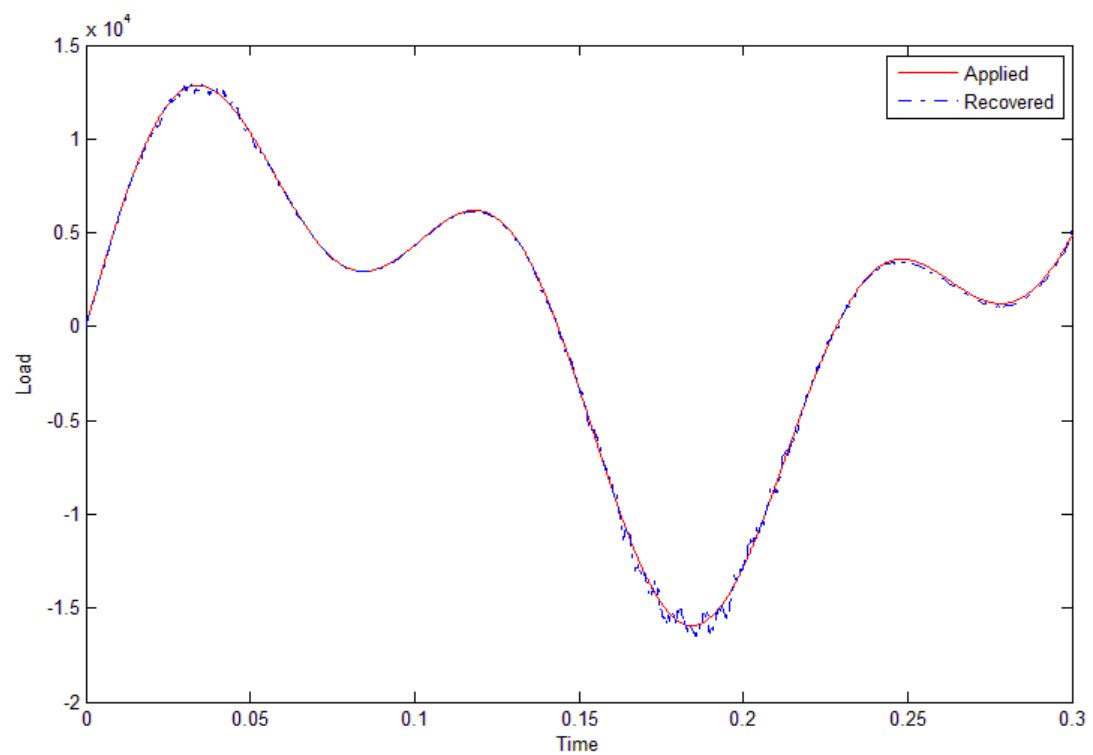# Chapter 9 - Conclusions and Future Research

It has been the primary endeavor of this dissertation to develop as well as bring together efficient algorithms and novel techniques to solve a distinct class of ill-conditioned inverse problems − identifying complex loads acting on a structure from experimentally measured structural response (strain, acceleration, etc.). To realize this technical goal, the techniques of D-optimal design for optimal sensor placements on the structure and model order reduction have extensively been used. The techniques are chiefly motivated from the observation that the quality of load estimates is sensitive to the locations where the sensors are mounted on the structure. Having developed the algorithms and techniques, they have been tested experimentally on simple structures and numerically through relatively complex simulations.

The first development involves a time domain technique for estimating dynamic loads acting on a structure from strain time response measured at a finite number of optimally placed strain gages on the structure. The approach is based on the fact that the strain response of an elastic vibrating system can be expressed as a linear superposition of its strain modes. Since the strain modes as well as the normal displacement modes are intrinsic dynamic characteristics of a system, the dynamic loads exciting a structure are estimated by measuring induced strain fields. The accuracy of estimated loads depends on the number and placement of gages on the instrumented structure. A solution procedure based on the construction of a D-optimal design augmented by finite element method is implemented to determine the optimum locations and orientations of strain gages that will provide the most precise load estimates. It is observed that the loads

recovered from the unreduced model are highly underestimated due to large amount of truncation errors resulting from few retained modes. The number of strain gages that can be used places a limit on the number of modes that can be retained in the analysis. To overcome this limitation, a novel approach based on model order reduction is proposed that results in significant improvement in dynamic load estimation.

Two original load identification algorithms are proposed based on acceleration measurements at optimally located accelerometers on a structure. The first algorithm utilizes the sparse nature of the mass, damping and stiffness matrices to help select the optimum locations of the accelerometers on the structure such that precise load estimates are obtained. Excellent agreement between the applied and recovered loads is observed when acceleration data from optimum locations of accelerometers is used. This approach, however, suffers from the limitation that the accelerometers need to be collocated with the forces, which is not always feasible. To deal with the aforementioned shortcoming, an alternate algorithm is presented for estimating dynamic loads acting on the structure from acceleration time response measured experimentally at a finite number of optimally placed non-collocated accelerometers on the structure. D-optimal design technique is used to determine the optimum accelerometer locations such that best possible load estimates are obtained from the measured acceleration data. It is observed that the loads recovered from optimally placed accelerometer data and unreduced model are highly underestimated due to large amount of truncation error resulting from few retained modes. Acceptable load estimates are obtained by utilizing Craig-Bampton model order reduction technique in load recovery. Excellent agreement in the applied and the

recovered loads is observed with the introduction of reduced modal matrix based algorithm that works in conjunction with optimum accelerometer locations.

The goals of this thesis have been not only to propose novel algorithms for solving the inverse problem of load identification but also to improve upon existing methodologies for force estimation. One of the techniques studied casts the load estimation problem as a minimization problem of error which is defined as the difference between the measured structural response and the response predicted from the model. Dynamic programming is used to solve the minimization problem. It is known that the quality of load estimates depends on the locations of sensors on the structure. To improve the precision of load estimates, the technique of D-optimal design in conjunction with finite element method is utilized to determine the optimum sensor locations. It is observed that the loads recovered based on accelerations measured from optimally placed accelerometers on the structure are in excellent agreement with the applied loads. One of the disadvantages of the dynamic programming technique is that the amount of computation increases dramatically as the order of the model increases. To overcome this limitation, a technique based on Craig-Bampton model order reduction is proposed. It is observed that the load recovered using the reduced model shows an initial discrepancy, but later follows the applied load closely. It is inferred that with the introduction of model order reduction and without compromising on the quality of load estimates, the computation time can be reduced by as much as 98%. This result indicates that the dynamic programming technique of load identification, in conjunction with model order reduction, is worthy of application to higher order problems of increased complexity.

A computational technique has also been studied where the loads exciting a structure are estimated by convolving the structural response with the inverse Markov parameters. The inverse Markov parameters, in turn, are computed from the forward Markov parameters using a linear prediction algorithm. The forward Markov parameters represent the response of the system to applied unit impulse and thus contain the dynamic properties of the system. They can be obtained analytically as well as experimentally. The computation of the inverse Markov parameters from forward Markov parameters, like all inverse problems, suffers from ill-conditioning. The computed inverse Markov parameters are not always bounded, thus rendering their convolution with the structural response to diverge. The accuracy of the inverse Markov parameters, and thereby the quality of input load estimates, depends on the locations of sensors on the structure. To improve the precision of load estimates, the technique of D-optimal design, in conjunction with finite element method, is utilized to determine the optimum sensor locations. It is observed that the algorithm predicts the optimum sensor locations to be as close to the loads as possible. This should not be considered as a limitation to the application of the proposed technique since if certain locations around the force application points are not available for sensor placement, they can initially be excluded from the candidate set. Furthermore, if the sensor positions seem to be too congested mutually, additional criteria may be instructed such as if a particular spot is chosen as a potential sensor location, then certain area around that location may be excluded from the candidate set. The loads recovered based on accelerations measured from optimally placed accelerometers on the structure are observed to be in excellent agreement with the applied loads.

The load identification techniques developed and proposed in this dissertation rely on the D-optimal design algorithm for the determination of optimal sensor locations such that accurate load estimates are obtained. Further improvement in the quality of the load estimates is realized through the Craig-Bampton model order reduction. Though the D-optimal design algorithm is efficient and quite popular among the design optimization community, it suffers from the limitation of getting stuck in local optima often times, which may not yield the best possible locations for sensor placements. Future research in this area will focus on experimenting with more efficient and robust optimization techniques that can be utilized to determine optimal sensor locations on the structure. While the Craig-Bampton model order reduction technique worked well when applied in the context of load identification schemes, experimenting with several other well-established model order reduction techniques and studying their effect on the load estimates is further suggested.

Application of the load identification techniques developed in this thesis has been studied experimentally using a cantilevered beam and numerically using spring-mass system, cantilevered beam and other simple geometries where one or two sinusoidal loads are exciting the structure. Spring-mass systems are relatively simple to deal with than beams; complicated structures seem more amenable to load identification testing and implementation than simpler ones. The real interest of the proposed techniques lies in the case of complicated structures where complex loads are acting. Implementation and testing of the proposed approaches on complicated structures towards identification of multiple complex loads forms another potential area of research.

References

[1]   Adams, R., & Doyle, J. (2002). Multiple Force Identification for Complex Structures. *Experimental Mechanics, 42* (1), 25-36.

[2]   Allen, M. S., & Carne, T. G. (2008). Comparison of Inverse Structural Filter (ISF) and Sum of Weighted Accelerations Technique (SWAT) Time Domain Force Identification Methods. *Mechanical Systems and Signal Processing, 22*, 1036-1054.

[3]   Atkinson, A. C., & Donev, A. N. (1992). *Optimum Experimental Designs.* New York: Oxford University Press.

[4]   Bartlett, F., & Flannelly, W. G. (1979). Model Verification of Force Determination for Measuring Vibratory Loads. *Journal of the American Helicopter Society, 24* (2), 10-18.

[5]   Bernasconi, O., & Ewins, D. J. (1989). Modal Strain/Stress Fields. *Journal of Modal Analysis, 4* (2), 68-76.

[6]   Boukria, Z., Perrotin, P., & Bennani, A. (2011). Experimental Impact Force Location and Identification Using Inverse Problems: Application for a Circular Plate. *International Journal of Mechanics, 5* (1), 48-55.

[7]   Budynas, R. G. (1999). *Advanced Strength and Applied Stress Analysis.* New York: McGraw Hill.

[8]   Busby, H. R., & Trujillo, D. M. (1987). Solution of an Inverse Dynamics Problem Using an Eigenvalue Reduction Technique. *Computers & Structures, 25* (1), 109–117.

[9]   Carne, T. G., Mayes, R. L., & Bateman, V. I. (1992). Force Reconstruction Using a Sum of Weighted Accelerations Technique. *Proceedings of the 10th International Modal Analysis Conference (IMAC)*, (pp. 291-298). San Diego, CA.

[10]   Chatterjee, S., & Hadi, A. S. (1988). *Sensitivity Analysis in Linear Regression.* New York: John Wiley.

[11]   Craig, R. R., & Bampton, M. C. (1968). Coupling of Substructures for Dynamic Analysis. *American Institute of Aeronautics and Astronautics (AIAA) Journal, 6* (7), 1313-1319.

[12]   Desanghere, G. (1983). Identification of External Forces Based on Transfer-function Measurements: Frequency Response Method. *Proceedings of the 8th International Seminar on Modal Analysis*, (pp. 1-28). Leuven, Belgium.

[13] Desanghere, G., & Snoeys, R. (1985). Indirect Identification of Excitation Forces by Modal Coordinate Transformation. *Proceedings of the 3rd International Modal Analysis Conference (IMAC)*, (pp. 685-690). Orlando, FL.

[14] Dhingra, A. K., & Hunter, T. G. (2003). Dynamic Strain Measurements For Structural Modeling. *Proceedings of the National Agency for Finite Element Methods and Standards (NAFEMS) World Congress*. Orlando, FL.

[15] Ewins, D. J. (2000). *Modal Testing: Theory, Practice, and Application*. Baldock, England: Research Studies Press Ltd.

[16] Friswell, M. I., Garvey, S. D., & Penny, J. E. (1995). Model Reduction Using Dynamic and Iterated IRS Techniques. *Journal of Sound and Vibration, 186* (2), 311-323.

[17] Galil, Z., & Kiefer, J. (1980). Time- and Space-Saving Computer Methods, Related to Mitchell's DETMAX, for Finding D-Optimum Designs. *Technometrics, 22* (3), 301-313.

[18] Genaro, G., & Rade, D. A. (1998). Input Force Identification in the Time Domain. *Proceedings of the 16th International Modal Analysis Conference (IMAC)*, (pp. 124-129). Santa Barbara, CA.

[19] Guyan, R. J. (1965). Reduction of Stiffness and Mass Matrices. *American Institute of Aeronautics and Astronautics (AIAA) Journal, 3* (2), 380.

[20] Hansen, M., & Starkey, J. M. (1990). On Predicting and Improving the Condition of Modal-Model-Based Indirect Force Measurement Algorithms. *Proceedings of the 8th International Modal Analysis Conference (IMAC)*, (pp. 115-120). Kissimmee, FL.

[21] Hashemi, R., & Kargarnovin, M. H. (2007). Vibration Base Identification of Impact Force using Genetic Algorithm. *International Journal of Mechanical Systems Science and Engineering, 1* (4), 204-210.

[22] Hillary, B. (1983). *Indirect Measurement of Vibration Excitation Forces*. PhD Thesis, Imperial College, Department of Mechanical Engineering, London.

[23] Hillary, B., & Ewins, D. J. (1984). The Use of Strain Gauges in Force Determination and Frequency Response Function Measurements. *Proceedings of the 2nd International Modal Analysis Conference (IMAC)*, (pp. 627-634). Orlando, FL.

[24] Hollandsworth, P. E., & Busby, H. R. (1989). Impact Force Identification Using the General Inverse. *International Journal of Impact Engineering, 8* (4), 315-322.

[25] Inoue, H., Harrigan, J. J., & Reid, S. R. (2001). Review of Inverse Analysis for Indirect Measurement of Impact Force. *Applied Mechanics Reviews, 54* (6), 503-524.

[26] Johnson, M., & Nachtsheim, C. J. (1983). Some Guidelines for Constructing Exact D-optimal Designs on Convex Design Spaces. *Technometrics, 25* (3), 271-277.

[27] Kammer, D. C. (1998). Input Force Reconstruction Using a Time Domain Technique. *Journal of Vibration and Acoustics, 120* (4), 868-874.

[28] Kammer, D. C. (1991). Sensor Placement for On-Orbit Modal Identification and Correlation of Large Space Structures. *Journal of Guidance, Control and Dynamics, 14* (2), 251-259.

[29] Koutsovasilis, P., & Beitelschmidt, M. (2008). Comparison of Model Reduction Techniques for Large Mechanical Systems - A Study on An Elastic Rod. *Multibody System Dynamics, 20* (2), 111-128.

[30] Li, D., Zhuge, H., & Wang, B. (1989). The Principle and Technique of Experimental Strain Modal Analysis. *Proceedings of the 7th International Modal Analysis Conference (IMAC)*, (pp. 1285-1289). Las Vegas, NV.

[31] Liu, J. J., Ma, C. K., Kung, I. C., & Lin, D. C. (2000). Input Force Estimation of a Cantilever Plate by using a System Identification Technique. *Computer Methods in Applied Mechanics and Engineering, 190* (11), 1309-1322.

[32] Lu, Z. R., & Law, S. S. (2007). Identification of System Parameters and Input Force from Output Only. *Mechanical Systems and Signal Processing, 21* (5), 2099-2111.

[33] Ma, C. K., Chang, J. M., & Lin, D. C. (2003). Input Forces Estimation of Beam Structures by an Inverse Method. *Journal of Sound and Vibration, 259* (2), 387-407.

[34] Masroor, S. A., & Zachary, L. W. (1991). Designing an All-Purpose Force Transducer. *Experimental Mechanics, 31* (1), 33-35.

[35] Mignolet, M. P., & Choi, B. K. (2003). Robust Optimal Positioning of Strain Gages on Blades. *ASME Journal of Turbomachinery, 125* (1), 155-164.

[36] Mitchell, T. J. (1974). An Algorithm for the Construction of "D-optimal" Experimental Designs. *Technometrics, 16* (2), 203-210.

[37] Nashed, M. Z. (1976). *Generalized Inverses and Applications.* Academic Press.

[38] Neter, J., Wasserman, W., & Kutner, M. H. (1990). *Applied Linear Statistical Models.* Richard D. Irwin, Inc.

[39] O'Callahan, J. C. (1989). A Procedure for an Improved Reduced System (IRS) Model. *Proceedings of the 7th International Modal Analysis Conference (IMAC)*, (pp. 17-21). Las Vegas, NV.

[40] Okubo, N., Tanabe, S., & Tatsuno, T. (1985). Identification of Forces Generated by a Machine Under Operating Condition. *Proceedings of the 3rd International Modal Analysis Conference (IMAC)*, (pp. 920-927). Orlando, FL.

[41] Paz, M. (1985). *Structural Dynamics: Theory and Computation.* New York: Van Nostrand Reinhold Company, Inc.

[42] Qu, Z.-Q. (2004). Model Order Reduction Techniques with Applications in Finite Element Analysis. New York: Springer.

[43] Sommerfeld, J. L., & Meyer, R. A. (1999). Correlation and Accuracy of a Wheel Force Transducer as Developed and Tested on a Flat-Trac® Tire Test System. *International Congress & Exposition.* (Paper Number: 1999-01-0938). Detroit, MI.

[44] Starkey, J. M., & Merrill, G. L. (1989). On the Ill-Conditioned Nature of Indirect Force Measurement Techniques. *International Journal of Analytical and Experimental Modal Analysis, 4* (3), 103-108.

[45] Steltzner, A. D., & Kammer, D. C. (1999). Input Force Estimation Using an Inverse Structural Filter. *Proceedings of the 17th International Modal Analysis Conference (IMAC)*, (pp. 954-960). Kissimmee, FL.

[46] Stevens, K. K. (1987). Force Identification Problems - An Overview. *Proceedings of the 1987 SEM Conference on Experimental Mechanics*, (pp. 838-844). Houston, TX.

[47] Szwedowicz, J., Senn, S. M., & Abhari, R. S. (2002). Optimum Strain Gage Application to Bladed Assemblies. *ASME Journal of Turbomachinery, 124* (4), 606-613.

[48] Trujillo, D. M., & Busby, H. R. (1997). *Practical Inverse Analysis in Engineering.* CRC Press.

[49] Tsang, W. F. (1990). Use of Dynamic Strain Measurements for the Modeling of Structures. *Proceedings of the 8th International Modal Analysis Conference (IMAC)*, (pp. 1246-1251). Kissimmee, FL.

[50] Wickham, M. J., Riley, D. R., & Nachtsheim, C. J. (1995). Integrating Optimal Experimental Design into the Design of a Multi-Axis Load Transducer. *Journal of Engineering for Industry, 117* (3), 400-405.

[51] Wu, A. L., & Loh, C. H. (2007). Input Force Estimation Using System Identification Techniques. *Proceedings of the 8th Pacific Conference on Earthquake Engineering (PCEE).* Singapore.

[52] Yam, L. H., Leung, T. P., Li, D. B., & Xue, K. Z. (1996). Theoretical and Experimental Study of Modal Strain Energy. *Journal of Sound and Vibration, 191* (2), 251-260.

CURRICULUM VITAE

Deepak Kumar Gupta

Place of Birth: Varanasi, Uttar Pradesh, India

Education

Doctor of Philosophy (Ph.D.) in Engineering, December 2013
University of Wisconsin – Milwaukee, Wisconsin, US

Master of Science (M.S.) in Mechanical Engineering, May 2010
University of Wisconsin – Milwaukee, Wisconsin, US

Bachelor of Technology (B. Tech.) in Mechanical Engineering, July 2007
Harcourt Butler Technological Institute, Kanpur, Uttar Pradesh, India

Industrial Experience

Jan 2011 – Present, Senior Seismic Engineer, Konecranes Nuclear Equipment & Services, LLC, New Berlin, Wisconsin, US

July 2007 – July 2008, Graduate Engineering Trainee, Volvo-Eicher Commercial Vehicles Ltd., Dhar, Madhya Pradesh, India

June 2005 – July 2005, Intern, Diesel Locomotive Works (DLW), Varanasi, Uttar Pradesh, India

Research Experience

June 2010 – Oct 2013, University of Wisconsin – Milwaukee, Wisconsin, US
Topic: *Inverse Methods for Load Identification Augmented by Optimal Sensor Placement and Model Order Reduction*

Sep 2008 – Aug 2009, University of Wisconsin – Milwaukee, Wisconsin, US
Topic: *Shape, Sizing, RBDO and Topology Optimization of Trusses and Structures*

June 2006 – July 2006, Indian Institute of Technology, Kanpur, Uttar Pradesh, India
Topic: *Suppression of Cup-burner Flame Using Nitrogen Gas*

Teaching Experience

Sep 2009 – Dec 2010, Teaching Assistant, Introduction to Finite Elements, University of Wisconsin – Milwaukee, Wisconsin, US

June 2009 – Aug 2009, Instructor, Upward Bound Math and Science, University of Wisconsin – Milwaukee, Wisconsin, US

Papers in Refereed Journals and Peer Reviewed Conference Proceedings

- Gupta, D. K., & Dhingra, A. K. (2013). Input Load Identification from Optimally Placed Strain Gages using D-optimal Design and Model Reduction. *Mechanical Systems and Signal Processing, 40* (2), 556-570.
- Dhingra, A. K., Hunter, T. G., & Gupta, D. K. (2013). Load Recovery in Components Based on Dynamic Strain Measurements. *Journal of Vibration and Acoustics*, *135*(5).
- Gupta, D. K., & Dhingra, A. K. (2013). An Inverse Approach on Load Identification from Optimally Placed Accelerometers. *Proceedings of the ASME 2013 International Design Engineering Technical Conferences.* Portland, OR.
- Gupta, D. K., & Dhingra, A. K. (2013). Verification and Validation of Load Reconstruction Technique Augmented by Finite Element Analysis. *ASME Verification & Validation Symposium.* Las Vegas, NV.
- Gupta, D. K., & Dhingra, A. K. (2012). Input Force Identification In Time Domain Using Optimally Placed Accelerometers. *Proceedings of the ASME 2012 International Mechanical Engineering Congress & Exposition.* Houston, TX.
- Gupta, D. K., & Dhingra, A. K. (2012). Load Transducer Design Using Inverse Method With Model Reduction. *Proceedings of the ASME 2012 International Design Engineering Technical Conferences.* Chicago, IL.

Awards and Recognition

- Member of American Society of Mechanical Engineers (ASME).
- Awarded Chancellor's Award by the department of Mechanical Engineering at the University of Wisconsin – Milwaukee for excellent research and academic performance (GPA 4.0/4.0).
- Amongst the top 5 students in the undergraduate batch of Mechanical Engineering of 65 students.
- Awarded distinction in international mathematics competition organized by the University of New South Wales, Australia.